FACULTY OF PHYSICS AND ASTRONOMY

UNIVERSITY OF HEIDELBERG

Diploma thesis
in Physics

submitted by
Andreas Deschner
born in Schwetzingen, Germany

Heidelberg
2008

Worldline Numerics and Non-Abelian Gauge Theories

This diploma thesis has been carried out by
Andreas Deschner
at the Institut für Theoretische Physik

under the supervision of
Prof. Dr. Holger Gies

Weltliniennumerik und nichtabelsche Eichtheorien

Abstract

In dieser Arbeit wird die Methode der Weltliniennumerik zum ersten Mal auf nichtabelsche SU(2)-Hintergrundfelder angewandt. Das pseudoabelsche Feld wird in zwei Eichungen untersucht. Wir können zeigen, dass Weltliniennumerik für diese Felder in der Lage ist, sowohl die Eichinvarianz, als auch die Pfadordnung zu berücksichtigen. Zum ersten Mal wird für ein konstantes nichtabelsches Feld, das wir PNA Feld nennen, die renormierte effektive Ein-Schleifen-Lagrange-Dichte berechnet. Untersuchungen des Erwartungswertes des Wegner-Wilson-Loops für das Instanton ergeben, dass die Eichinvarianz gebrochen ist. Das Problem wird dann auf eine Eigenschaft des BPST-Instantons zurückgeführt: Die Summe bestimmter Beiträge zum numerisch ausgewerteten Ausdruck für $\mathrm{tr}[\mathbf{G}_{\mu\nu}\mathbf{G}_{\mu\nu}]$ muss mit sehr hoher Genauigkeit verschwinden, um richtige Ergebnisse zu ermöglichen. Um die erforderliche Genauigkeit zu erreichen, wird eine Methode zur Verbesserung der Rotationsinvarianz des diskretisierten Weltlinienensembles vorgeschlagen. Erste Betrachtungen legen den Schluss nahe, dass die weltliniennumerischen Ergebnisse sehr langsam konvergieren. Wir folgern daraus, dass Felder, die hinsichtlich der numerischen Auswertung von $\mathrm{tr}[\mathbf{G}_{\mu\nu}\mathbf{G}_{\mu\nu}]$ ein ähnliches Verhalten wie das BPST-Instanton zeigen, für Standard-Weltliniennumerik eine große Herausforderung darstellen. Des Weiteren wird Weltliniennumerik verwendet, um die Auswirkungen einer Störung der Art $\delta_a \cos(kx_1)\cos(kx_2)$ auf das effektive Potential der 0-Komponente eines konstanten SU(2) Eichfeldes im thermischen Gleichgewicht, deren Erwartungswert als Confinement-Ordnungsparameter dienen kann, zu bestimmen. Die numerischen Daten deuten an, dass das veränderliche Feld gegenüber dem konstanten Feld begünstigt ist. Sollte unser Resultat von weiteren Studien bestätigt werden, könnte es von großer Bedeutung für die Untersuchung von Hochtemperatureigenschaften des Quark-Gluon-Plasmas sein.

Worldline Numerics and Non-Abelian Gauge Theories

Abstract

In this thesis worldline numerics is for the first time used to treat non-abelian SU(2) background fields. Investigating the pseudo-abelian field in two gauges, we are successful in showing that worldline numerics is, for these fields, able to preserve gauge invariance as well as to respect path ordering. For the first time the one-loop effective action for a constant non-abelian field, which we call PNA field, is calculated. Evaluating the Wilson loop expectation value for the instanton, we find gauge invariance to be broken. A detailed analysis enables us to track the problem down to the distinct feature of the BPST instanton that a very precise cancellation of contributions to the numerically evaluated expression for $\mathrm{tr}[\mathbf{G}_{\mu\nu}\mathbf{G}_{\mu\nu}]$ is necessary to allow for correct results. To achieve this precision, a method to improve the rotational invariance of the discretised worldline ensemble is proposed. First numerical tests, however, indicate that, also using this method, the worldline numerical results converge very slowly. It is concluded that gauge fields that require such cancellations pose a serious challenge to standard worldline numerics. Furthermore, worldline numerics is used to investigate the effect that a perturbation of the kind $\delta_a \cos(kx_1)\cos(kx_2)$ has on the one-loop effective potential of the zero-component of a constant SU(2) gauge field in thermal equilibrium, whose expectation value can serve as an order parameter for confinement. The numerical data indicates a varying field to be favoured over the constant field. Should further studies confirm our result, this could be of high relevance to the study of high temperature properties of the quark-gluon plasma.

"When the going gets weird,
the weird turn pro."

Hunter S. Thompson

Contents

1 Introduction

The calculation of one-loop effective actions for given background gauge fields has been of great interest to physicists for a long time. The first calculations were performed in 1936 by Heisenberg and Euler [1] and Weisskopf [2], who computed the renormalised one-loop effective action of a background field of constant field strength in spinor and scalar QED respectively, in order to investigate how a constant external field changes the properties of the vacuum. This is most remarkable since at the time the formal framework that justifies subtracting divergent terms to get finite results, which is now known as charge-renormalisation, did not exist. They were able to quantify how quantum fluctuations cause non-linear interactions between electro-magnetic fields. The study of effective actions of constant background fields, which are today called Heisenberg-Euler actions, has become prototypical for a wide physical field, which computes fluctuation induced effects in background fields using effective actions as computational tools.

To calculate a one-loop effective action, one needs to evaluate a functional determinant of a partial differential operator. This is a highly delicate task (see e.g. [3]). Apart from the constant field case, there are only very few field configurations for which one was able to perform an analytical computation of the one-loop effective action (see e.g. [4]). For a long time the discretisation of space-time on a lattice was the only method to compute the one-loop effective action that was not restricted to highly symmetric background fields. Therefore one very often had to rely on approximation schemes like the semi-classical approach (see e.g. [4–7]) and the heat-kernel expansion (see e.g. [8–11]) to learn about the effective action for a given background field.

In 2002 a method called *worldline numerics* was proposed [12, 13] and in the following years developed into a useful and elegant tool for the computation of one-loop effective actions for a wide class of background fields. Since its introduction, the worldline numerical method has been used on a variety of problems such as the pair production in inhomogeneous fields [14], the Casimir effect [15–20] and chiral fermions [21]. It is based on the worldline formalism that had its first appearance in Feynman's seminal paper in which he laid the foundations of modern QED [22]. After its invention, the worldline formalism was only rarely used for actual calculations, and it took until the 1990s for it to be rediscovered and used to do numerous computations (see e.g. [23–27]). For a review on the worldline formalism see [8].

Worldline numerics is a Monte Carlo method to evaluate a worldline expression for the one-loop effective action. Instead of a functional determinant, the worldline expression contains an integral over an auxiliary parameter called the proper time and a one-dimensional path integral over closed loops. Using Monte Carlo tech-

niques to evaluate this path integral, it suffices to only discretise a one-dimensional space, which is associated with the proper time. Uniformly distributed numbers can analytically be mapped onto the necessary Monte Carlo ensembles, which makes the Monte Carlo evaluation of the path integral very efficient. Of course also a lattice implementation of the path integral is possible and was actually used to investigate matter determinants in background Yang-Mills fields [28].

In this thesis we perform a first test of the ability of worldline numerics to cope with non-abelian gauge theories, i.e. to calculate the one-loop effective action for SU(2) background fields. We thereby investigate the effect of fluctuations of a matter field up to one-loop order. This is done for three background field configurations: the pseudo-abelian field, a non-abelian field, which does not depend on space-time and is called the PNA field, and the instanton background field. The first two were chosen in order to gain experience with the behaviour of the method when it is used on fields of very different structure. The instanton was chosen because it is physically interesting (see [29–31]; for a compilation of important publications [32]), and because there exists an analytical result [33]. This gives us the luxury to compare an outcome of the worldline numerical computation with analytically correct results.

Additionally to matter determinants in a given background field, we calculate the one-loop effective potential for an SU(2) gauge field at finite temperature in order to derive an upper bound for the Polyakov loop expectation value, that can serve as an order parameter for confinement [34, 35]. The Polyakov loop expectation value being zero signals confinement; it being unequal to zero signals deconfinement. Here there are no matter fluctuations to take into account but the fluctuations of the gauge field, which makes it necessary to evaluate a gluon as well as a ghost determinant. For a constant field there exists an analytical solution to the problem [36], and going from there we consider the field $a(x) = a + \delta_a \cos(kx_1)\cos(kx_2)$, which is a constant field a that is perturbed in two space-time directions.

1.1 Outline

In chapter 2 the key quantities and concepts of the thesis are introduced. The worldline representation of the one-loop effective action is derived and then worked on in order to simplify its numerical implementation. To introduce the notations used, a short summary of the most important properties of an SU(2) gauge theory is given. Furthermore, the renormalisation of the one-loop effective action is explained.

In chapter 3 we focus on the numerical aspects of the computation of the one-loop effective action. First the Monte Carlo evaluation of the one-loop effective action is explained. Then a method to implement the renormalisation and a method to test the quality of the numerical results using the inverse mass expansion are described. A summary of the numerical method is also given.

In chapter 4 the application of the worldline numerical method to two simple background fields, the pseudo-abelian background field and a constant field, which we call the PNA field, is presented. In order to learn how well worldline numerics can reproduce the gauge invariance of the Wilson loop expectation value, we calculate the Wilson loop expectation value for the pseudo-abelian background field in two gauges. Both results are then compared to the inverse mass expansion. For the PNA field, we compute the Wilson loop expectation value and compare it to the inverse mass expansion. Then the renormalised effective Lagrangian density of the PNA field is computed.

In chapter 5 we investigate how useful worldline numerics is to calculate the one-loop effective action of an instanton background field. First the necessary instanton related quantities are introduced and an approximation to the one-loop effective action, which is called the derivative expansion, is explained. The Wilson loop expectation value is computed in two gauges, the regular gauge and the singular gauge. We find that the worldline numerical results for the Wilson loop expectation value are not gauge invariant. The problem is pinned down to not sufficiently precisely computed worldline correlation functions. We then propose a method to improve how well worldline numerics reproduces the Lorentz structure of worldline correlation functions by rotating the loop cloud. Afterwards, it is explained that also with a rotated loop cloud today's computers do not allow for the computation of the Wilson loop expectation value to a precision that would make a sensible calculation of the one-loop effective action for the regular instanton possible.

In chapter 6 we compute of the one-loop effective potential of the zero-component of an SU(2) gauge field in thermal equilibrium. The first two sections are devoted to the explanation of how one can investigate a QFT at finite temperature and how we have to amend the worldline numerical method in order to do so. Then the relation between the Polyakov loop expectation value, confinement and the expectation value of the zero-component of the gauge field is explained. We prepare the one-loop effective potential of the zero-component of the gauge field for the numerical implementation which is undertaken afterwards.

In the last chapter a summary of the results that are obtained in this thesis is given and possibilities for future work are outlined.

2 The effective action and the worldline

In this chapter the key quantities and concepts of the thesis are introduced. The worldline representation of the one-loop effective action is derived and then worked on in order to simplify its numerical implementation. To introduce the notations used, a short summary of the most important properties of an SU(2) gauge theory is given. Furthermore, the renormalisation of the one-loop effective action is explained.

2.1 The effective action

One of the main tasks in quantum field theory is to calculate correlation or Green's functions as they contain the complete physical information about a QFT. They are the vacuum expectation values of the time-ordered products of field operators, i.e.

$$G^{(n)}(x_1, x_2, ..., x_n) = \langle 0|T(\phi(x_1)\phi(x_2)...\phi(x_n))|0\rangle \ . \tag{2.1}$$

Connected Green's functions can always be composed using free two point Green's functions and the sum of all one particle irreducible (1PI) Green's functions, which are Green's functions whose Feynman graph cannot be cut into two pieces by cutting only one internal line. The hard part is to calculate the sum of all one particle irreducible Green's functions $\Gamma^{(n)}(x_1, x_2, ..., x_n)$. This can be done differentiating the effective action Γ. The effective action can in a Legendre transformation like manner be obtained from the generating functional for connected Green's functions W, which is given by

$$W = -i \ln Z[J] \ , \tag{2.2}$$

where

$$Z[J] = \int \mathcal{D}\phi \, e^{\, iS + i\int \mathrm{d}x \, J^\dagger \phi + i\int \mathrm{d}x \, J\phi^\dagger} \tag{2.3}$$

is the generating functional. S is the action of the system, J and ϕ denote vectors, whose properties depend on the theory under consideration. J is called the source term or the current. If we now introduce a new variable $\phi_\mathrm{c}(x) = \frac{\delta W}{\delta J(x)}$, we can define the effective action

$$\Gamma[\phi_\mathrm{c}] := W - \int \mathrm{d}x \, J^\dagger \phi_\mathrm{c} \ - \int \mathrm{d}x \, J\phi_\mathrm{c}^\dagger \ . \tag{2.4}$$

After spending some time differentiating one will find that

$$\Gamma^{(n)}(x_1, x_2, ..., x_n) = \frac{\delta^n \Gamma}{\delta\phi_\mathrm{c}(x_1) \ldots \delta\phi_\mathrm{c}(x_n)} \ . \tag{2.5}$$

Throughout this thesis we work in an Euclidean setting. This means that the time axis is rotated clockwise in the complex plane by ninety degrees. One calls this a Wick rotation. Then the action

$$S = \int \mathrm{d}^4x\, \mathcal{L} = \int_{-\infty}^{\infty} \mathrm{d}x_0 \int \mathrm{d}^3x\, \mathcal{L} \tag{2.6}$$

becomes

$$\int_{i\infty}^{-i\infty} \mathrm{d}x_0 \int \mathrm{d}^3x\, \mathcal{L} = -i \int_{-\infty}^{\infty} \mathrm{d}\tilde{x}_0 \int \mathrm{d}^3x\, \mathcal{L}(i\tilde{x}_0) = i \int \mathrm{d}^4x_\mathrm{E}\, \mathcal{L}_\mathrm{E} =: iS_\mathrm{E}\ . \tag{2.7}$$

For the other quantities defined so far, we find the correspondences

$$\begin{array}{lcl} Z & \Longrightarrow & Z_\mathrm{E} = \int \mathcal{D}\phi\, e^{-S_\mathrm{E} + \int \mathrm{d}x\, J^\dagger\phi + \int \mathrm{d}x\, J\phi^\dagger} \\ W & \Longrightarrow & W_\mathrm{E} = \ln Z_\mathrm{E} \\ \Gamma & \Longrightarrow & \Gamma_\mathrm{E} = -W_\mathrm{E} + \int \mathrm{d}x\, J^\dagger\phi_\mathrm{c} + \int \mathrm{d}x\, J\phi_\mathrm{c}^\dagger\ . \end{array} \tag{2.8}$$

Working in an Euclidean space makes life much easier. The path integral in Z does not have to be taken over a vigorously oscillating expression but a nice exponential function of a real action.

Since we will only deal with Euclidean quantities, the subscript E will be omitted from now on.

2.2 The one-loop effective action

To derive the one-loop effective action, we will now employ the steepest-descent-method, which means that we are going to expand the exponential in the path integral that was used to define Z about a stationary point, where $-S + \int \mathrm{d}x\, J^\dagger\phi + \int \mathrm{d}x\, J\phi^\dagger$ has an extremum, because one hopes the region close to this point to dominate the whole integration. This point will be called ϕ_0 and it meets the requirements

$$\frac{\delta}{\delta\phi_i}[-S + \int \mathrm{d}x\, J^\dagger\phi + \int \mathrm{d}x\, J\phi^\dagger]\,\big|_{\phi=\phi_0} = 0 \tag{2.9}$$

$$\frac{\delta}{\delta\phi_i^*}[-S + \int \mathrm{d}x\, J^\dagger\phi + \int \mathrm{d}x\, J\phi^\dagger]\,\big|_{\phi=\phi_0} = 0\ . \tag{2.10}$$

Neglecting every contribution of order higher than one, we now expand the exponent about ϕ_0. Had one not set $\hbar = 1$, we would see that $\hbar$ is the small parameter of the expansion. We find that

$$\begin{aligned} Z &\approx \int \mathcal{D}\phi\, e^{-S[\phi_0,\phi_0^\dagger] + \int \mathrm{d}x\, J^\dagger\phi_0 + \int \mathrm{d}x\, J\phi_0^\dagger - \frac{1}{2}\phi_i^* \frac{\delta^2 S}{\delta\phi_i^*\delta\phi_j}\phi_j} \\ &= e^{-S[\phi_0,\phi_0^\dagger] + \int \mathrm{d}x\, J^\dagger\phi_0 + \int \mathrm{d}x\, J\phi_0^\dagger} \int \mathcal{D}\phi\, e^{-\frac{1}{2}\phi_i^* \frac{\delta^2 S}{\delta\phi_i^*\delta\phi_j}\phi_j}\ . \end{aligned} \tag{2.11}$$

Because of the extremality conditions (2.9) and (2.10) all the linear terms have dropped out. For W and Γ we find that

$$W \approx -S[\phi_0, \phi_0^\dagger] + \int \mathrm{d}x\, J^\dagger \phi_0 + \int \mathrm{d}x\, J\phi_0^\dagger + \ln \int \mathcal{D}\phi\, e^{-\frac{1}{2}\phi_i^* \frac{\delta^2 S}{\delta\phi_i^* \delta\phi_j}\phi_j} \tag{2.12}$$

and

$$\begin{aligned}\Gamma \approx S[\phi_0, \phi_0^\dagger] - \ln \int \mathcal{D}\phi\, e^{-\frac{1}{2}\phi_i^* \frac{\delta^2 S}{\delta\phi_i^* \delta\phi_j}\phi_j} - \int \mathrm{d}x\, J^\dagger \phi_0 - \int \mathrm{d}x\, J\phi_0^\dagger \\ + \int \mathrm{d}x\, J^\dagger \phi_\mathrm{c} + \int \mathrm{d}x\, J\phi_\mathrm{c}^\dagger\,.\end{aligned} \tag{2.13}$$

For ϕ_c this means that

$$\phi_\mathrm{c} = \phi_\mathrm{c}(x) = \frac{\delta W}{\delta J(x)} \approx \phi_0\,, \tag{2.14}$$

and finally we get

$$\Gamma \approx S[\phi_0, \phi_0^\dagger] - \ln \int \mathcal{D}\phi\, e^{-\frac{1}{2}\phi_i^* \frac{\delta^2 S}{\delta\phi_i^* \delta\phi_j}\phi_j}\,. \tag{2.15}$$

The one-loop correction to the classical action is therefore given by

$$\Gamma^{(1)} = -\ln \int \mathcal{D}\phi\, e^{-\frac{1}{2}\phi_i^* \frac{\delta^2 S}{\delta\phi_i^* \delta\phi_j}\phi_j}\,. \tag{2.16}$$

It is the contribution to the effective action that is generated by all one-loop diagrams and is called the one-loop effective action. For a free theory the effective action Γ is equal to the classical action S. The one-loop effective action therefore has to be zero. In a free theory there just are no loops that could contribute to the effective action.

2.3 A little on SU(2) gauge theories

In this thesis we deal with an SU(2) gauge theory. It is therefore worthwhile to review some of the most important properties of this theory. This will serve us to introduce the necessary notations and conventions.

Let us suppose we have a free complex scalar field of isospin one half, i.e. a free two-component complex scalar field $\phi = (\phi_1, \phi_2)$, with which we want to deal in a quantum field theoretical way. We would choose the Lagrangian density to have the form

$$\mathcal{L} = \phi^\dagger(-\partial_\mu\partial_\mu + m^2)\phi\,. \tag{2.17}$$

The Lagrangian density and therefore everything observable is invariant under a global unitary transformation $\mathbf{U}$ of the fields as

$$\mathcal{L}(\phi') = \phi'^\dagger(\partial_\mu\partial_\mu + m^2)\phi' = \phi^\dagger \mathbf{U}^\dagger(\partial_\mu\partial_\mu + m^2)\mathbf{U}\phi = \phi^\dagger(\partial_\mu\partial_\mu + m^2)\mathbf{U}^\dagger\mathbf{U}\phi = \mathcal{L}(\phi)\,, \tag{2.18}$$

where, as in the rest of the section, gauge transformed quantities are indicated by a dash, and we used that $\mathbf{U}$ is unitary and therefore $\mathbf{U}^\dagger = \mathbf{U}^{-1}$. Throughout this thesis bold symbols are used for matrix-valued quantities.

We will work with SU(2) transformations. This means that in the fundamental representation all the $\mathbf{U}$s can be written as an exponential of elements of the Lie algebra of the Hermitian matrices of two dimensions:

$$\mathbf{U} = \exp[-i\Theta^a \mathbf{T}^a] \,, \tag{2.19}$$

or with $\mathbf{U}$ depending on x:

$$\mathbf{U}(x) = \exp[-i\Theta^a(x) \mathbf{T}^a] \,, \tag{2.20}$$

where $a = 1, 2, 3$, Θ^a are real numbers and the $\mathbf{T}^a$ are the basis of the real vector space of the Hermitian 2×2 matrices. We choose

$$\mathbf{T}^a = \frac{\boldsymbol{\sigma}^a}{2} \,, \tag{2.21}$$

where the $\boldsymbol{\sigma}^a$ are the Pauli matrices, which has the consequences that

$$\mathrm{tr}[\mathbf{T}^a \mathbf{T}^b] = \frac{1}{2}\delta^{ab} \;,\; [\mathbf{T}^a, \mathbf{T}^b] = i\,\epsilon^{abc}\mathbf{T}^c \tag{2.22}$$

and

$$\mathbf{T}^a \mathbf{T}^b = \frac{1}{4}\big[\delta^{ab}\mathbf{1} + i\,\epsilon^{abc}\boldsymbol{\sigma}^c\big] \,. \tag{2.23}$$

We will also use another representation of SU(2): the adjoint representation. In this representation the generators of the group $\mathbf{T}^a$ are given by the structure constants of the algebra in the following way:

$$T^a{}_{jk} = i\,\epsilon^{akj} \,. \tag{2.24}$$

We now require the gauge transformations to be locally possible as well, i.e.

$$S[\phi] = S[\mathbf{U}(x)\phi] \,. \tag{2.25}$$

In order to make equation (2.25) correct, we have to amend the Lagrangian density. It is the derivatives which cause the problem, but we can solve it by introducing the gauge field $\mathbf{A}_\mu$ so that

$$S = \int \mathrm{d}^4x\, \phi^\dagger(-\mathbf{D}_\mu\mathbf{D}_\mu + m^2)\phi \;=\; \int \mathrm{d}^4x\, \phi^\dagger(-(\partial_\mu + \mathbf{A}_\mu)(\partial_\mu + \mathbf{A}_\mu) + m^2)\phi \,. \tag{2.26}$$

The $\mathbf{D}_\mu$ are called covariant derivatives. Of course $\mathbf{A}_\mu$ has to transform in a special way to make the action locally gauge invariant. We want

$$\begin{aligned} \phi'^\dagger(\partial_\mu + \mathbf{A}'_\mu)(\partial_\mu + \mathbf{A}'_\mu)\phi' &= \phi^\dagger\,\mathbf{U}^\dagger(\partial_\mu + \mathbf{A}'_\mu)\mathbf{U}\;\mathbf{U}^\dagger(\partial_\mu + \mathbf{A}'_\mu)\mathbf{U}\,\phi \\ &= \phi^\dagger\,(\partial_\mu + \mathbf{A}_\mu)\;(\partial_\mu + \mathbf{A}_\mu)\,\phi \end{aligned} \tag{2.27}$$

to hold. It follows that

$$\mathbf{U}^\dagger(\partial_\mu + \mathbf{A}'_\mu)\mathbf{U}\,\phi = \mathbf{U}^{-1}(\partial_\mu + \mathbf{A}'_\mu)\mathbf{U}\,\phi = (\partial_\mu + \mathbf{A}_\mu)\,\phi \tag{2.28}$$

and therefore that

$$\mathbf{A}'_\mu = \mathbf{U}\mathbf{A}_\mu\mathbf{U}^{-1} - [\partial_\mu\mathbf{U}]\mathbf{U}^{-1}\ . \tag{2.29}$$

Equation (2.29) tells us how $\mathbf{A}_\mu$ behaves under a gauge transformation. In analogy to the U(1) case, the electro-magnetic field, we assume that the gauge field can be written as $\mathbf{A}_\mu = -igA^a_\mu\mathbf{T}^a$, where we call the A^a_μ the components of the field. The strength of the gauge field interaction is governed by the coupling constant g.

There is another very useful quantity: the field-strength-tensor

$$\mathbf{G}_{\mu\nu} = \partial_\mu\mathbf{A}_\nu - \partial_\nu\mathbf{A}_\mu + [\mathbf{A}_\mu, \mathbf{A}_\nu]\ . \tag{2.30}$$

Just as the field, $\mathbf{G}_{\mu\nu}$ can be written as a linear combination of the $\mathbf{T}^a$:

$$\mathbf{G}_{\mu\nu} = -igG^a_{\mu\nu}\mathbf{T}^a\ . \tag{2.31}$$

Plugging in the definition of the gauge field, one finds that

$$\begin{aligned}\mathbf{G}_{\mu\nu} =& -ig\partial_\mu A^a_\nu\mathbf{T}^a + ig\partial_\nu A^a_\mu\mathbf{T}^a - g^2[A^a_\mu\mathbf{T}^a, A^a_\nu\mathbf{T}^a]\\ =& -ig\left[\partial_\mu A^a_\nu - \partial_\nu A^a_\mu + g\epsilon^{abc}A^b_\mu A^c_\nu\right]\mathbf{T}^a\ ,\end{aligned} \tag{2.32}$$

where in the last line the second equation in (2.22) was used. The components of the field strength tensor are therefore given by

$$G^a_{\mu\nu} = \partial_\mu A^a_\nu - \partial_\nu A^a_\mu + g\epsilon^{abc}A^b_\mu A^c_\nu\ . \tag{2.33}$$

Under gauge transformations it behaves according to

$$\begin{aligned}\mathbf{G}'_{\mu\nu} &= \partial_\mu\mathbf{A}'_\nu - \partial_\nu\mathbf{A}'_\mu + [\mathbf{A}'_\mu, \mathbf{A}'_\nu]\\ &= \mathbf{U}\mathbf{G}_{\mu\nu}\mathbf{U}^{-1}\ .\end{aligned} \tag{2.34}$$

With equation (2.34), it is easy to show that $\mathrm{tr}[\mathbf{G}_{\mu\nu}\mathbf{G}_{\mu\nu}]$ is gauge invariant as

$$\mathrm{tr}[\mathbf{G}'_{\mu\nu}\mathbf{G}'_{\mu\nu}] = \mathrm{tr}[\mathbf{U}\mathbf{G}_{\mu\nu}\mathbf{U}^{-1}\mathbf{U}\mathbf{G}_{\mu\nu}\mathbf{U}^{-1}] = \mathrm{tr}[\mathbf{G}_{\mu\nu}\mathbf{G}_{\mu\nu}]\ . \tag{2.35}$$

In terms of the components $G^a_{\mu\nu}$ we can write

$$\begin{aligned}\mathrm{tr}[\mathbf{G}_{\mu\nu}\mathbf{G}_{\mu\nu}] &= g^2\mathrm{tr}[iG^a_{\mu\nu}\mathbf{T}^a iG^b_{\mu\nu}\mathbf{T}^b]\\ &= -g^2\mathrm{tr}[G^a_{\mu\nu}G^b_{\mu\nu}\mathbf{T}^a\mathbf{T}^b]\\ &= -\frac{g^2}{4}G^a_{\mu\nu}G^b_{\mu\nu}\mathrm{tr}[\delta^{ab}\mathbf{1} + i\epsilon^{abc}\boldsymbol{\sigma}^c]\\ &= -\frac{g^2}{2}(G^a_{\mu\nu})^2\ ,\end{aligned} \tag{2.36}$$

where we used (2.23) and the vanishing trace of the Pauli matrices. We therefore have found another possible building block for a locally gauge invariant action, which could, for example, look like

$$\begin{aligned} S_{\mathrm{YM}} &= \int \mathrm{d}^4x \left[\frac{1}{2g^2}\mathrm{tr}[\mathbf{G}_{\mu\nu}\mathbf{G}_{\mu\nu}] + \phi^\dagger(-\mathbf{D}^2 + m^2)\phi\right] \\ &= \int \mathrm{d}^4x \left[-\frac{1}{4}(G^a_{\mu\nu})^2 + \phi^\dagger(-\mathbf{D}^2 + m^2)\phi\right] . \end{aligned} \tag{2.37}$$

It is also customary to work with rescaled components of the gauge potential and the field strength tensor so that

$$A^a_\mu \to \tfrac{1}{g}A^a_\mu \quad \text{and} \quad G^a_{\mu\nu} \to \tfrac{1}{g}G^a_{\mu\nu} . \tag{2.38}$$

We will do so when investigating the instanton and the Polyakov loop expectation value.

2.4 Deriving a worldline expression

Using the content of the last section, we can now proceed to investigate the one-loop effective action. This time in the special case of an SU(2) theory. Equation (2.16) tells us that

$$\exp[-\Gamma^{(1)}] = \mathcal{N}\int \mathcal{D}\phi\, e^{-\frac{1}{2}\phi^*_i \frac{\delta^2 S}{\delta\phi^*_i \delta\phi_j}\phi_j} , \tag{2.39}$$

where $\mathcal{N}$ serves to normalise $\Gamma^{(1)}$ such that

$$\Gamma^{(1)}[\mathbf{A} = 0] = 0 , \tag{2.40}$$

which must hold because for a free theory (in our case a theory without a background field) the effective action is equal to the classical action and any correction of S must therefore vanish. Inserting the action S_{YM}, which is given in (2.37), yields

$$\exp[-\Gamma^{(1)}] = \mathcal{N}\int \mathcal{D}\phi\, e^{-\frac{1}{2}\int \mathrm{d}^4x\, \phi^\dagger(\mathbf{D}^2+m^2)\phi} . \tag{2.41}$$

Because

$$\mathcal{N}\int \mathcal{D}\phi\, e^{-\frac{1}{2}\int \mathrm{d}^4x\, \phi^\dagger(\mathbf{D}^2+m^2)\phi} = \mathcal{N}'\det(-\mathbf{D}^2 + m^2)^{-1} , \tag{2.42}$$

we can write

$$\exp[-\Gamma^{(1)}] = \mathcal{N}'\det(-\mathbf{D}^2 + m^2)^{-1} . \tag{2.43}$$

The exponent of $\det(-\mathbf{D}^2 + m^2)$ is not $-1/2$ because ϕ is a complex field. This requires us to integrate over all the ϕ_i and ϕ^*_i. The equations (2.40) and (2.43) give

$$\begin{aligned} \Gamma^{(1)} &= -\ln\mathcal{N}' + \ln\det(-\mathbf{D}^2 + m^2) \\ &= \ln\frac{\det(-\mathbf{D}^2 + m^2)}{\det(-\partial^2 + m^2)} . \end{aligned} \tag{2.44}$$

Using the $\ln\det = \mathrm{Tr}\ln$ rule, this takes the form

$$\Gamma^{(1)} = \mathrm{Tr}\ln(-\mathbf{D}^2 + m^2) - \mathrm{Tr}\ln(-\partial^2 + m^2)\ , \tag{2.45}$$

or in proper time representation (which is explained in section A.1)

$$\Gamma^{(1)} = -\mathrm{tr}\int_0^\infty \frac{\mathrm{d}T}{T}\,\mathrm{Tr}(e^{-(-\mathbf{D}^2+m^2)T} - e^{-(-\partial^2+m^2)T})\ . \tag{2.46}$$

We divided the trace into two traces; the colour trace tr, which takes care of the fact that the Lagrangian density is a 2×2 matrix, and Tr, which is the trace of the differential operator. The integration variable T is called the proper time. Traces can be calculated in any coordinate frame since they are invariant under a coordinate change. As the basis, we choose the eigenvectors of the space operator, which are well known from quantum mechanics. We get that

$$\Gamma^{(1)} = -\mathrm{tr}\int_0^\infty \frac{\mathrm{d}T}{T}\int \mathrm{d}^D x\left[\langle x|e^{-(-\mathbf{D}^2+m^2)T}|x\rangle - \langle x|e^{-(-\partial^2+m^2)T}|x\rangle\right], \tag{2.47}$$

where D is the number of space-time dimensions of the system that is scrutinised. The matrix element $\langle x|(e^{-(-\mathbf{D}^2+m^2)T}|x\rangle$ is very similar to a transition amplitude in ordinary quantum mechanics and one can find a path integral expression for the matrix element in very much the same way one does it in a quantum mechanics course to introduce the Feynman path integral. As one can retrace in section A.2, the result is:

$$\Gamma^{(1)} = -\mathrm{tr}\int_0^\infty \frac{\mathrm{d}T}{T}e^{-m^2T}\int \mathrm{d}^D x\left[\int_{x(0)=x}^{x(T)=x}\mathcal{D}x\left[\mathrm{P}e^{-\int_0^T \mathrm{d}\tau[\frac{\dot{x}^2}{4}+\dot{x}_\mu \mathbf{A}_\mu]} - e^{-\int_0^T \mathrm{d}\tau[\frac{\dot{x}^2}{4}]}\right]\right]. \tag{2.48}$$

The P denotes path ordering. It is necessary because in general the gauge fields $\mathbf{A}(x)$ do not commute and $e^{\mathbf{A}(x_1)}e^{\mathbf{A}(x_2)} \neq e^{\mathbf{A}(x_1)+\mathbf{A}(x_2)}$. It is defined by

$$\mathrm{P}e^{\mathbf{A}(t_1)+\mathbf{A}(t_2)+\cdots+\mathbf{A}(t_n)} := e^{\mathbf{A}(t_1)}e^{\mathbf{A}(t_2)}\ldots e^{\mathbf{A}(t_n)}\ ,$$
$$\text{with } t_1 > \cdots > t_n\ . \tag{2.49}$$

2.5 Making the one-loop effective action suit numerical evaluation

What we have found for the one-loop effective action is already quite nice, but it can be made much nicer (for a numerical analysis) with only a few manipulations. First we realise that

$$\int_{x(0)=x}^{x(T)=x}\mathcal{D}x\, e^{-\int_0^T \mathrm{d}\tau\left[\frac{\dot{x}^2}{4}\right]} = \langle x|T\partial^2|x\rangle = \frac{1}{(4\pi T)^{\frac{D}{2}}}\ . \tag{2.50}$$

After factoring out $\int_{x(0)=x}^{(T)=x} \mathcal{D}x\, e^{-\int_0^T \mathrm{d}\tau \left[\frac{\dot{x}^2}{4}\right]}$ and using (2.50), equation (2.48) becomes

$$\Gamma^{(1)} = -\frac{1}{(4\pi)^{\frac{D}{2}}}\mathrm{tr}\int_0^\infty \frac{\mathrm{d}T}{T^{1+\frac{D}{2}}} e^{-m^2T}\int \mathrm{d}^D x \left[\mathcal{N}\int_{x(0)=x}^{x(T)=x}\mathcal{D}x\big[\mathrm{P}e^{-\int_0^T \mathrm{d}\tau[\frac{\dot{x}^2}{4}+\dot{x}_\mu \mathbf{A}_\mu]}\big] - \mathbf{1}\right], \tag{2.51}$$

where

$$\mathcal{N} = \left[\int_{x(0)=x}^{x(T)=x}\mathcal{D}x\, e^{-\int_0^T \mathrm{d}\tau[\frac{\dot{x}^2}{4}]}\right]^{-1}, \tag{2.52}$$

and $\mathbf{1}$ is the 2×2 unit matrix. Now we rearrange the integration itself. Because

$$\int \mathrm{d}^D x \int_{x(0)=x}^{x(T)=x}\mathcal{D}x = \int_{x(0)=x(T)}\mathcal{D}x = \int \mathrm{d}^D x_{\mathrm{cm}} \int_{\tilde{x}(0)=\tilde{x}(T)}\mathcal{D}\tilde{x}\,, \tag{2.53}$$

where

$$\int_0^T \mathrm{d}\tau\, \tilde{x}(\tau) = 0\,, \tag{2.54}$$

we find for the one-loop effective action:

$$\Gamma^{(1)} = -\frac{1}{(4\pi)^{\frac{D}{2}}}\mathrm{tr}\int_0^\infty \frac{\mathrm{d}T}{T^{1+\frac{D}{2}}} e^{-m^2T}\int \mathrm{d}^D x_{\mathrm{cm}} \left[\mathcal{N}\int \mathcal{D}\tilde{x}\big[\mathrm{P}e^{-\int_0^T \mathrm{d}\tau[\frac{\dot{\tilde{x}}^2}{4}+\dot{\tilde{x}}_\mu \mathbf{A}_\mu(x_{\mathrm{cm}}+\tilde{x})]}\big] - \mathbf{1}\right]. \tag{2.55}$$

The path integral has to be taken over closed loops with "centre of mass" zero. Instead of integrating over the common starting (and end) points of the loops, over which the path integral is taken, we now integrate over the common "centre of mass" of the loops.

To derive the promised nice expression, we only have to scale the parametrisation of the loops so that the integral in the exponent runs from zero to one by changing the integration variable from τ to $t = \frac{\tau}{T}$ and to introduce unit loops $y(t) = \frac{1}{\sqrt{T}}x(Tt)$. The new integration variable t is called the proper time parameter. We find that

$$\begin{aligned}\int_0^T \mathrm{d}\tau \frac{\dot{x}^2}{4} &= \int_0^T \mathrm{d}\tau \frac{1}{4}\Big(\sqrt{T}\frac{\mathrm{d}}{\mathrm{d}\tau}y\Big(\frac{\tau}{T}\Big)\Big)^2 = \int_0^T \mathrm{d}\tau \frac{1}{4}\Big(\sqrt{T}\frac{\mathrm{d}}{\mathrm{d}\tau}y\Big(\frac{\tau}{T}\Big)\Big)^2 \\ &= \int_0^1 \mathrm{d}t\, \frac{\dot{y}^2}{4}\end{aligned} \tag{2.56}$$

and

$$\begin{aligned}\int_0^T \mathrm{d}\tau \dot{x}_\mu \mathbf{A}_\mu(x_{\mathrm{cm}}+x) &= \int_0^T \mathrm{d}\tau\Big(\sqrt{T}\frac{\mathrm{d}}{\mathrm{d}\tau}y\Big(\frac{\tau}{T}\Big)\Big)\mathbf{A}_\mu\Big(x_{\mathrm{cm}}+\sqrt{T}y\Big(\frac{\tau}{T}\Big)\Big) \\ &= \sqrt{T}\int_0^1 \mathrm{d}t\, \dot{y}_\mu\, \mathbf{A}_\mu(x_{\mathrm{cm}}+\sqrt{T}\,y(t))\,,\end{aligned} \tag{2.57}$$

where the dot denotes differentiation with respect to the integration variable.

Thanks to the use of unit loops, the weight $\exp\left[\int_0^1 \mathrm{d}t\, \dot{y}^2/4\right]$, with which the loops contribute to the path integral, is now T independent. This makes a sensible (time efficient) numerical treatment of the one-loop effective action possible.

Introducing the Wilson loop $W := \operatorname{tr} \mathrm{P} \exp\left[-\oint \mathrm{d}x_\mu\, \mathbf{A}_\mu(x)\right]$ and its gauge invariant expectation value

$$\langle W \rangle = \left[\frac{\int_{y(0)=y(1)} \mathcal{D}y\, e^{-\int_0^1 \mathrm{d}t\, \frac{\dot{y}^2}{4}}\, W}{\int_{y(0)=y(1)} \mathcal{D}y\, e^{-\int_0^1 \mathrm{d}t\, \frac{\dot{y}^2}{4}}} \right] , \tag{2.58}$$

we can write down a neat expression for the one-loop effective action:

$$\Gamma^{(1)} = -\frac{1}{(4\pi)^{\frac{D}{2}}} \int_0^\infty \frac{\mathrm{d}T}{T^{1+\frac{D}{2}}} e^{-m^2 T} \int \mathrm{d}^D x_{\mathrm{cm}} \left[\langle W \rangle - 2\right] . \tag{2.59}$$

Equation (2.59) is the starting point of the numerical analysis.

2.6 The proper time T seen as a "zooming" parameter

Writing out all the dependencies, we find the Wilson loop expectation value to be

$$\langle W \rangle = \frac{\int \mathcal{D}y\, e^{-\int_0^1 \mathrm{d}t\, \frac{\dot{y}^2}{4}}\ \operatorname{tr} P e^{-\sqrt{T}\int_0^1 \mathrm{d}t\, \dot{y}_\mu\, \mathbf{A}_\mu\left(x_{\mathrm{cm}}+\sqrt{T}\, y(t)\right)}}{\int \mathcal{D}y\, e^{-\int_0^1 \mathrm{d}t\, \frac{\dot{y}^2}{4}}} , \tag{2.60}$$

where the path integral is taken over all closed loops of a common "centre of mass" x_{cm}. The Wilson loop expectation value depends on x_{cm} and the proper time T. Every loop contributes to the path integral according to its weight $\exp\left[-\int_0^1 \mathrm{d}t\, \dot{y}^2/4\right]$. Loops who stay close to the origin dominate the path integration. One can therefore think of the loops that affect the result of the integration as a cloud surrounding x_{cm}. The gauge field $\mathbf{A}_\mu$ is evaluated at $x_{\mathrm{cm}} + \sqrt{T}\, y(t)$. How far away from x_{cm} a loop of given weight collects information about the gauge field is therefore governed by T. A small T means that the main contribution to $\langle W \rangle$ comes from $\mathbf{A}_\mu$ evaluated close to x_{cm}, while for very big T also the remote behaviour of the gauge field is of importance. Thinking of the loops as a cloud, this means that the cloud swells as one makes T bigger. One could call T a "zooming" parameter which controls how far away from x_{cm} the gauge field contributes to the Wilson loop expectation value.

2.7 Renormalisation

The T-integration in equation (2.59) deserves some more consideration. Making use of the inverse mass or heat-kernel expansion (see e.g. [8–11]), we can write the

one-loop effective action as

$$\begin{aligned}\Gamma^{(1)} =& -\frac{1}{(4\pi)^{\frac{D}{2}}}\int \mathrm{d}^D x_{\mathrm{cm}} \int_0^\infty \frac{\mathrm{d}T}{T^{1+\frac{D}{2}}} e^{-m^2T}[\frac{T^2}{12}\mathrm{tr}[(\mathbf{G}_{\mu\nu})^2] + O(T^4)] \\ =& -\frac{1}{(4\pi)^{\frac{D}{2}}}\int \mathrm{d}^D x_{\mathrm{cm}} \int_0^\infty \frac{\mathrm{d}T}{T^{\frac{D}{2}-1}} e^{-m^2T}[\frac{1}{12}\mathrm{tr}[(\mathbf{G}_{\mu\nu})^2] + O(T^2)] \,. \end{aligned} \tag{2.61}$$

In the small T limit the integrand in (2.61) is proportional to $T^{1-\frac{D}{2}}$. For $D \geq 4$ the integral therefore diverges; the one-loop effective action is infinite. As we saw, T is a "zooming" parameter. For small T we look at small distances and large momentum scales. The integrand is therefore UV-divergent. In order to deal with this UV-divergence, we have to regularise and renormalise $\Gamma^{(1)}$. Because all our calculations are done in 4 space-time dimensions, we will set $D = 4$.

The regularisation is done by imposing a cutoff on our integration, i.e. by choosing a lower boundary of our integration interval that is nonzero to make the one-loop effective action finite. We take it to be $1/\Lambda^2$. The regularised one-loop effective action in four dimensions reads

$$\Gamma^{(1)}_{\mathrm{reg}} = -\frac{1}{(4\pi)^2}\int \mathrm{d}^4 x_{\mathrm{cm}} \int_{\frac{1}{\Lambda^2}}^\infty \frac{\mathrm{d}T}{T^3} e^{-m^2T}\left[\langle W\rangle - 2\right] . \tag{2.62}$$

For the divergent term, which we will call $\Delta\Gamma^{(1)}_\Lambda$, we find with the aid of the exponential integral, which is given in equation (A.3), that

$$\begin{aligned}\Delta\Gamma^{(1)}_\Lambda =& -\frac{1}{12(4\pi)^2}\int \mathrm{d}^4 x_{\mathrm{cm}} \int_{\frac{1}{\Lambda^2}}^\infty \frac{\mathrm{d}T}{T} e^{-m^2T}\mathrm{tr}[(\mathbf{G}_{\mu\nu})^2] \\ =& \frac{1}{12(4\pi)^2}\left(\mathrm{C_E} + \ln\left(\frac{m^2}{\Lambda^2}\right) + O\left(\frac{m^2}{\Lambda^2}\right)\right)\int \mathrm{d}^4 x_{\mathrm{cm}}\mathrm{tr}[(\mathbf{G}_{\mu\nu})^2] \\ =& -\frac{g^2}{392\pi^2}\left(\mathrm{C_E} + \ln\left(\frac{m^2}{\Lambda^2}\right) + O\left(\frac{m^2}{\Lambda^2}\right)\right)\int \mathrm{d}^4 x_{\mathrm{cm}}(G^a_{\mu\nu})^2 \,. \end{aligned} \tag{2.63}$$

This means that adding a term of the kind

$$\Delta\tilde{\Gamma}^{(1)}_\Lambda = \frac{g^2}{392\pi^2}\left(\mathrm{C_E} + \ln\left(\frac{\mu^2}{\Lambda^2}\right)\right)\int \mathrm{d}^4 x_{\mathrm{cm}}(G^a_{\mu\nu})^2 \tag{2.64}$$

to $\Gamma^{(1)}_{\mathrm{reg}}$ yields a result that does not diverge as Λ goes to infinity. We name this result $\Gamma^{(1)}_\Lambda$. The μ that appears in (2.64) parametrises different renormalisation schemes, and one has the freedom to identify it with the renormalisation point. The renormalisation is then done by adding and subtracting $\Delta\tilde{\Gamma}^{(1)}$ to the classical action and letting Λ go to infinity. After addition and subtraction of $\Delta\tilde{\Gamma}^{(1)}$, the Λ

dependent effective action, up to one loop order, reads

$$\begin{aligned}\Gamma_\Lambda &= \int \mathrm{d}^4x \left[-\frac{1}{4}(G^a_{\mu\nu})^2 + \phi^\dagger(-\mathbf{D}^2+m^2)\phi - \Delta\tilde{\Gamma}^{(1)}_\Lambda + \Delta\tilde{\Gamma}^{(1)}_\Lambda + \Gamma^{(1)}_{\mathrm{reg}}\right] \\ &= \int \mathrm{d}^4x \left[-\frac{1}{4}\left(1+\frac{g^2}{98\pi^2}\left(\mathrm{C_E}+\ln\left(\frac{\mu^2}{\Lambda^2}\right)\right)\right)(G^a_{\mu\nu})^2 \right. \\ &\qquad \left. +\phi^\dagger(-\mathbf{D}^2+m^2)\phi + \Gamma^{(1)}_\Lambda\right] \ . \end{aligned} \tag{2.65}$$

We now define the renormalised field $\mathbf{A}_R$ and the renormalised coupling g_R by

$$\mathbf{A}^2_R = Z\mathbf{A}^2 \quad \text{and} \quad g^2_R = Z^{-1}g^2 \ , \tag{2.66}$$

where

$$Z = 1+\frac{g^2}{98\pi^2}\left(\mathrm{C_E}+\ln\left(\frac{\mu^2}{\Lambda^2}\right)\right) \ . \tag{2.67}$$

The definition of $\mathbf{A}_R$ and g_R makes sure that all terms of the form $g\mathbf{A}$ do not change when using the renormalised quantities instead of the bare ones. The equations (2.66) and (2.67) allow us to derive the beta function at one-loop order:

$$\beta(g^2_{\mathrm{R}}) = \mu\,\partial_\mu g^2_{\mathrm{R}} = -\frac{g^4_{\mathrm{R}}}{49\pi^2} \ , \tag{2.68}$$

where the well known minus sign signals asymptotic freedom. Expressing everything in renormalised quantities and letting Λ go to infinity, we find the, up to one-loop order, renormalised effective action Γ_{ren} to be

$$\Gamma_{\mathrm{ren}} = \lim_{\Lambda\to\infty}\int \mathrm{d}^4x \left[-\frac{1}{4}(G^a_{\mu\nu})^2_{\mathrm{ren}} + \phi^\dagger(-\mathbf{D}^2+m^2)\phi + \Gamma^{(1)}_\Lambda\right] \ . \tag{2.69}$$

For the renormalised one-loop effective action we get that

$$\begin{aligned}\Gamma^{(1)}_{\mathrm{ren}} &= \lim_{\Lambda\to\infty}\int \mathrm{d}^4x\,\Gamma^{(1)}_\Lambda \\ &= \Gamma^{(1)} + \lim_{\Lambda\to\infty}\frac{1}{12(4\pi)^2}\int \mathrm{d}^4x_{\mathrm{cm}}\int_{\frac{1}{\Lambda^2}}^\infty \frac{\mathrm{d}T}{T}e^{-\mu^2T}\mathrm{tr}[(\mathbf{G}_{\mu\nu})^2] \\ &= -\frac{1}{(4\pi)^2}\int \mathrm{d}^4x_{\mathrm{cm}}\int_0^\infty \frac{\mathrm{d}T}{T^3}\left[e^{-m^2T}(\langle W\rangle - 2) - \frac{T^2}{12}e^{-\mu^2T}\mathrm{tr}[(\mathbf{G}_{\mu\nu})^2]\right] \ . \end{aligned} \tag{2.70}$$

Setting $\mu = m$ (on-shell renormalisation) we find the key result of this section:

$$\Gamma^{(1)}_{\mathrm{ren}} = -\frac{1}{(4\pi)^2}\int \mathrm{d}^4x_{\mathrm{cm}}\int_0^\infty \frac{\mathrm{d}T}{T^3}e^{-m^2T}\left[\langle W\rangle - 2 - \frac{T^2}{12}\mathrm{tr}[(\mathbf{G}_{\mu\nu})^2]\right] \ . \tag{2.71}$$

3 The worldline-numerical method

In this chapter we focus on the numerical aspects of the computation of the one-loop effective action. First the Monte Carlo evaluation of the one-loop effective action is explained. Then a method to implement the renormalisation is described. A summary of the numerical method is also given.

3.1 Worldline numerics and the Wilson loop

The only tricky part of a quantitative evaluation of the one-loop effective action, as it is given in equation (2.59), is the computation of the Wilson loop expectation value. We use Monte Carlo techniques to overcome this problem. In order to do so, we have to generate an appropriate loop ensemble $\mathcal{E}_{n_L}$ with n_L loops ${}^j y_\mu(t)$, which are distributed according to their weight in the path integral $\exp\big[-\int_0^1 \mathrm{d}t\, \dot{y}^2/4\big]$, calculate the Wilson loop W_j for every loop and then compute the W_js' arithmetic mean. Increasing the number of loops will make such an estimate of the Wilson loop expectation value more accurate:

$$\langle W\rangle = \lim_{n_L\to\infty}\left[\frac{\sum_{j=1}^{n_L} W_j}{n_L}\right] . \tag{3.1}$$

Because of the finite performance of modern day computers, we sadly cannot generate continuous loops. Therefore an ensemble of discretised loops will have to do and the proper time parameter to be discretised. Such an ensemble will be called the loop cloud. This is the *only* discretisation necessary; space-time remains continuous. The continuous four-dimensional loops $y_\mu(t)$ become a $4\times n_p$ matrix $y=\{y_\mu^k\}$, with n_p being the number of points used to discretise the loop. For notational convenience we will also use $y_0\equiv y_{n_p}$ and $y_{n_p+1}\equiv y_1$. The probability distribution of the loops can then be written as

$$P[\{y_i\}] = \delta(y_1+\cdots+y_{n_p})\exp\Big[-\frac{n_p}{4}\sum_{k=1}^{n_p}(y_k-y_{k-1})^2\Big] , \tag{3.2}$$

where we omitted the normalisation because it is not relevant to our purpose. The delta function serves to make sure that the "centre of mass" is zero. We also suppressed the space-time coordinates since the probability distribution factorises for different directions in the Euclidean space. To get one four-dimensional loop, we can therefore generate four one-dimensional loops as the rows of y.

The discretised loops are obtained using the v-loop algorithm (as proposed in [15], where one can also find other methods), which maps Gaussian distributed numbers onto just such loops we need for our calculation. The v-loop algorithm is given in section A.3. The Gaussian distributed numbers are generated with the Box-Müller method [37], which requires uniformly distributed numbers. The uniformly distributed numbers are generated with the random number generator `ranlxd`. That we can analytically map uniformly generated random numbers onto our loops, without costly additional means (required by many other Monte Carlo algorithms, e.g. the Metropolis acceptance-rejection decision), makes loop generation using the v-loop algorithm very efficient.

The loop cloud consists of n_L loops. Its entries ${}^j y_k^\mu$ carry three indices: j denotes on which loop we are, k which point on the loop we are dealing with and μ which space-time component of the point is addressed.

Having generated the loop cloud, we can estimate the Wilson loop expectation value according to

$$\begin{aligned}\langle W\rangle =& \frac{1}{n_L}\sum_{j=1}^{n_L} W_j \\ =& \frac{1}{n_L}\sum_{j=1}^{n_L} \mathrm{tr}\Big[\prod_{k=1}^{n_p} \mathbf{U}_k^j\Big] \\ =& \frac{1}{n_L}\sum_{j=1}^{n_L} \mathrm{tr}\Big[\prod_{k=1}^{n_p} e^{-\sqrt{T}\,(\ {}^j y_{k+1}^\mu - \ {}^j y_k^\mu)\,\mathbf{A}_\mu\left(x_{\mathrm{cm}}+\sqrt{T}\,\left(\frac{{}^j y_{k+1}+\ {}^j y_k}{2}\right)\right)}\Big]\ . \end{aligned} \tag{3.3}$$

Note that it is essential to perform the multiplications of the phases $\mathbf{U}_k$ in (3.3) in the correct order, e.g.

$$\mathbf{U}_1\mathbf{U}_2\ldots\mathbf{U}_{n_p} \quad \text{or} \quad \mathbf{U}_{n_p}\mathbf{U}_{n_p-1}\ldots\mathbf{U}_1\ , \tag{3.4}$$

but not

$$\mathbf{U}_2\mathbf{U}_1\mathbf{U}_3\ldots\mathbf{U}_{n_p}\ . \tag{3.5}$$

In doing so we take care of the path ordering, which is required because we are dealing with a non-abelian gauge field and the $\mathbf{U}_k$s in general do not commute. Additionally to the freedom the cyclic invariance of the trace gives us, we have the freedom to choose one of the two directions given in (3.4). The reason is that because of the probability distribution (3.2) only the squared difference of adjacent points determines the probability of a loop to be part of the loop cloud. Relabelling the points on a loop as indicated in (3.4), leaves the squared differences of adjacent points unchanged. The relabelled loop is just as good a part of the loop cloud as the loop we started with.

The quality of our estimate of the Wilson loop expectation value depends on the two parameters n_p (the number of points per loop) and n_L (the number of loops). Discretising the proper time parameter results in a systematic error, while only

using a finite number of loops causes a statistical one. Provided that we have chosen n_p large enough for the systematic error to be much smaller than the statistical error, a sensible error S_{WEV} of our Monte Carlo calculation is given by the standard error

$$S_{WEV} = \frac{1}{\sqrt{n_L(n_L-1)}} \sqrt{\sum_{k=1}^{n_L} (W_k - \langle W \rangle)^2} \,. \tag{3.6}$$

How large n_p should be depends on the background gauge field. To ensure that the error caused by discretising the proper time parameter is small, most of the distances between adjacent points $\sqrt{T}|y_k - y_{k+1}|$, at which the gauge field is evaluated, should be smaller than any characteristic length scale of the field. The distance of adjacent points on a loop $d = y_k - y_{k+1}$ is distributed according to

$$\begin{aligned} P[y_k - y_{k+1} = d] =& \frac{1}{\mathcal{N}} \int \mathrm{d}y_{k-1} \int \mathrm{d}y_k \int \mathrm{d}y_{k+1} \int \mathrm{d}y_{k+2} \; \Big[\delta(d - y_k + y_{k+1}) \\ & \times e^{-\frac{n_p}{4} \sum_{j=k-1}^{k+1} (y_j - y_{j+1})^2} \Big] \\ =& \frac{1}{\mathcal{N}} \int \mathrm{d}y_{k-1} \int \mathrm{d}y_k \int \mathrm{d}y_{k+2} \; e^{-\frac{n_p}{4} \left((y_{k-1} - y_k)^2 + d^2 + ((d - y_k) - y_{k+2})^2 \right)} \\ =& \frac{1}{\mathcal{N}'} \; e^{-\frac{n_p}{4} d^2} \,, \end{aligned} \tag{3.7}$$

where $\mathcal{N}'$ normalises the probability distribution to one. This is a normal distribution with variance $\sigma^2 = 2/n_p$, centred at 0. The distance between about 68% of the adjacent points on a loop of the loop cloud is therefore smaller than $\sigma = \sqrt{2/n_p}$. Taking into account that the gauge field is evaluated at $\sqrt{T}(\frac{y_k + y_{k+1}}{2})$ and not $\frac{y_k + y_{k+1}}{2}$, we find that n_p should be chosen such that for values of T that dominate the proper time integral $\sigma_T = \sqrt{2T/n_p}$ is smaller than the characteristic length scales of the background gauge field.

3.1.1 The multiplication of the phases

As can be seen in (3.3), the worldline numerical method to calculate the Wilson loop expectation value requires us to multiply n_p matrices

$$\mathbf{U}_k = e^{-\sqrt{T}\,(y^\mu_{k+1} - y^\mu_k)\,\mathbf{A}_\mu\left(x_{\mathrm{cm}} + \sqrt{T}\,\left(\frac{y_{k+1} + y_k}{2}\right)\right)} \,, \tag{3.8}$$

which are elements of SU(2). This means that they can be written as

$$\mathbf{U}_k = e^{i \Theta^a_k \mathbf{T}^a} \,, \tag{3.9}$$

where as before

$$\mathbf{T}^a = \frac{\boldsymbol{\sigma}^a}{2} \tag{3.10}$$

and $\boldsymbol{\sigma}^a$ are the Pauli matrices. Multiplying the $\mathbf{U}_k$s by brute force, we would have to calculate exponential functions of matrices to obtain the $\mathbf{U}_k$s and then perform n_p multiplications of 2×2 matrices.

Although this would certainly work, we recommend using a different method, which is more elegant, easier to implement numerically and much more efficient. We make use of the fact that a matrix $\mathbf{A} \in \mathrm{SU}(2)$ satisfies:

$$\begin{aligned}\mathbf{A} &= e^{i\Theta^a \mathbf{T}^a} \\ &= \cos\Big(\frac{|\Theta|}{2}\Big)\mathbf{1} + i\frac{\Theta^a \boldsymbol{\sigma}^a}{|\Theta|}\sin\Big(\frac{|\Theta|}{2}\Big) \\ &= a^0\mathbf{1} + ia^j\boldsymbol{\sigma}^j \ , \end{aligned} \tag{3.11}$$

where 1 again denotes the 2×2 unit matrix,

$$a^0 = \cos\Big(\frac{|\Theta|}{2}\Big) \quad \text{and} \quad a^j = \frac{\Theta^j}{|\Theta|}\sin\Big(\frac{|\Theta|}{2}\Big) \ . \tag{3.12}$$

$$\tag{3.13}$$

Multiplying $\mathbf{A}, \mathbf{B} \in \mathrm{SU}(2)$, we therefore find that

$$\begin{aligned}\mathbf{AB} =& \big[a^0\mathbf{1} + ia^j\boldsymbol{\sigma}^j\big]\big[b^0\mathbf{1} + ib^l\boldsymbol{\sigma}^l\big] \\ =& a^0b^0\mathbf{1} + ib^0a^j\boldsymbol{\sigma}^j + ia^0b^l\boldsymbol{\sigma}^l - a^jb^l\boldsymbol{\sigma}^j\boldsymbol{\sigma}^l \\ =& a^0b^0\mathbf{1} + i(b^0a^j + a^0b^j)\boldsymbol{\sigma}^j - a^jb^l\boldsymbol{\sigma}^j\boldsymbol{\sigma}^l \ , \end{aligned} \tag{3.14}$$

where the b^μ are defined analogously to the a^μ in (3.11). Because

$$\boldsymbol{\sigma}^j\boldsymbol{\sigma}^l = \delta^{jl}\mathbf{1} + i\epsilon^{jli}\boldsymbol{\sigma}^i \ , \tag{3.15}$$

we can write

$$\begin{aligned}\mathbf{AB} =& a^0b^0\mathbf{1} + i(b^0a^j + a^0b^j)\boldsymbol{\sigma}^j - a^jb^l(\delta^{jl}\mathbf{1} + i\epsilon^{jli}\boldsymbol{\sigma}^i) \\ =& (a^0b^0 + a^jb^j)\mathbf{1} + i(b^0a^j + a^0b^j - \epsilon^{ilj}a^ib^l)\boldsymbol{\sigma}^j \ . \end{aligned} \tag{3.16}$$

In (3.3) we are only interested in the trace of the product of the $\mathbf{U}_k$s. By repetitive application of (3.16) we can calculate the product of the $\mathbf{U}_k$s bypassing matrix multiplications entirely. After the multiplication the trace is also easy to derive. The Pauli matrices are traceless and the only contribution comes from the term containing the unit matrix. The trace is therefore just two times the real number the unit matrix is multiplied with. Another numerical advantage of this method is that all the quantities necessary for the calculation are real.

3.2 Numerical implementation of the renormalisation

A sensible numerical implementation of the renormalisation is also not trivial. As explained in section 2.7 the renormalised one-loop effective action is given by

$$\Gamma^{(1)}_{\mathrm{ren}} = -\frac{1}{(4\pi)^2}\int \mathrm{d}^4x_{\mathrm{cm}} \int_0^\infty \frac{\mathrm{d}T}{T^3} e^{-m^2T}\left[\langle W\rangle - 2 - \frac{T^2}{12}\mathrm{tr}[(\mathbf{G}_{\mu\nu})^2]\right] \ . \tag{3.17}$$

The Wilson loop expectation value is calculated using worldline techniques. The value we get for $\langle W \rangle$ therefore differs from the analytic "true" value, which we will call $\langle W \rangle_{\text{anal}}$, by some value $\Delta\langle W \rangle$, i.e.

$$\langle W \rangle = \langle W \rangle_{\text{anal}} + \Delta\langle W \rangle \; . \tag{3.18}$$

For the one-loop effective action this means that

$$\begin{aligned} \Gamma^{(1)}_{\text{ren}} = &- \frac{1}{(4\pi)^2} \int \mathrm{d}^4 x_{\text{cm}} \int_0^\infty \frac{\mathrm{d}T}{T^3} e^{-m^2 T} \left[\langle W \rangle_{\text{anal}} - 2 - \frac{T^2}{12} \mathrm{tr}[(\mathbf{G}_{\mu\nu})^2] \right] \\ &- \frac{1}{(4\pi)^2} \int \mathrm{d}^4 x_{\text{cm}} \int_0^\infty \frac{\mathrm{d}T}{T^3} e^{-m^2 T} \, \Delta\langle W \rangle \; . \end{aligned} \tag{3.19}$$

The first line in (3.19) is the value we want to calculate; the integral in the second line is the error we have to face as a result of the Monte Carlo character of the computation. Because of the factor T^{-3}, even the smallest $\Delta\langle W \rangle$ results in an artificial UV divergence. The error becomes uncontrollable and the result of (3.17) unusable.

This problem can be circumvented by fitting $\langle W \rangle$ to a polynomial P. In this context the inverse mass expansion provides us with two important pieces of information:

- The first two coefficients of even order are known.
- All the coefficients of odd order vanish.

P can therefore be chosen as:

$$P = a_0 + a_1 T^2 + a_2 T^4 + a_3 T^6 + \dots \; , \tag{3.20}$$

where

$$a_0 = 2 \quad \text{and} \quad a_1 = \frac{1}{12} \mathrm{tr}[(\mathbf{G}_{\mu\nu})^2] \; . \tag{3.21}$$

$$\tag{3.22}$$

Close to $T = 0$ one expects the polynomial to follow the behaviour of the Wilson loop expectation value quite well and substitutes $\langle W \rangle$ by P. As one can see in (3.17), the first two coefficients in P are subtracted because of the renormalisation. We can integrate over a polynomial P', that starts with a_2:

$$P' = a_2 T^4 + a_3 T^6 + a_4 T^8 + \dots \; . \tag{3.23}$$

After the whole fitting procedure, we end up with the following expression for the

renormalised one-loop effective action:

$$\begin{aligned}\Gamma^{(1)}_{\text{ren}} =& -\frac{1}{(4\pi)^2}\int \mathrm{d}^4x_{\text{cm}}\int_0^{T_0}\frac{\mathrm{d}T}{T^3}e^{-m^2T}\,P' \\ &-\frac{1}{(4\pi)^2}\int \mathrm{d}^4x_{\text{cm}}\int_{T_0}^{\infty}\frac{\mathrm{d}T}{T^3}e^{-m^2T}\,[\langle W\rangle - 2 - \frac{T^2}{12}\mathrm{tr}[(\mathbf{G}_{\mu\nu})^2] \\ =& -\frac{1}{(4\pi)^2}\int \mathrm{d}^4x_{\text{cm}}\int_0^{T_0}\mathrm{d}T e^{-m^2T}\,[a_2T^1 + a_3T^3 + a_4T^5 + \dots] \\ &-\frac{1}{(4\pi)^2}\int \mathrm{d}^4x_{\text{cm}}\int_{T_0}^{\infty}\frac{\mathrm{d}T}{T^3}e^{-m^2T}\,[\langle W\rangle - 2 - \frac{T^2}{12}\mathrm{tr}[(\mathbf{G}_{\mu\nu})^2]\,. \end{aligned} \tag{3.24}$$

The polynomial must of course be truncated and T_0 chosen small enough to ensure the error one makes to remain small.

It is by no means indispensable to use the knowledge of the inverse mass expansion. One could also fit to a general polynomial and then omit all the terms of order smaller than 3 to ensure a finite result (taking the renormalisation into account).

3.2.1 The fitting procedure as a quality check

Because there is only very little analytical knowledge of the Wilson loop expectation value that one could compare the algorithm's outcomes to, opportunities to test how well the algorithm can deal with the background field under investigation are of high value to us. The fitting procedure can be used as such a test. Setting $a_0 = 2$ and fitting $\langle W\rangle$ to P, we expect the fit to give us $a_1 \approx \frac{1}{12}\mathrm{tr}[(\mathbf{G}_{\mu\nu})^2]$. Anything else would not only be a big surprise but also a reason to mistrust the algorithm's results. Because the data points we use for the fit are correlated, the usual means to estimate the errors and the quality of the fitted parameters and the fit itself are not applicable in this case. To get an estimate of the error of a_1, we therefore have to resort to the jackknife method, which means to divide the loop cloud into a number of sub ensembles, calculate a_1 for every sub ensemble and finally determine the standard error treating the different a_1s as independent results. For the fit we used the routine `svdfit` from [38].

3.3 Summary of the numerical method

The expression we want to evaluate numerically is

$$\begin{aligned}\Gamma^{(1)}_{\text{ren}} =& -\frac{1}{(4\pi)^2}\int \mathrm{d}^4x_{\text{cm}}\int_0^{T_0}\mathrm{d}T e^{-m^2T}\,[a_2T^1 + a_3T^3 + a_4T^5] \\ &-\frac{1}{(4\pi)^2}\int \mathrm{d}^4x_{\text{cm}}\int_{T_0}^{\infty}\frac{\mathrm{d}T}{T^3}e^{-m^2T}\,[\langle W\rangle - 2 - \frac{T^2}{12}\mathrm{tr}[(\mathbf{G}_{\mu\nu})^2]\,, \end{aligned} \tag{3.25}$$

where the a_i are obtained using a fitting procedure (see section 3.2) and we believe the polynomial, that was the result of the fit, to be a good approximation of the

Wilson loop expectation value for $T < T_0$. The Romberg integration routine `qromo` implemented with `midpnt` and `midinf` from [38] was used for the integration. For every x requested by the routines that perform the x-integration, we have to perform a T-integration, picking up information about the UV- and the IR-behaviour of the background field, while scaling the loop cloud from very small to very big. For very small T, this procedure does not work and we need to fit the Wilson loop expectation value to a polynomial in order to determine a_2, a_3, a_4. To evaluate the Wilson loop expectation value, we first of all need to generate the loop cloud. For this we use the v-loop algorithm (see section A.3). The loop cloud ${}^j y_k^\mu$ is an object equipped with three indices:

- the number of the loop: j
- the number of the point on loop j: k
- the coordinate of the point k on loop j: μ .

The Wilson loop expectation value can then be calculated employing equation (3.3):

$$\langle W \rangle = \frac{1}{n_L} \sum_{j=1}^{n_L} \mathrm{tr}\Big[\prod_{k=1}^{n_p} e^{-\sqrt{T}\,(\ {}^j y_{k+1}^\mu - \ {}^j y_k^\mu)\, \mathbf{A}_\mu \left(x_{\mathrm{cm}} + \sqrt{T}\, \left(\frac{{}^j y_{k+1} + \ {}^j y_k}{2} \right) \right)} \Big] \,, \tag{3.26}$$

performing the product as explained in section 3.1.1.

With a fixed number of points n_p, the mean distance of adjacent points grows as T becomes bigger. Integrating over all $T > 0$ with a fixed n_p, we could have to face some trouble since for a good resolution of our method we need the values of the background field evaluated at adjacent points to differ only slightly. Physically relevant background fields, however, have to fall off quickly because their contribution to the action $\int \mathrm{d}^4x\, \frac{1}{2}\mathrm{tr}[\mathbf{G}_{\mu\nu}\mathbf{G}_{\mu\nu}]$ has to be finite, which means that $\mathrm{tr}[\mathbf{G}_{\mu\nu}\mathbf{G}_{\mu\nu}]$ has to vanish faster than x^{-4} as one approaches infinity. This causes the majority of the values of the background field evaluated at adjacent points on the loop to differ only slightly, even if the adjacent points do not, because at a big T the loop cloud is huge. Furthermore, the factor T^{-3} in the integrand damps contributions of a big T. These two effects justify the use of a loop cloud of fixed n_p in the integration.

4 Application to two simple fields

In this chapter the application of the worldline numerical method to two simple background fields, the pseudo-abelian background field and the PNA field, is presented.

4.1 The pseudo-abelian background field

While quite some experience with the worldline numerical method has been gained treating Abelian background fields, there has only been one attempt to use a worldline numerical method in the non-abelian case [28], employing random walk worldline loops on a hyper cubic lattice (and not as proposed here loops generated by the v-loop algorithm). As a first go we therefore chose a background field configuration, that is essentially Abelian: the pseudo-abelian field. Its only nonzero components are given by

$$A_2^3 = -Hx_3 \quad \text{and} \quad A_3^3 = Hx_2 \,, \tag{4.1}$$

with H being real and $H > 0$. The choice of name is now obvious. Because the background field $\mathbf{A}_\mu$ is just the third Pauli matrix times some real number, it commutes with itself everywhere in the four-dimensional Euclidean space. The path ordering can be dropped and the integration in the exponent can be performed. The only remaining effect of the non-abelian decent of the problem is the trace, which has to be taken after performing the product. It is an SU(2) gauge field; just an Abelian one. Inserting (4.1) into the definition of the Wilson loop and using what we just said, we find that

$$\begin{aligned} W_{\mathrm{ps}} &= \operatorname{tr} \mathrm{P} \exp\Big[-\oint \mathrm{d}t\, \dot{x}_\mu\, \mathbf{A}_\mu(x) \Big] \\ &= \operatorname{tr} \mathrm{P} \exp\Big[\oint \mathrm{d}t\, igH[\dot{x}_3 x_2 - \dot{x}_2 x_3] \mathbf{T}^3 \Big] \\ &= \exp\Big[\frac{igH}{2} \oint \mathrm{d}t\, [\dot{x}_3 x_2 - \dot{x}_2 x_3] \Big] + \exp\Big[-\frac{igH}{2} \oint \mathrm{d}t\, [\dot{x}_3 x_2 - \dot{x}_2 x_3] \Big] \\ &= 2\cos\Big[\frac{gH}{2} \oint \mathrm{d}t\, [\dot{x}_3 x_2 - \dot{x}_2 x_3] \Big] \,, \end{aligned} \tag{4.2}$$

and for the Wilson loop expectation value (defined in equation (2.58)) that

$$\langle W_{\mathrm{ps}} \rangle(gH) = 2 \left[\frac{\int_{y(0)=y(1)} \mathcal{D}y\, e^{-\int_0^1 \mathrm{d}t\, \frac{\dot{y}^2}{4}}\, \cos\Big[\frac{gHT}{2} \int_0^1 \mathrm{d}t\, [\dot{y}_3 y_2 - \dot{y}_2 y_3] \Big]}{\int_{y(0)=y(1)} \mathcal{D}y\, e^{-\int_0^1 \mathrm{d}t\, \frac{\dot{y}^2}{4}}} \right] . \tag{4.3}$$

The subscript ps indicates the pseudo-abelian case. The x_{cm} dependency has been omitted as the $\langle W_{\mathrm{ps}}\rangle$ does not depend on x_{cm} because all the contributions containing x_{cm} are loop integrals over a total derivative and therefore zero.

4.1.1 $\Gamma^{(1)}$ of the pseudo-abelian background field

For the pseudo-abelian background field we cannot only utilise the knowledge gained using worldline numerics on Abelian fields but also compare to an analytically known result. A closed expression for the one-loop effective Lagrangian density for a scalar particle in an electro-magnetic background field of constant field strength has been derived by Victor Weisskopf as early as 1936 [2]. A special case of an electro-magnetic field of constant field strength, the constant magnetic field, corresponds to the pseudo-abelian background field. The one-loop Lagrangian density of a constant magnetic field of field strength $B > 0$ has been calculated to be:

$$\mathcal{L}^{(1)}_{\mathrm{km}}(eB) = \frac{1}{(4\pi)^2}\int_0^\infty \frac{dT}{T^3}\, e^{-m^2T}\Big[\frac{eBT}{\sinh(eBT)} - 1 + \frac{(eB)^2}{6}\,T^2\Big]\,, \tag{4.4}$$

where e is the electromagnetic charge and the subscript km shall indicate quantities corresponding to the constant magnetic field. As is derived in the remainder of this section, we find for the renormalised one-loop Lagrangian density of the pseudo-abelian field $\mathcal{L}^{(1)}_{\mathrm{ps}}$ that

$$\begin{aligned}\mathcal{L}^{(1)}_{\mathrm{ps}}(gH) &= 2\,\mathcal{L}^{(1)}_{\mathrm{km}}(gH)\\ &= \frac{1}{(4\pi)^2}\int_0^\infty \frac{dT}{T^3}\, e^{-m^2T}\Big[2\frac{gHT}{\sinh(gHT)} - 2 + \frac{(gH)^2}{3}\,T^2\Big]\,.\end{aligned} \tag{4.5}$$

To start the derivation we remember that vector potential A_{km} of a constant magnetic field of field strength $B > 0$ that points into the x_1 direction can be chosen to be $A_{\mathrm{km}} = (0, -\frac{B}{2}x_3, \frac{B}{2}x_2, 0)$. With some caution all the formulae that we have derived in this thesis are applicable to a U(1) as well as to an SU(2) gauge theory, for which they were originally derived. The expression for the renormalised Lagrangian density in a constant magnetic background field for example reads

$$\mathcal{L}^{(1)}_{\mathrm{km}}(eB) = \frac{1}{(4\pi)^2}\int_0^\infty \frac{dT}{T^3}\, e^{-m^2T}\Big[\langle W\rangle_{\mathrm{km}} - 1 + \frac{1}{12}e^2(F_{\mu\nu})^2\,T^2\Big]\,, \tag{4.6}$$

where $F_{\mu\nu}$ is field strength tensor and the traces have disappeared because in U(1) gauge field theories there are no colour indices one could trace over. $F_{\mu\nu}$'s only nonzero components are $F_{23} = -F_{32} = B$. For the squared field strength we can write $(F_{\mu\nu})^2 = F_{\mu\nu}F_{\mu\nu} = 2B^2$. With (4.6) and (4.4), we find that

$$\begin{aligned}\mathcal{L}^{(1)}_{\mathrm{km}}(eB) &= \frac{1}{(4\pi)^2}\int_0^\infty \frac{dT}{T^3}\, e^{-m^2T}\Big[\langle W\rangle_{\mathrm{km}} - 1 + \frac{(eB)^2}{6}\,T^2\Big]\\ &= \frac{1}{(4\pi)^2}\int_0^\infty \frac{dT}{T^3}\, e^{-m^2T}\Big[\frac{eBT}{\sinh(eBT)} - 1 + \frac{(eB)^2}{6}\,T^2\Big]\,.\end{aligned} \tag{4.7}$$

By comparison of the two lines in (4.7), we find the analytic expression for the Wilson loop expectation value of a constant magnetic field to be

$$\langle W\rangle_{\mathrm{km}} = \frac{eBT}{\sinh(eBT)} \,. \tag{4.8}$$

Using the definition of the Wilson loop expectation value, we get that

$$\begin{aligned}\langle W\rangle_{\mathrm{km}} &= \frac{\int_{y(0)=y(1)} \mathcal{D}y\, e^{-\int_0^1 \mathrm{d}t\, \frac{\dot{y}^2}{4}} \exp\left[\frac{ieBT}{2}\int_0^1 \mathrm{d}t\,[\dot{y}_3\, y_2 - \dot{y}_2\, y_3]\right]}{\int_{y(0)=y(1)} \mathcal{D}y\, e^{-\int_0^1 \mathrm{d}t\, \frac{\dot{y}^2}{4}}} \\ &= \frac{\int_{y(0)=y(1)} \mathcal{D}y\, e^{-\int_0^1 \mathrm{d}t\, \frac{\dot{y}^2}{4}} \cos\left[\frac{ieBT}{2}\int_0^1 \mathrm{d}t\,[\dot{y}_3\, y_2 - \dot{y}_2\, y_3]\right]}{\int_{y(0)=y(1)} \mathcal{D}y\, e^{-\int_0^1 \mathrm{d}t\, \frac{\dot{y}^2}{4}}} \\ &\quad - i\frac{\int_{y(0)=y(1)} \mathcal{D}y\, e^{-\int_0^1 \mathrm{d}t\, \frac{\dot{y}^2}{4}} \sin\left[\frac{ieBT}{2}\int_0^1 \mathrm{d}t\,[\dot{y}_3\, y_2 - \dot{y}_2\, y_3]\right]}{\int_{y(0)=y(1)} \mathcal{D}y\, e^{-\int_0^1 \mathrm{d}t\, \frac{\dot{y}^2}{4}}} \,. \end{aligned} \tag{4.9}$$

As we have already seen several times, the paths contribute to the path integral according to their weight $\exp\big[-\int_0^1 \mathrm{d}t\,\dot{y}^2/4\big]$, which only depends on the squared derivative of the loop. Paths of opposite direction have the same weight. Let us consider some path y_+ which gives the phase

$$\alpha := \int_{y_+} \mathrm{d}t\,[\dot{y}_3\, y_2 - \dot{y}_2\, y_3] \tag{4.10}$$

to the cosine and sine functions in (4.9). Parameterising y_+ in the opposite direction we end up with a path $y_-$of the same weight, which contributes

$$\int_{y_-} \mathrm{d}t\,[\dot{y}_3\, y_2 - \dot{y}_2\, y_3] = -\int_{y+} \mathrm{d}t\,[\dot{y}_3\, y_2 - \dot{y}_2\, y_3] = -\alpha \,. \tag{4.11}$$

This does not bother the cosine terms in (4.9), but the sine terms cancel each other:

$$\cos(\alpha) + i\sin(\alpha) + \cos(-\alpha) + i\sin(-\alpha) = 2\cos(\alpha) \,. \tag{4.12}$$

Hence the Wilson loop expectation value in a constant magnetic field is:

$$\begin{aligned}\langle W\rangle_{\mathrm{km}}(eBT) &= \frac{\int_{y(0)=y(1)} \mathcal{D}y\, e^{-\int_0^1 \mathrm{d}t\, \frac{\dot{y}^2}{4}} \cos\left[\frac{ieB}{2}\int_0^1 \mathrm{d}t\,[\dot{y}_3\, y_2 - \dot{y}_2\, y_3]\right]}{\int_{y(0)=y(1)} \mathcal{D}y\, e^{-\int_0^1 \mathrm{d}t\, \frac{\dot{y}^2}{4}}} \\ &= \frac{1}{2}\langle W\rangle_{\mathrm{ps}}(eBT) \,, \end{aligned} \tag{4.13}$$

where in the last line (4.3) was used. With (4.8) this yields that

$$\langle W\rangle_{\mathrm{ps}} = 2\,\frac{gHT}{\sinh(gHT)} \,, \tag{4.14}$$

which concludes the derivation of equation (4.5).

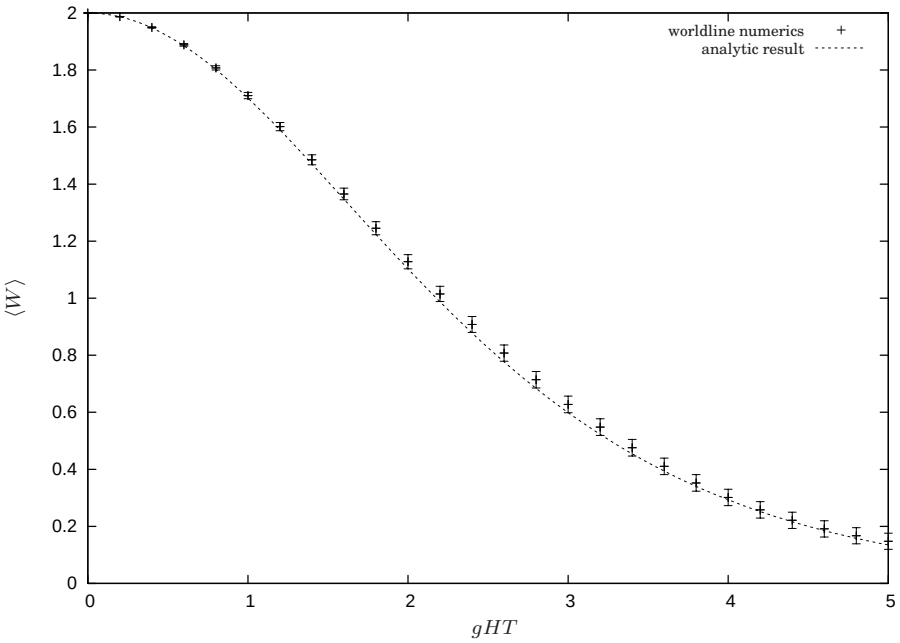

Figure 4.1: Comparison of the analytical and the worldline numerical results for the Wilson loop expectation value in a pseudo-abelian background field. 2500 loops of 1001 points were used for the computation.

4.1.2 Comparison to the worldline numerical calculation

As we can see in figure 4.1, the worldline numerical method to calculate the Wilson loop expectation value in a pseudo-abelian background field reproduces the analytical results nicely. This is, however, hardly surprising because the worldline numerical method has been successfully used for the treatment of QED background gauge fields several times [12–14] and the actual calculations of the Wilson loop expectation value in a pseudo-abelian field and a magnetic field of constant field strength are very similar. The non-abelian nature of the background field was not expected to cause any difficulties. Because we are using the same loop cloud for every point, the numerical data lies on a smooth curve. The results we obtain for different gHT are highly correlated.

4.1.3 The non-abelian pseudo-abelian background field

By calculating the Wilson loop in a pseudo-abelian background field, we have gained some trust in the worldline method. However, the pseudo-abelian case is essentially Abelian. To really test the worldline method on a non-abelian background field, we should use a field where the $\mathbf{A}_\mu$ do not commute. Of course we still want to be able to compare to an analytically correct result. Making use of the gauge invariance of the Wilson loop, we can easily find such a field and still know the Wilson loop

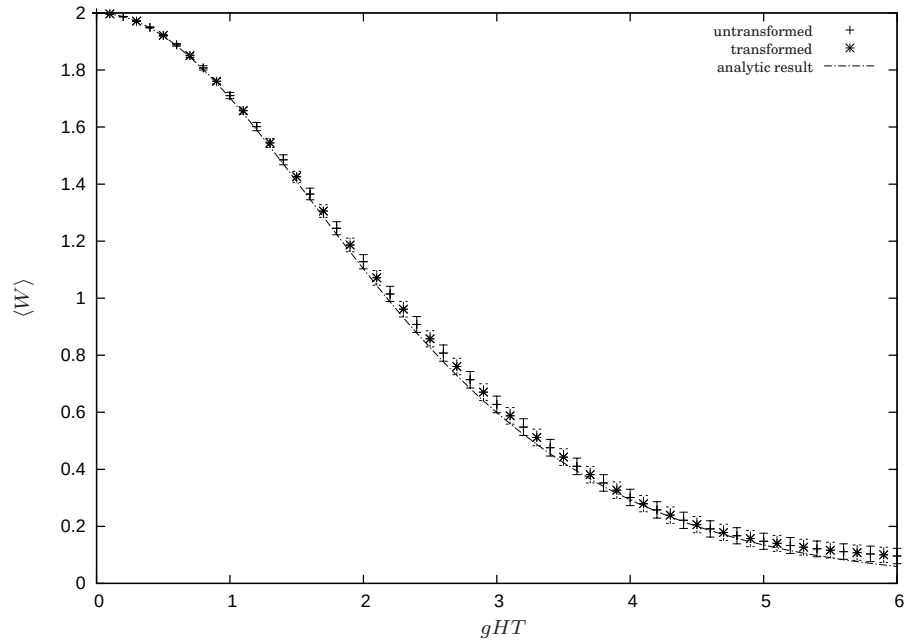

Figure 4.2: Wilson loop expectation value in a pseudo-abelian field and a gauge transformed pseudo-abelian field. The analytical result is also shown. 2500 loops of 1001 points were used for the computation.

expectation value. We perform a gauge transformation on the pseudo-abelian gauge field to ensure the gauge field to be properly non-abelian. The gauge transformation $\mathbf{U}$ that we use is

$$\mathbf{U} = e^{ix^a \mathbf{T}^a} \ . \tag{4.15}$$

With (2.29) and after a lengthy but straightforward calculation, we find the gauge transformed field $\mathbf{A}'_\mu$ to be

$$\begin{aligned} \mathbf{A}'_\mu = &- iA'^a_\mu \mathbf{T}^a = -i[A^a_\mu \cos(x) - \epsilon^{uja} \hat{x}^u A^j_\mu \sin(x) + 2A^u_\mu \hat{x}^u \hat{x}^a \sin^2\left(\frac{x}{2}\right) \\ &+ \hat{x}_\mu \hat{x}^a + \frac{1}{x}\sin(x)(\delta^a_\mu - \hat{x}_\mu \hat{x}^a) + \frac{2}{x}\sin^2\left(\frac{x}{2}\right)\epsilon^{ua}_\mu \hat{x}^u]\mathbf{T}^a \ , \end{aligned} \tag{4.16}$$

where $x = |x|$ and $\hat{x}_\mu = \frac{x_\mu}{x}$. Inserting the pseudo-abelian field (4.1), we end up with a properly non-abelian background field, whose Wilson loop expectation value is analytically known.

In figure 4.2 we see the result of the worldline numerical calculation of the pseudo-abelian and the gauge transformed pseudo-abelian field together with the analytical result. We again find that the worldline method reproduces the analytical result nicely. The gauge transformation does *not* impair our ability to use the worldline method. We also see that our algorithm is capable of dealing with the path ordering necessary for a non-abelian background field. It actually looks like using the gauge transformed field yields exactly the same results as using the untransformed field.

This, however, is not the case as can be very nicely seen comparing both cases to the inverse mass expansion.

4.1.4 Comparison to the inverse mass expansion

As explained in subsection 3.2.1, we have another way of testing the worldline numerical method using the knowledge of the first two coefficients of the inverse mass expansion:

$$\langle W \rangle = 2 + \frac{T^2}{12}\mathrm{tr}[(\mathbf{G}_{\mu\nu})^2] + O(T^4) \; . \tag{4.17}$$

With the definition of the pseudo-abelian field (equation (4.1)), we find for the field strength tensor that

$$\begin{aligned} \mathbf{G}_{\mu\nu} &= \partial_\mu \mathbf{A}_\nu - \partial_\nu \mathbf{A}_\mu + [\mathbf{A}_\mu, \mathbf{A}_\nu] \\ &= -igG^3_{\mu\nu}\mathbf{T}^3 \; , \end{aligned} \tag{4.18}$$

with

$$G^3_{\mu\nu} = 2H \begin{pmatrix} 0 & 0 & 0 & 0 \\ 0 & 0 & 1 & 0 \\ 0 & -1 & 0 & 0 \\ 0 & 0 & 0 & 0 \end{pmatrix} \; . \tag{4.19}$$

Equation (2.36) allows us to easily calculate the second coefficient in the inverse mass expansion. It is given by

$$\begin{aligned} \frac{T^2}{12}\mathrm{tr}[(\mathbf{G}_{\mu\nu})^2] &= -\frac{g^2T^2}{24}(G^3_{\mu\nu})^2 \\ &= -\frac{1}{3}\, g^2H^2T^2 \end{aligned} \tag{4.20}$$

Fitting the polynomial $P = 2 + a_1(gHT)^2 + a_2(gHT)^3 + a_3(gHT)^4 + a_4(gHT)^6 + a_5(gHT)^8$ to the numerical data for the Wilson loop expectation value, the resulting a_1 should be close to $-\frac{1}{3}$.

In figure 4.1.4 we have a plot of a_1 for the transformed pseudo-abelian and the untransformed pseudo-abelian field. The Wilson loop expectation value was evaluated at ten different values of gHT ranging from $gHT_0/10$ to gHT_0. The coefficient a_1 is plotted against gHT_0. As we can see in 4.1.4 (a), the numerical result agrees with the expected value of $-1/3$ in the untransformed as well as the transformed case. In figure 4.1.4, however, we find differences between the two cases; while choosing a bigger interval between the ten points that we use for the fit almost does not affect the result for a_1 in the untransformed pseudo-abelian case, in the transformed case the result becomes worse quite fast. The deviation from the analytical expectations is, however, very small. Both gauge fields are equally well treatable with the worldline numerical method.

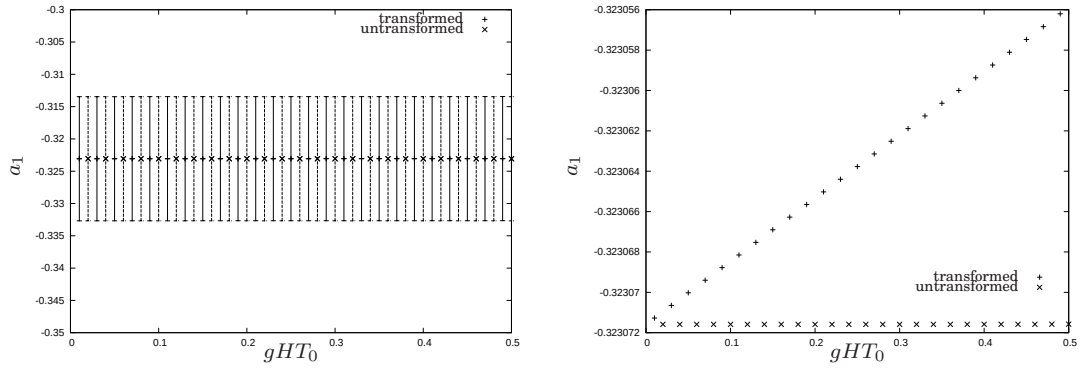

(a) with errors (b) without errors

Figure 4.3: The coefficient a_1 given by a fit of the Wilson loop expectation value to the polynomial P for different T_0. The gauge transformed and the untransformed pseudo-abelian gauge field are shown. 2500 loops of 1001 points were used for the computation.

4.2 The PNA field

We have now seen an example of a successful use of worldline numerics in a properly non-abelian background field. To gain some more experience with non-abelian background fields, we now turn the PNA field, whose one-loop effective potential in a pure SU(2) theory was calculated in [39], and compute its one-loop effective Lagrangian density.

The PNA field has no coordinate dependence at all. In some sense it is a purely non-abelian field (hence the name Purely Non-Abelian). The components of the PNA field are:

$$A^i_j = a\delta^i_j \quad \text{and} \quad A^i_0 = 0\,, \tag{4.21}$$

where $j, i = 1, 2, 3$ and $a > 0$.

4.2.1 The Wilson loop expectation value

Since the zero-component of the PNA field is zero, the problem is essentially three-dimensional. A three-dimensional loop cloud therefore suffices to calculate the Wilson loop expectation value. In figure 4.4 we have a plot of the Wilson loop expectation value. It seems well behaved and trustworthy. Instead of showing an exponential decrease of the Wilson loop expectation value, the worldline numerical method gives us a quantity that oscillates irregularly around zero. The result is compatible with an exponential decrease. In the integration necessary to calculate the one-loop effective Lagrangian density, these oscillations do not worry us because they are damped by the factor T^{-3}. We can, however, learn something about the effect of different loop clouds. We know that the Wilson loop expectation value should

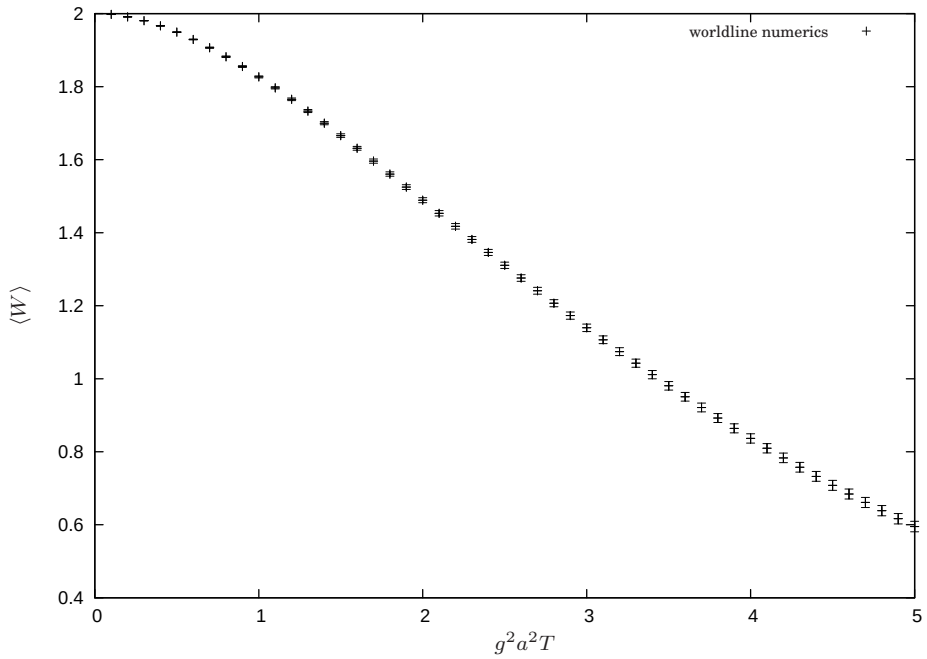

Figure 4.4: The Wilson loop expectation value in a PNA field. 3000 loops of 1001 points were used for the computation.

decrease and almost be zero for large g^2a^2T. We thus have a parameter range in which we have knowledge of an expected outcome.

Because the oscillations are an artefact of the discretisation of the loops, one would expect them to become smaller as one chooses loops with more points. This has only a minor effect as can be seen in figure 4.5 (a)-(c). What is effective is to increase the number of loops. This can be seen in figure 4.5 (c)-(e). The computation of the Wilson loop expectation value for the loop cloud used in figure 4.5 (a) takes about 10 times longer than for the loop cloud used in figure 4.5 (e). We see that there is no point in wasting precious computing time in using a large number of points per loop n_p.

4.2.2 Comparison with the inverse mass expansion

To learn how reliable the results close to $T = 0$ are, we again employ the inverse mass expansion. Because the field is independent of x, the partial derivatives of the field are zero and the field strength tensor is given by

$$\mathbf{G}_{\mu\nu} = [\mathbf{A}_\mu, \mathbf{A}_\nu] \; . \tag{4.22}$$

For μ or ν being zero we find that

$$\mathbf{G}_{\mu\nu} = 0 \; . \tag{4.23}$$

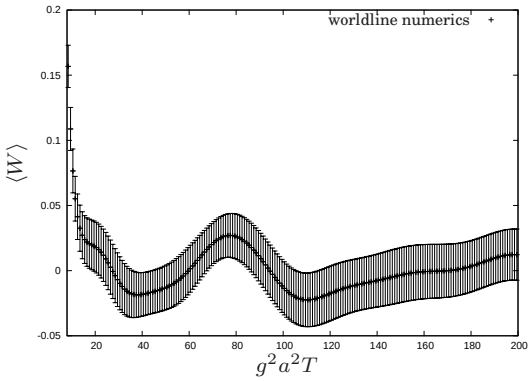

(a) 3000 loops, 10001 points

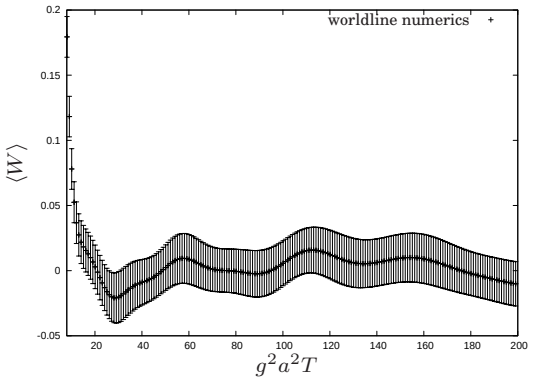

(b) 3000 loops, 1001 points

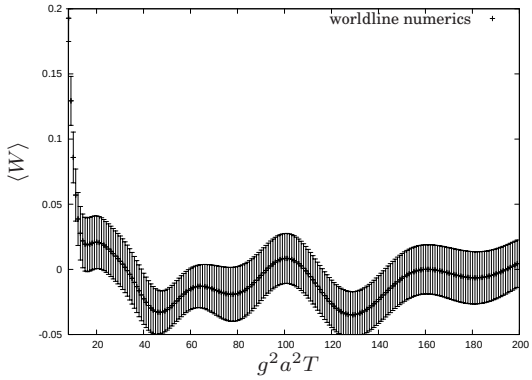

(c) 3000 loops, 101 points

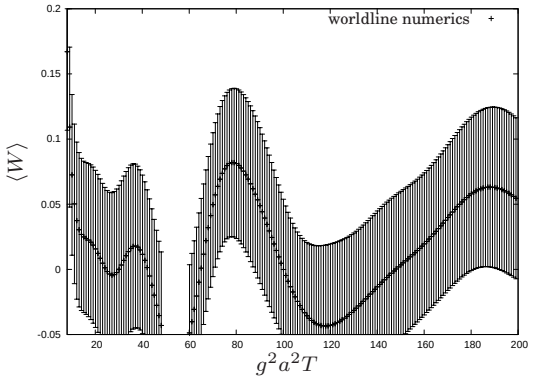

(d) 300 loops, 101 points

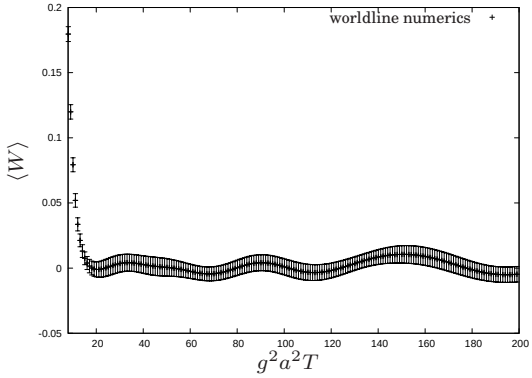

(e) $30,000$ loops, 101 points

Figure 4.5: The Wilson loop expectation value in a PNA field at high g^2a^2T computed with a variety of loop clouds.

For $\mu = i$ and $\nu = j$, with $i, j = 1, 2, 3$, we find that

$$\begin{aligned}\mathbf{G}_{\mu\nu} &= \mathbf{G}_{ij} \\ &= [\mathbf{A}_i, \mathbf{A}_j] \\ &= -(ga)^2 \delta_j^b \delta_i^a [\mathbf{T}^a, \mathbf{T}^b] \\ &= -i(ga)^2 \delta_j^b \delta_i^a \epsilon^{abc} \mathbf{T}^c \\ &= -i(ga)^2 \epsilon^{ijc} \mathbf{T}^c \ . \end{aligned} \tag{4.24}$$

We have thus found the components of the field strength tensor as defined in (2.31):

$$\begin{aligned} G^a_{\mu\nu} &= 0 && \text{if } \mu = 0 \text{ or } \nu = 0 \ , \\ G^a_{\mu\nu} &= ga^2 \epsilon^{\mu\nu a} && \text{otherwise} \ . \end{aligned} \tag{4.25}$$

For the second coefficient in the inverse mass expansion is this means that

$$\begin{aligned} \frac{T^2}{12} \mathrm{tr}[(\mathbf{G}_{\mu\nu})^2] &= -\frac{g^2 T^2}{24} G^a_{\mu\nu} G^a_{\mu\nu} \\ &= -\frac{(a^2 g^2 T)^2}{24} \epsilon^{ija} \epsilon^{ija} \\ &= -\frac{(a^2 g^2 T)^2}{24} (\delta_{jj}\delta_{aa} - \delta_{ja}\delta_{aj}) \\ &= -\frac{(a^2 g^2 T)^2}{24} (9 - 3) \\ &= -\frac{(a^2 g^2 T)^2}{4} \ . \end{aligned} \tag{4.26}$$

Fitting to the polynomial $P = 2 + a_1 T^2 + a_2 T^4 + a_3 T^6 + a_4 T^8$, we therefore expect $a_1 \approx -(ga)^4/4$.

For the fit we again calculated the Wilson loop expectation value at $T = T_0/n$, where $n = 1, \ldots, 10$. In figure 4.6 we can see that using T_0 very close to zero yields the desired result.

4.2.3 The one-loop effective Lagrangian density

We have seen that the worldline numerical method gives us reasonable results for the PNA field and are therefore able to calculate the one-loop effective Lagrangian density $\mathcal{L}^{(1)}$. It is given by:

$$\mathcal{L}^{(1)} = -\frac{1}{(4\pi)^2} \int_0^\infty \frac{\mathrm{d}T}{T^3} e^{-m^2 T} \left[\langle W \rangle - 2 - \frac{T^2}{12} \mathrm{tr}[(\mathbf{G}_{\mu\nu})^2] \right] . \tag{4.27}$$

Our findings, which were computed following the recipe given in section 3.3, with ten points at T_0/n, where $n = 1, \ldots, 10$ and $T_0 = 0.1$, used for the fit, are shown in figure 4.7. To compute the errors, we used the jackknife method, which was explained in the context of the fitting procedure in subsection 3.2.1.

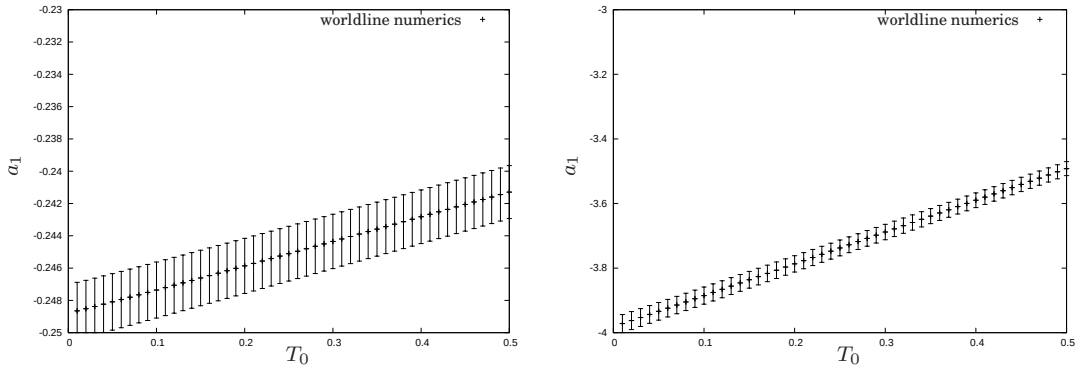

(a) $ga = 1$ (b) $ga = 2$

Figure 4.6: The coefficient a_1 given by a fit of the Wilson loop expectation value to the polynomial P for different T_0 in the PNA field with $ga = 1$ and $ga = 2$. 30,000 loops of 101 points were used for the computation.

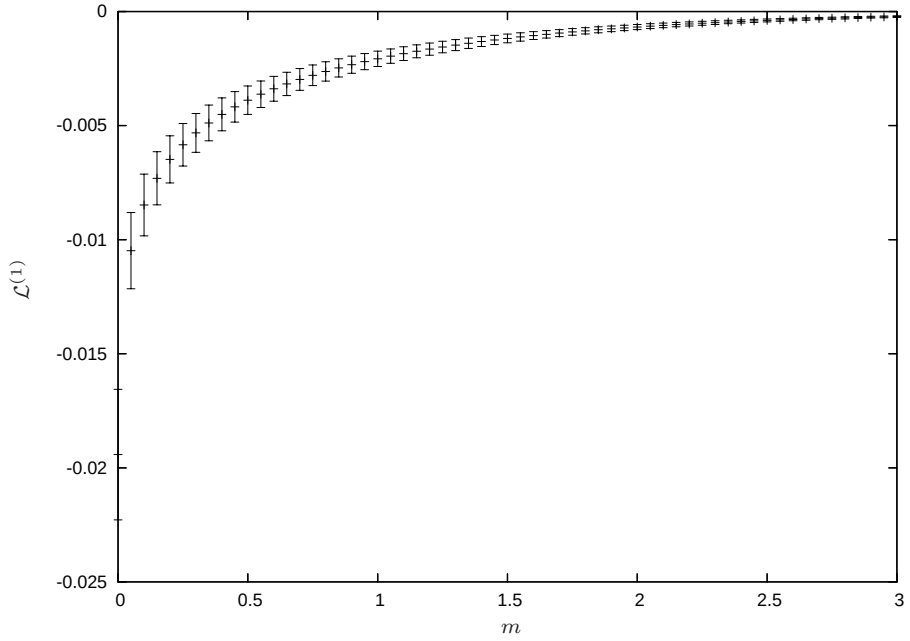

Figure 4.7: The one-loop effective Lagrangian density for $ga = 1$. 1000 loops of 101 points were used for the computation.

Since this is the first time this matter determinant has been calculated we have no means to compare it to any previous work. It is, however, possible to derive an analytical result for the one-loop effective Lagrangian density computed by us [40]. Once this calculation has been performed it will be possible to assess the quality

of the worldline numerical result, but since there are no indications of numerical problems we are confident that the numerical data is accurate.

5 The instanton

The instanton is a background field that is physically interesting (see [29–31]; for a compilation of important publications [32]), and the one-loop effective action in a one instanton background field has been derived in [33]. It is therefore a case in which we have both: a physically interesting background field and a way to see whether or not a result for the one-loop effective action is correct. We will use the instanton in two different gauges: the regular gauge (BPST instanton) and the singular gauge (singular instanton). The numerical results are compared to an approximation of the Wilson loop expectation value, which is called the derivative expansion. We find that the worldline numerical results for the Wilson loop expectation value are not gauge invariant. The problem is pinned down to not sufficiently precisely computed worldline correlation functions. We then propose a method to improve how well worldline numerics reproduces the Lorentz structure of worldline correlation functions by rotating the loop cloud. Afterwards, it is explained that also with a rotated loop cloud today's computers do not allow for the computation of the Wilson loop expectation value to a precision that would make a sensible calculation of the one-loop effective action for the regular instanton possible.

5.1 Non-numerical preliminaries

In this section the necessary quantities are introduced and some instanton specific analytic work is done. The instanton is given in two gauges and the derivative expansion is explained.

5.1.1 The BPST instanton

Working with the instanton background field, we will use rescaled components of the gauge potential and the field strength tensor:

$$A^a_\mu \to \tfrac{1}{g} A^a_\mu \quad \text{and} \quad G^a_{\mu\nu} \to \tfrac{1}{g} G^a_{\mu\nu} \; . \tag{5.1}$$

Belavin et al. [41] found what is called the BPST instanton solution. It is given by

$$\mathbf{A}^a_\mu(x) = \frac{2\eta_{a\mu\nu} x_\nu}{x^2 + \rho^2} \; , \tag{5.2}$$

where $x^2 = x_\mu x_\mu$ and the 't Hooft symbol $\eta_{a\mu\nu}$ is given by:

$$\eta_{a\mu\nu} = \begin{cases} \epsilon_{a\mu\nu} & \mu,\, \nu = 1,\, 2,\, 3, \\ \delta_{a\mu} & \nu = 0, \\ -\delta_{a\nu} & \mu = 0 \; . \end{cases} \tag{5.3}$$

The parameter ρ corresponds to the size of the instanton. The components of the field strength tensor are

$$\mathbf{G}^a_{\mu\nu} = -\frac{4\rho^2\eta_{a\mu\nu}}{(x^2+\rho^2)^2}\ , \tag{5.4}$$

and the trace of the squared field strength is

$$\mathrm{tr}[\mathbf{G}_{\mu\nu}\mathbf{G}_{\mu\nu}] = -\frac{96\rho^4}{(x^2+\rho^2)^4}\ . \tag{5.5}$$

Because $\mathbf{A}_\mu$ falls off like x^{-1}, one would expect the components of the field strength tensor to show a x^{-2} behaviour. As we can see in (5.4), this is not the case and the $\mathbf{G}_{\mu\nu}$ fall off like x^{-4}. Writing $\mathrm{tr}[\mathbf{G}_{\mu\nu}\mathbf{G}_{\mu\nu}]$ in terms of $\mathbf{A}_\mu$, we find that

$$\begin{aligned}\mathrm{tr}[\mathbf{G}_{\mu\nu}\mathbf{G}_{\mu\nu}] =& \mathrm{tr}\big[\partial_\mu\mathbf{A}_\nu - \partial_\nu\mathbf{A}_\mu + [\mathbf{A}_\mu,\mathbf{A}_\nu]\big]\big[\partial_\mu\mathbf{A}_\nu - \partial_\nu\mathbf{A}_\mu + [\mathbf{A}_\mu,\mathbf{A}_\nu]\big]\\ =& 2\,\mathrm{tr}\big[\partial_\mu\mathbf{A}_\nu\partial_\mu\mathbf{A}_\nu - \partial_\nu\mathbf{A}_\mu\partial_\mu\mathbf{A}_\nu\big]\\ &+ 2\,\mathrm{tr}\big[\mathbf{A}_\mu\mathbf{A}_\nu[\mathbf{A}_\mu,\mathbf{A}_\nu]\big] - 4\,\mathrm{tr}\big[(\partial_\mu\mathbf{A}_\nu)[\mathbf{A}_\mu,\mathbf{A}_\nu]\big]\ ,\end{aligned} \tag{5.6}$$

where all the derivatives act only on the field next to them. The large-x-behaviour depends very strongly on the precise balance between the three terms on the right hand side of equation (5.6).

5.1.2 The instanton in singular gauge

Using the singular instanton, in equation (5.6) no non-trivial cancellation of terms that vanish slower than x^{-4} takes place. It can be obtained from the BPST instanton by performing the gauge transformation $\mathbf{U} = i\frac{x_\mu}{x}\mathbf{T}^+_\mu$, where $\mathbf{T}^+_\mu = (-i\mathbf{1}, \mathbf{T}^a)$ (see [42], [43]). For the components of the singular instanton one finds that

$$A^a_\mu(x) = 2\frac{x_\nu}{x^2}\frac{\overline{\eta}_{a\mu\nu}\rho^2}{x^2+\rho^2}\ . \tag{5.7}$$

The definition of $\overline{\eta}_{a\mu\nu}$ is the same as the definition of $\eta_{a\mu\nu}$ (equation (5.3)), with the last two equations multiplied by -1. Because it is gauge invariant, $\mathrm{tr}[\mathbf{G}_{\mu\nu}\mathbf{G}_{\mu\nu}]$ is the same for the singular instanton as for the regular instanton, but all contributions to $\mathrm{tr}[\mathbf{G}_{\mu\nu}\mathbf{G}_{\mu\nu}]$ as given in equation (5.6) fall off as x^{-4}. Its large-x-behaviour does not depend very sensitively on the balance between the terms on the right hand side of (5.6). The non-trivial behaviour the BPST instanton shows for large x has been traded for a non-trivial behaviour of the singular instanton close to the origin. The singular instanton diverges as one approaches the origin. We therefore do not expect the straightforward worldline numerical analysis to be of any value close to the origin. The standard discretisation will run into the same difficulties as are known from the path integral formulation of the hydrogen problem in quantum mechanics (see [44]). Further away from the origin, however, we expect the numerical results to be reliable and comparisons between the BPST instanton and the singular instanton to be meaningful.

5.1.3 The derivative expansion

The numerical results are not only compared to each other but also to a quantity that behaves similarly to the Wilson loop expectation value and is motivated by the derivative expansion approximation.

In Abelian gauge theories the derivative expansion approach enables one to get an approximate value of the one-loop effective action even if the background field is inhomogeneous, which in most cases renders the analytical derivation of the one-loop effective action impossible. The idea is to expand the one-loop effective action about a field of constant field strength tensor. The first coefficient of the series is then just the one-loop effective action corresponding to that field. In many cases (scale of variation of the background field larger than Compton wave length of the electron) taking only the first coefficient into account yields surprisingly good results (see e.g. [4]).

In [45] Dunne et al. propose an approximate solution for the one-loop effective action in an instanton background field, which is motivated by the derivative expansion used for Abelian fields. They argue, that because the instanton field is self dual a good choice for a background field to expand about would be a covariantly constant self dual field that points into one direction in colour space:

$$A^a_\mu = n^a\, A_\mu \quad \text{and} \quad G^a_{\mu\nu} = n^a\, G_{\mu\nu}\ , \tag{5.8}$$

with n^a being a normalised three-dimensional vector. The one-loop effective Lagrangian of such fields is analytically known. It is (see [46]) given by

$$\mathcal{L}^{(1)} = \mathrm{tr}\frac{1}{(4\pi)^2}\int_0^\infty \frac{\mathrm{d}T}{T^3} e^{-m^2T}\left(\frac{sT\hat{n}}{\sinh(sT\hat{n})}\right)^{\frac{D}{2}}\ , \tag{5.9}$$

where $\hat{n} = n^a\boldsymbol{\sigma}^a$, $s^2\mathbf{1} = 2\,\mathrm{tr}[(\mathbf{G}_{\mu\nu})^2]$, $\boldsymbol{\sigma}^a$ are the Pauli matrices and D is the number of dimensions. Setting $D = 4$ we find that

$$\mathcal{L}^{(1)} = \frac{1}{(4\pi)^2}\int_0^\infty \frac{\mathrm{d}T}{T^3} e^{-m^2T}\left(\frac{sT}{\sinh(sT)}\right)^{2}\ . \tag{5.10}$$

Now an assumption is made that this solution can also be utilised for the instanton field, and one uses the s of the instanton:

$$s = \sqrt{\frac{192\rho^4}{(r^2+\rho^2)^4}}\ . \tag{5.11}$$

This yields what we will call the derivative expansion approximation of the one-loop effective Lagrangian density:

$$\mathcal{L}^{(1)}_{DE} = \frac{1}{(4\pi)^2}\int_0^\infty \frac{\mathrm{d}T}{T^3} e^{-m^2T} 2\left(\frac{\frac{\sqrt{12}\rho^2}{(r^2+\rho^2)^2}T}{\sinh(\frac{\sqrt{12}\rho^2}{(r^2+\rho^2)^2}T)}\right)^{2}\ . \tag{5.12}$$

The result of a calculation of the one-loop effective action with this Lagrangian agrees surprisingly well with the known analytical result [45]. Keeping in mind that the derivative expansion approximation is by no means in a strict sense derived, but rather guessed and found to be useful, we will compare the worldline numerical results of the Wilson loop expectation value to the analogous quantity in (5.12)

$$\langle W\rangle_{\mathrm{DE}} = 2\left(\frac{\frac{\sqrt{12}\rho^2}{(r^2+\rho^2)^2}T}{\sinh(\frac{\sqrt{12}\rho^2}{(r^2+\rho^2)^2}T)}\right)^2 . \tag{5.13}$$

We of course do not expect actual agreement of $\langle W\rangle_{\mathrm{DE}}$ and $\langle W\rangle$ but think that since the integration over $\langle W\rangle_{\mathrm{DE}}$ gives an almost correct result they should behave similarly. Moreover, the derivative expansion should become reliable at large r, where the field varies slowly.

5.1.4 Renormalisation

The unrenormalised (and unregularised) one-loop effective action in an BPST instanton background field is given by (see equation (2.59)

$$\begin{aligned}
\Gamma^{(1)} &= -\frac{1}{(4\pi)^2}\int \mathrm{d}^4x \int_0^\infty \frac{\mathrm{d}T}{T^3} e^{-m^2T}\left[\langle W\rangle - 2\right] \\
&= -\frac{1}{(4\pi)^2}\int \mathrm{d}^4x \int_0^\infty \frac{\mathrm{d}T}{T^3} e^{-m^2T}\left[\mathrm{tr}\frac{\int \mathcal{D}y\, e^{-\int_0^1 \mathrm{d}t\,\frac{\dot y^2}{4}}\; P e^{-\sqrt{T}\int_0^1 \mathrm{d}t\,\dot y_\mu \mathbf{A}_\mu(x+\sqrt{T}\,y(t))}}{\int \mathcal{D}y\, e^{-\int_0^1 \mathrm{d}t\,\frac{\dot y^2}{4}}} - 2\right] \\
&= -\frac{1}{(4\pi)^2}\int \mathrm{d}^4x \int_0^\infty \frac{\mathrm{d}T}{T^3} e^{-m^2T}\left[\mathrm{tr}\frac{\int \mathcal{D}y\, e^{-\int_0^1 \mathrm{d}t\,\frac{\dot y^2}{4}}\; P e^{i\sqrt{T}\int_0^1 \mathrm{d}t\,\dot y_\mu \frac{2\eta_{a\mu\nu}(x+\sqrt{T}y)_\nu}{(x+\sqrt{T}y)^2+\rho^2}}}{\int \mathcal{D}y\, e^{-\int_0^1 \mathrm{d}t\,\frac{\dot y^2}{4}}} - 2\right] .
\end{aligned} \tag{5.14}$$

A change of variables $T \to \rho^2 T$ and $x_\mu \to \rho x_\mu$ yields that

$$\begin{aligned}
\Gamma^{(1)} &= -\frac{1}{(4\pi)^2}\int \mathrm{d}^4x \int_0^\infty \frac{\mathrm{d}T}{T^3} e^{-m^2\rho^2T}\left[\mathrm{tr}\frac{\int \mathcal{D}y\, e^{-\int_0^1 \mathrm{d}t\,\frac{\dot y^2}{4}}\; P e^{i\sqrt{T}\int_0^1 \mathrm{d}t\,\dot y_\mu \frac{2\eta_{a\mu\nu}(x+\sqrt{T}y)_\nu}{(x+\sqrt{T}y)^2+1}}}{\int \mathcal{D}y\, e^{-\int_0^1 \mathrm{d}t\,\frac{\dot y^2}{4}}} - 2\right] \\
&= -\frac{1}{(4\pi)^2}\int \mathrm{d}^4x \int_0^\infty \frac{\mathrm{d}T}{T^3} e^{-m^2\rho^2T}\left[\langle W\rangle(\rho=1) - 2\right] ,
\end{aligned} \tag{5.15}$$

where $\langle W\rangle(\rho=1)$ is the Wilson loop expectation value in an instanton background with $\rho = 1$. We find that

$$\Gamma^{(1)}(\rho, m) = \Gamma^{(1)}(m\rho) . \tag{5.16}$$

Using what we found for the renormalised one-loop effective action in section 2.7, we can, in the instanton case, write:

$$\begin{aligned}\Gamma^{(1)}_{\text{ren}} &= \lim_{\Lambda\to\infty}\left[\Gamma^{(1)}_{\text{reg}}(m\rho) + \frac{1}{(4\pi)^2}\int \mathrm{d}^4x \int_{\frac{1}{\Lambda^2}}^{\infty}\frac{\mathrm{d}T}{T}e^{-\mu^2\rho^2T}\frac{1}{12}\mathrm{tr}[(\mathbf{G}_{\mu\nu}(\rho=1))^2]\right] \\ &= \lim_{\Lambda\to\infty}\left[\Gamma^{(1)}_{\text{reg}}(m\rho) + \frac{1}{12(4\pi)^2}\left(-C_{\text{E}} + \ln(\Lambda^2) - \ln(\mu^2\rho^2)\right)\int \mathrm{d}^4x\,\mathrm{tr}[(\mathbf{G}_{\mu\nu}(\rho=1)^2]\right].\end{aligned} \tag{5.17}$$

Because

$$\begin{aligned}\frac{1}{12(4\pi)^2}\int \mathrm{d}^4x\,\mathrm{tr}[(\mathbf{G}_{\mu\nu}(\rho=1))^2] &= \frac{1}{12(4\pi)^2}\int \mathrm{d}^4x\,\frac{96}{(x^2+1)^4} \\ &= \int \mathrm{d}x\,\frac{x^3}{(x^2+1)^4} \\ &= \frac{1}{12}\,,\end{aligned} \tag{5.18}$$

it is possible to divide $\Gamma^{(1)}_{\text{ren}}$ in a part that only depends on $m\rho$, and a part that only depends on $\mu\rho$:

$$\Gamma^{(1)}_{\text{ren}} = \frac{1}{6}\ln(\mu\rho) + \bar{\Gamma}^{(1)}(m\rho)\,. \tag{5.19}$$

$\bar{\Gamma}^{(1)}(m\rho)$ is called the modified one-loop effective action. Since $\bar{\Gamma}^{(1)}$ depends only on $m\rho$, there is no loss of generality if we set $\rho = 1$. We do that if not stated otherwise.

5.2 Worldline numerical results and problems

In this section the numerical results are presented and the problems that have been discovered are explained.

5.2.1 Wilson loop expectation value

For an instanton field every rotation can be undone by a gauge transformation (see e.g. [30]). Together with the gauge invariance of the Wilson loop expectation value (see e.g. [47]), this makes the Wilson loop expectation value even rotationally invariant. The Wilson loop expectation value then depends only on two variables: the proper time T and the distance x of the "centre of mass" of the loop cloud from the origin.

The results of the worldline numerical computation of the Wilson loop expectation value and the corresponding quantity associated with the derivative expansion $\langle W\rangle_{\text{DE}}$ are shown in the figures 5.1 and 5.2. We can see that the results of the worldline computation of the Wilson loop expectation value for the BPST instanton and the singular instanton do *not* agree. In figure 5.1 the Wilson loop expectation value $\langle W\rangle$ is plotted as a function of x and T, in figure 5.2 as a function of T at

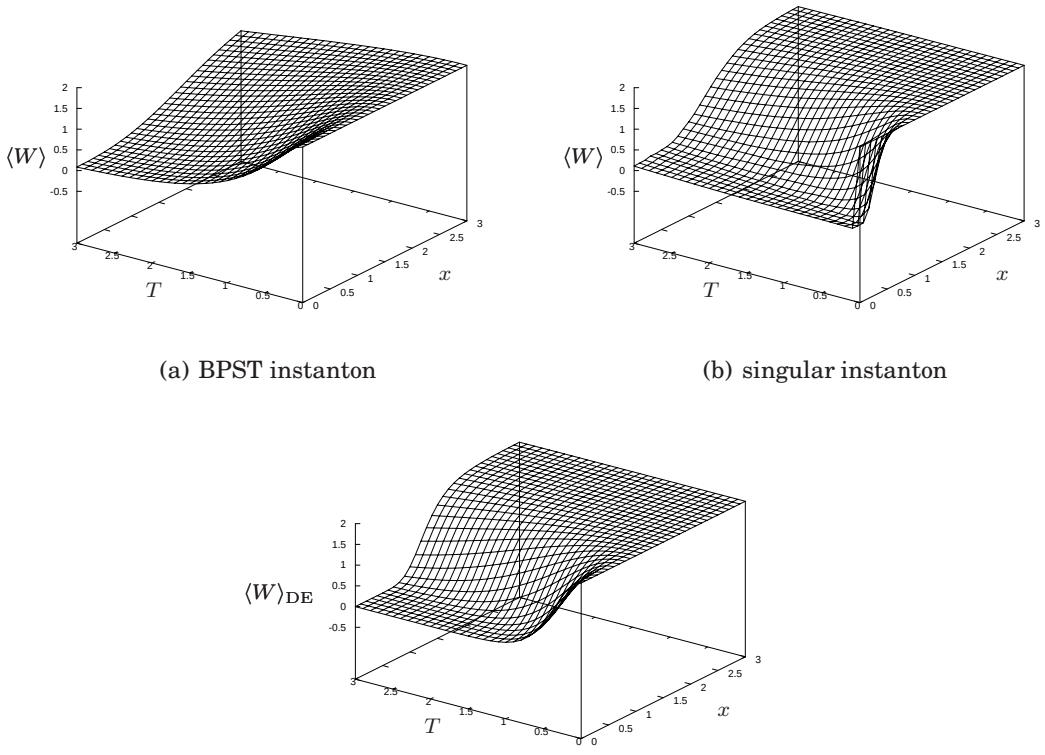

(a) BPST instanton

(b) singular instanton

(c) derivative expansion

Figure 5.1: Estimates of the Wilson loop expectation value of a BPST instanton (a), the singular instanton (b) and the derivative expansion (c). 1000 loops of 301 points were used for the computation.

several values of x. For small x (figure 5.2 (a)), where we do not expect any sensible results for the singular instanton, the singular instanton goes to zero almost instantaneously while the BPST instanton shows a behaviour, which is somewhat similar to the behaviour of $\langle W \rangle_{\mathrm{DE}}$. At $x = 1$ (figure 5.2 (b)) both instantons agree with $\langle W \rangle_{\mathrm{DE}}$ within their errors. For larger x (figure 5.2 (c)-(d)) it is the BPST instanton Wilson loop expectation value that goes to zero much more rapidly than the Wilson loop expectation value of the singular instanton as well as $\langle W \rangle_{\mathrm{DE}}$.

We see that worldline numerics applied in the proposed way is *not* able to com-

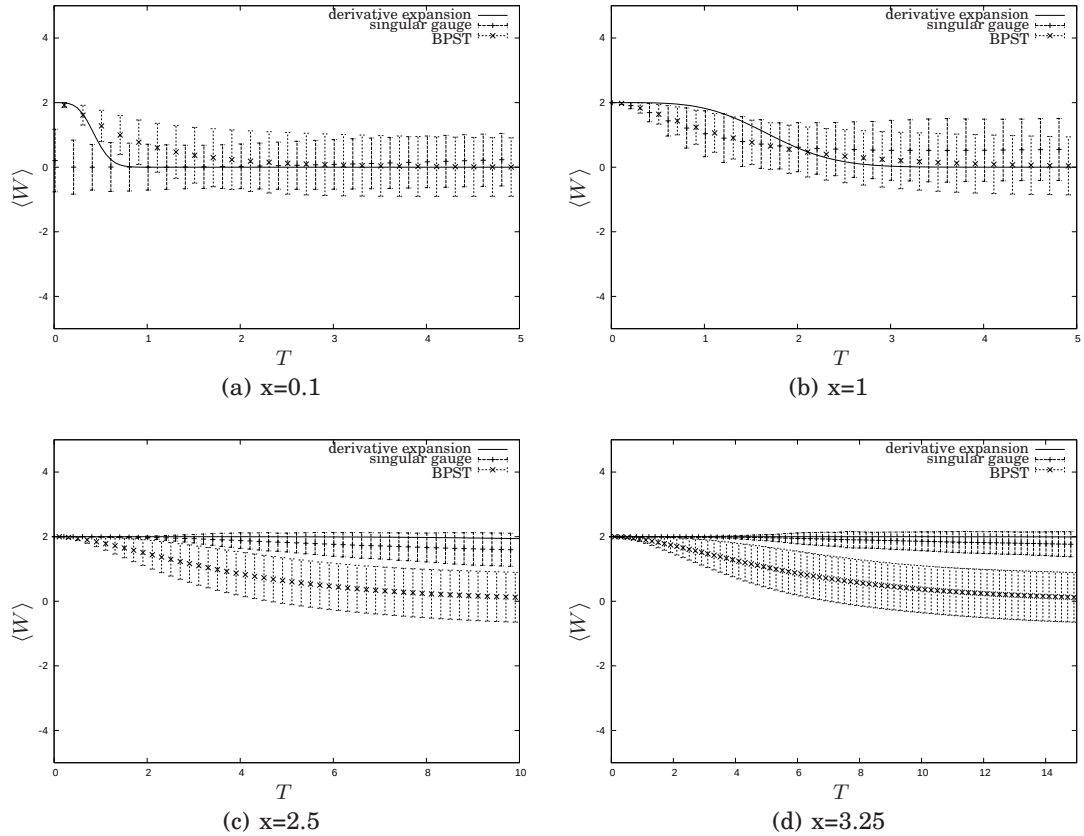

(a) x=0.1 (b) x=1

(c) x=2.5 (d) x=3.25

Figure 5.2: The Wilson loop expectation value of a BPST instanton, a singular instanton and the derivative expansion evaluated at a variety of x values. 3000 loops of 1001 points were used for the computation.

pute the correct Wilson loop expectation value for either the singular or the BPST instanton. For both background fields the Wilson loop expectation value should be equal since they are on the same gauge orbit, which means that one field is just a gauge transform of the other, and the Wilson loop expectation value is gauge invariant. That the singular instanton agrees with the $\langle W \rangle_{\mathrm{DE}}$ if we leave the region of its divergence lets us suspect the BPST instanton of being not easily treatable with standard worldline numerics. A comparison to the inverse mass expansion substantiates this suspicion.

5.2.2 Comparison to the inverse mass expansion

We again fit the Wilson loop expectation value evaluated at fixed x and $T = 0.01n$ with $n = 1, \ldots, 10$ to the polynomial $P = 2 + a_1 T^2 + a_2 T^4 + a_3 T^6 + a_4 T^8$. As above

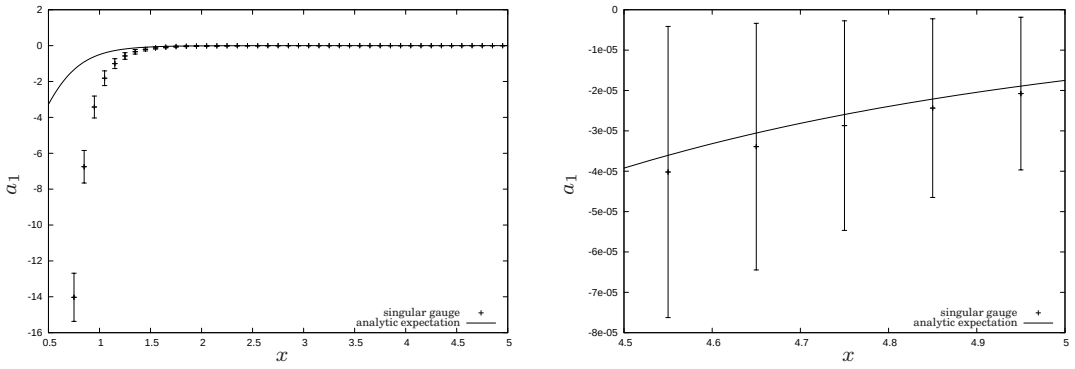

(a) (b)

Figure 5.3: The coefficient a_1 obtained by a fit to P for the singular instanton together with the analytically expected value of a_1 with $0.5 < x < 5$ (a) and $4.5 < x < 5$ (b). 3001 loops of 501 points were used for the computation.

we expect (setting $\rho = 1$) that

$$a_1 \approx \frac{1}{12}\mathrm{tr}[\mathbf{G}_{\mu\nu}\mathbf{G}_{\mu\nu}] = -\frac{8}{(x^2+1)^4}\,. \tag{5.20}$$

In figure 5.3 we find the results of the numerical computation for the singular instanton together with the analytically expected second coefficient in the inverse mass expansion. As can be seen on figure 5.3 (a), for small x the singular instanton really is pretty useless for a straightforward worldline numerical treatment, but the results become better as we go further away form the origin. At about $x = 2$ the numerical data fits the analytic expectation very well. Figure 5.3 (b) is a magnification of the upper right corner of figure 5.3 (a). We see that worldline numerics yields impressively good results for the singular instanton as long as we stay away from the origin.

In the case of the BPST instanton things look differently. Figure 5.4 (a) shows a_1 plotted against x ranging from zero to five. Only close to $x = 0$ the numerically obtained value agrees with the analytical expectation. If we go away from the origin, the deviation from the expected value has a maximum at about $x = 1$ and then it becomes small again. Although the absolute value of the deviation decreases for larger x, the numerical results are still very far away from the expected ones. As can be seen on the double logarithmic plot figure 5.4 (b), they differ by several orders of magnitude. The numerical a_1 agrees with the analytical expectation only very close to $x = 0$ within its errors. Away from $x = 0$ the worldline numerical results are a mess.

That the statistical errors are quite small hints at a systematic problem of some kind that is not solely caused by the use of a finite number of loops. Increasing the number of loops n_L or the number of points per loop n_p, indeed does not improve the

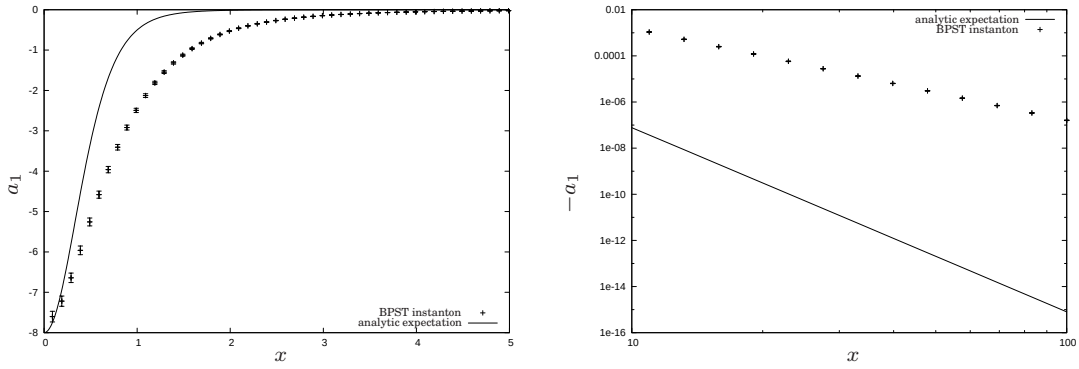

(a) (b)

Figure 5.4: The coefficient a_1 obtained by a fit to P for the BPST instanton together with the analytically expected value of a_1 with $0 < x < 5$ (a) and with inverted sign double logarithmically with $10 < x < 100$ (b). 3001 loops of 501 points were used for the computation.

results notably as is shown on figure 5.5 and figure 5.6, for which several different loop clouds were used.

In figure 5.6 (a) we see the worldline numerical a_1 calculated at $x = 100$, with a fixed number of points $n_p = 101$, plotted as a function of the number of loops n_L that were used in the computation. A logarithmic plot of 5.6 (a) is shown in figure 5.6 (b). It tells us that while increasing the n_L improves the result, it does so at terrible speed. Trying to reduce the error to a reasonable size by brute force, i.e. by enlarging the loop cloud, therefore does not work in practice.

In figure 5.7 we have an amended replot of figure 5.4 (b), in which we left out the error and added the function $f(x)$, which was obtained by fitting the function $f(x) = c\,(x-a)^b$ onto the Wilson loop expectation value in a BPST instanton background. The fit gave us: $c = 18.0748$, $b = -4.02788$ and $a = -0.21048$. The a_1 computed using worldline numerics does not fall off like x^{-8} as we would have expected (and the singular instanton Wilson loop expectation value does), but like x^{-4}.

5.2.3 The problem

The Wilson loop expectation value of two instanton background fields behave very differently. While the singular instanton behaves as expected, i.e. gives useless results close to $x = 0$ and sensible results for $x > 2.5$, the BPST instanton does not agree with any analytic knowledge we have. It deviates from the $\langle W \rangle_{\mathrm{DE}}$ to a large extent and the second coefficient obtained by a fit matches the analytical one only very close to $x = 0$.

Because our method works as well (and badly) as expected for the singular instanton, it is clear that the problem does not affect every non-abelian field. In addition to that, such a difficulty has not yet been observed in any of the calculations

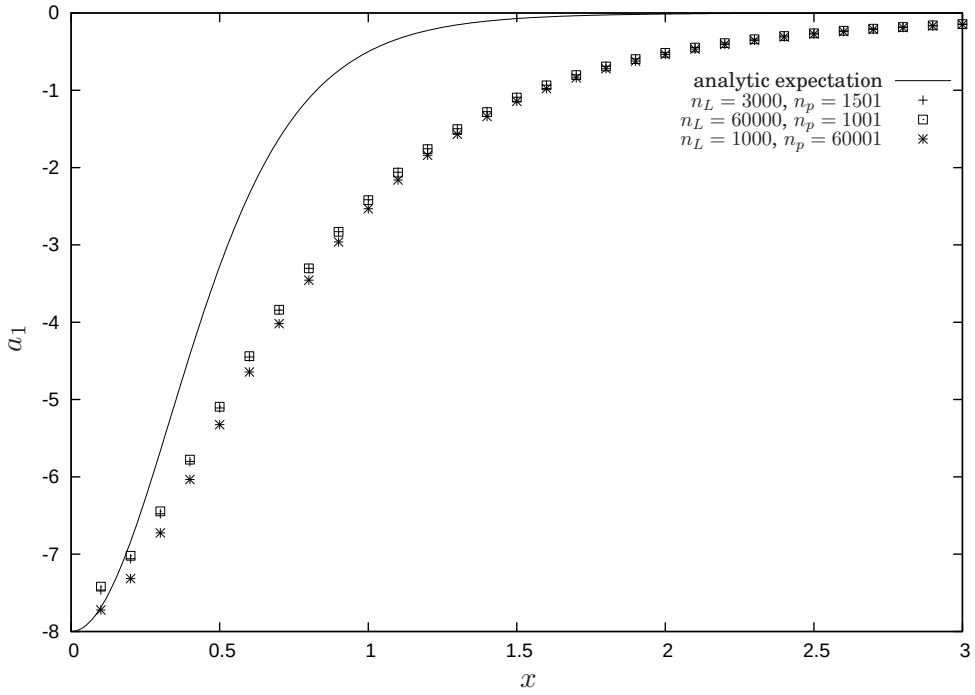

Figure 5.5: The analytically expected and the numerical value of a_1 for the BPST instanton computed with various loop clouds.

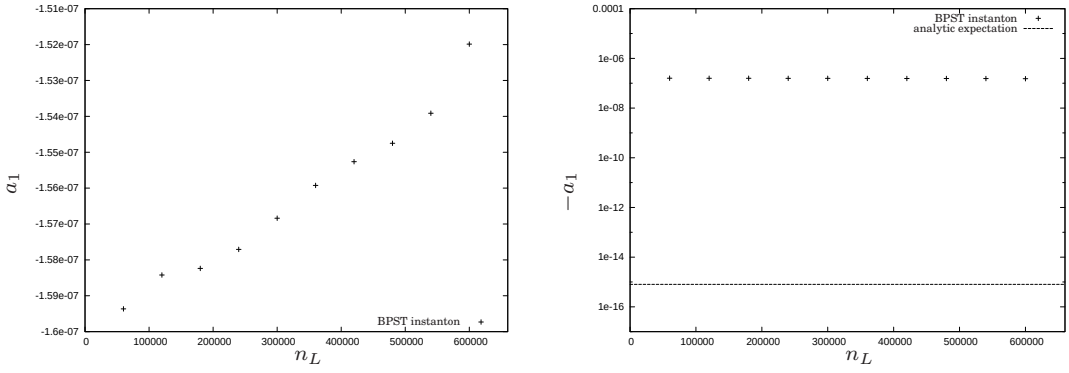

(a) (b)

Figure 5.6: The worldline numerical a_1 as a function of the number of loops n_L at fixed $x = 100$. In (b) a logarithmic plot of the a_1 and the analytic expected value is show. 101 points were used for the computation.

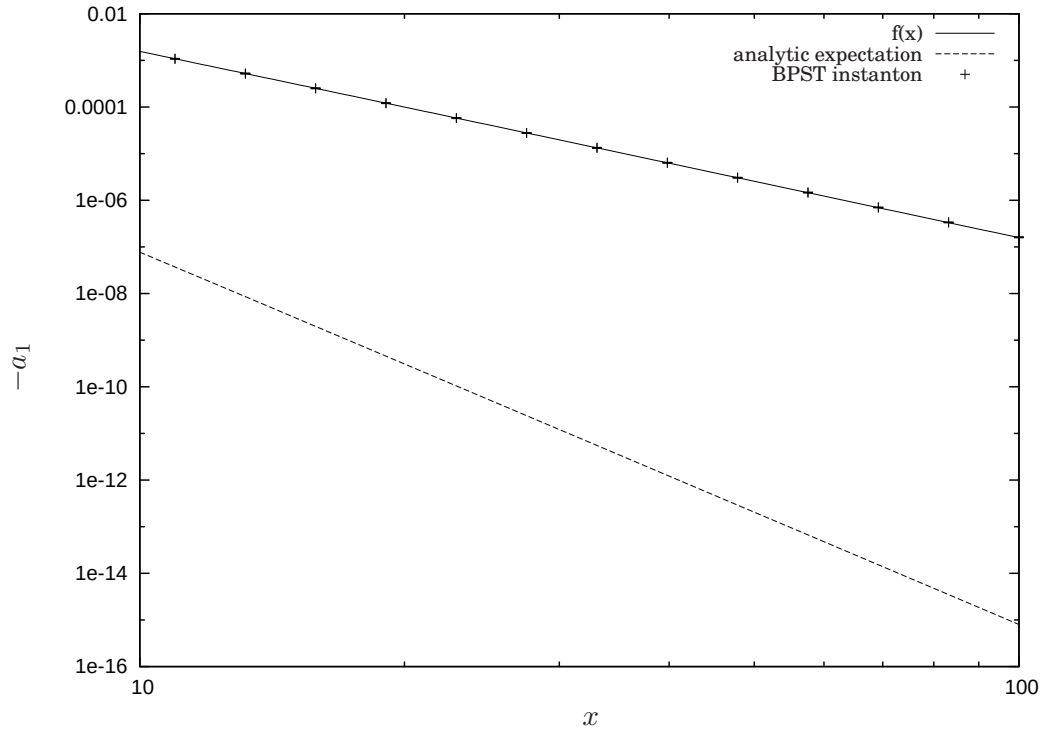

Figure 5.7: Double logarithmic plot of a_1, the analytically expected value and the function $f(x) = 18.0748\,(x + 0.21048)^{-4.02788}$, which was the result of a fit. 3000 loops of 501 points were used for the computation.

involving Abelian fields.

The unfavourable behaviour of the Wilson loop expectation value in a BPST instanton background field is certainly a non-abelian effect.

5.3 The inverse mass expansion in terms of the gauge field

To get a better idea of what is being calculated, we have a closer look at a_1, which is the coefficient of $O(T^2)$ in the inverse mass expansion, expressed entirely in terms of the gauge fields, as the computer calculates it, i.e. with a discretised proper time parameter. While this is certainly not the expression one can most easily digest, it clarifies the calculation performed by the computer a great deal, making it possible for us to track down possible weaknesses of the method. As is derived in section A.4.2, a Monte Carlo estimate of a_1, which we call a_{MC}, is given by

$$
\begin{aligned}
a_{\mathrm{MC}} = \mathrm{tr}\,\big\langle\; & -\frac{1}{6}\,\partial_\nu\partial_\alpha\partial_\beta\mathbf{A}_\mu(x)\sum_{n=1}^{n_p} y'^n_\mu\tilde{y}^n_\nu\tilde{y}^n_\alpha\tilde{y}^n_\beta \\
& +\frac{1}{2}\,\partial_\nu\partial_\alpha\mathbf{A}_\mu(x)\mathbf{A}_\beta(x)\sum_{n=1}^{n_p} y'^n_\beta y'^n_\mu\tilde{y}^n_\nu\tilde{y}^n_\alpha \\
& +\frac{1}{2}\,\partial_\nu\mathbf{A}_\mu(x)\partial_\beta\mathbf{A}_\alpha(x)\sum_{n=1}^{n_p} y'^n_\alpha y'^n_\mu\tilde{y}^n_\beta\tilde{y}^n_\nu \\
& -\frac{1}{2}\,\partial_\nu\mathbf{A}_\mu(x)\mathbf{A}_\alpha(x)\mathbf{A}_\beta(x)\sum_{n=1}^{n_p} y'^n_\mu y'^n_\alpha y'^n_\beta\tilde{y}^n_\nu \\
& +\frac{1}{24}\,\mathbf{A}_\mu(x)\mathbf{A}_\alpha(x)\mathbf{A}_\nu(x)\mathbf{A}_\beta(x)\sum_{n=1}^{n_p} y'^n_\mu y'^n_\alpha y'^n_\nu y'^n_\beta \\
& +\frac{1}{2}\,\partial_\nu\partial_\alpha\mathbf{A}_\mu(x)\mathbf{A}_\beta(x)\sum_{n=1}^{n_p}\sum_{j=1}^{n-1} y'^j_\beta y'^n_\mu\tilde{y}^n_\nu\tilde{y}^n_\alpha \\
& +\frac{1}{2}\,\mathbf{A}_\beta(x)\partial_\nu\partial_\alpha\mathbf{A}_\mu(x)\sum_{n=1}^{n_p}\sum_{j=1}^{n-1} y'^n_\beta y'^j_\mu\tilde{y}^j_\nu\tilde{y}^j_\alpha \\
& -\partial_\nu\mathbf{A}_\mu(x)\mathbf{A}_\beta(x)\mathbf{A}_\nu(x)\sum_{n=1}^{n_p}\sum_{j=1}^{n-1} y'^j_\nu y'^n_\mu y'^n_\beta\tilde{y}^n_\nu \\
& -\mathbf{A}_\nu(x)\partial_\nu\mathbf{A}_\mu(x)\mathbf{A}_\beta(x)\sum_{n=1}^{n_p}\sum_{j=1}^{n-1} y'^n_\nu y'^j_\mu y'^j_\beta\tilde{y}^j_\nu \\
& +\frac{1}{6}\,\mathbf{A}_\mu(x)\mathbf{A}_\alpha(x)\mathbf{A}_\beta(x)\mathbf{A}_\nu(x)\sum_{n=1}^{n_p}\sum_{j=1}^{n-1} y'^j_\nu y'^n_\beta y'^n_\alpha y'^n_\mu
\end{aligned}
$$

$$
\begin{aligned}
&+\frac{1}{6}\,\mathbf{A}_\nu(x)\mathbf{A}_\mu(x)\mathbf{A}_\alpha(x)\mathbf{A}_\beta(x)\sum_{n=1}^{n_p}\sum_{j=1}^{n-1} y'^{n}_{\nu}y'^{j}_{\beta}y'^{j}_{\alpha}y'^{j}_{\mu}\\
&+\partial_\nu\mathbf{A}_\mu(x)\partial_\alpha\mathbf{A}_\beta(x)\sum_{n=1}^{n_p}\sum_{j=1}^{n-1} y'^{n}_{\mu}\tilde{y}^{n}_{\nu}y'^{j}_{\alpha}\tilde{y}^{j}_{\beta}\\
&-\frac{1}{2}\partial_\nu\mathbf{A}_\mu(x)\mathbf{A}_\beta(x)\mathbf{A}_\alpha(x)\sum_{n=1}^{n_p}\sum_{j=1}^{n-1} y'^{n}_{\mu}\tilde{y}^{n}_{\nu}y'^{j}_{\alpha}y'^{j}_{\beta}\\
&-\frac{1}{2}\mathbf{A}_\beta(x)\mathbf{A}_\alpha(x)\partial_\nu\mathbf{A}_\mu(x)\sum_{n=1}^{n_p}\sum_{j=1}^{n-1} y'^{j}_{\mu}\tilde{y}^{j}_{\nu}y'^{n}_{\alpha}y'^{n}_{\beta}\\
&-\mathbf{A}_\mu(x)\mathbf{A}_\alpha(x)\partial_\beta\mathbf{A}_\nu(x)\sum_{n=1}^{n_p}\sum_{j=1}^{n-1}\sum_{r=1}^{j-1} y'^{n}_{\mu}y'^{j}_{\alpha}y'^{r}_{\nu}\tilde{y}^{r}_{\beta}\\
&-\mathbf{A}_\mu(x)\partial_\beta\mathbf{A}_\nu(x)\mathbf{A}_\alpha(x)\sum_{n=1}^{n_p}\sum_{j=1}^{n-1}\sum_{r=1}^{j-1} y'^{n}_{\mu}y'^{r}_{\alpha}y'^{j}_{\nu}\tilde{y}^{j}_{\beta}\\
&-\partial_\beta\mathbf{A}_\nu(x)\mathbf{A}_\mu(x)\mathbf{A}_\alpha(x)\sum_{n=1}^{n_p}\sum_{j=1}^{n-1}\sum_{r=1}^{j-1} y'^{j}_{\mu}y'^{r}_{\alpha}y'^{n}_{\nu}\tilde{y}^{n}_{\beta}\\
&+\frac{1}{2}\mathbf{A}_\mu(x)\mathbf{A}_\alpha(x)\mathbf{A}_\beta(x)\mathbf{A}_\nu(x)\sum_{n=1}^{n_p}\sum_{j=1}^{n-1}\sum_{r=1}^{j-1} y'^{n}_{\mu}y'^{j}_{\alpha}y'^{r}_{\beta}y'^{r}_{\nu}\\
&+\frac{1}{2}\mathbf{A}_\mu(x)\mathbf{A}_\alpha(x)\mathbf{A}_\beta(x)\mathbf{A}_\nu(x)\sum_{n=1}^{n_p}\sum_{j=1}^{n-1}\sum_{r=1}^{j-1} y'^{n}_{\mu}y'^{j}_{\alpha}y'^{j}_{\beta}y'^{r}_{\nu}\\
&+\frac{1}{2}\mathbf{A}_\mu(x)\mathbf{A}_\alpha(x)\mathbf{A}_\beta(x)\mathbf{A}_\nu(x)\sum_{n=1}^{n_p}\sum_{j=1}^{n-1}\sum_{r=1}^{j-1} y'^{n}_{\mu}y'^{n}_{\alpha}y'^{j}_{\beta}y'^{r}_{\nu}\\
&+\mathbf{A}_\mu(x)\mathbf{A}_\alpha(x)\mathbf{A}_\beta(x)\mathbf{A}_\nu(x)\sum_{n=1}^{n_p}\sum_{j=1}^{n-1}\sum_{r=1}^{j-1}\sum_{l=1}^{r-1} y'^{n}_{\mu}y'^{j}_{\alpha}y'^{r}_{\beta}y'^{l}_{\nu}\,\Big\rangle\,,
\end{aligned}
\tag{5.21}
$$

where

$$
y'^{n}_{\mu} = (y^{n}_{\mu} - y^{n-1}_{\mu}) \quad \text{and} \quad \tilde{y}^{n}_{\mu} = \frac{y^{n}_{\mu} + y^{n-1}_{\mu}}{2}\,, \tag{5.22}
$$

where n_p is the number of points on a loop used to perform the calculation. The $\langle \dots \rangle$ accounts for the fact that we have to calculate the expectation value as we are used to: by summing over all the loops in the loop cloud. Being derived by a Taylor expansion of the Monte Carlo estimate of the Wilson loop expectation value, a_{MC} given in (5.21) is the best result of the numerical evaluation of a_1 through the fitting procedure that we can hope for. This is because the fitting procedure does not give us an estimate of a_1 but of a_{MC}. In the limit $n_p, n_L \to \infty$, both, a_{MC}, which is the best possible outcome of the fitting procedure, and a_1, which is obtained the

usual way using the Schwinger-Fock gauge, should of course be equal, i.e.

$$\begin{aligned}\lim_{n_p,n_L\to\infty} a_{\mathrm{MC}} &= \frac{1}{12}\mathrm{tr}[(\mathbf{G}_{\mu\nu})^2] \\ &= \frac{1}{12}\big\{2\,\mathrm{tr}\big[\partial_\mu \mathbf{A}_\nu \partial_\mu \mathbf{A}_\nu - \partial_\mu \mathbf{A}_\nu \partial_\nu \mathbf{A}_\mu\big] \\ &\qquad + 2\,\mathrm{tr}\big[\mathbf{A}_\mu \mathbf{A}_\nu [\mathbf{A}_\mu, \mathbf{A}_\nu]\big] - 4\,\mathrm{tr}\big[(\partial_\mu \mathbf{A}_\nu)[\mathbf{A}_\mu, \mathbf{A}_\nu]\big]\big\}\ . \end{aligned} \tag{5.23}$$

The expectation value of a sum like (5.21) can be found by calculating the expectation value of every term. We thus are left with a whole bunch of expectation values of the kind $\langle \sum \dots \rangle$. In the continuum limit we find that

$$n_p\, y'^n_\mu = n_p\, (y^n_\mu - y^{n-1}_\mu) \to \dot{y}_\mu(t = n/n_p) \tag{5.24}$$

and

$$\tilde{y}^n_\mu = \frac{y^n_\mu + y^{n-1}_\mu}{2} \to y_\mu(t = n/n_p)\ . \tag{5.25}$$

The sums therefore become

$$\begin{aligned}\langle \sum_n^{n_p} \sum_j^{n-1} \dots \rangle \to & \langle \int_0^1 \mathrm{d}t \int_0^t \mathrm{d}t' \dots \rangle \\ &= \int_0^1 \mathrm{d}t \int_0^t \mathrm{d}t' \dots \langle \dots \rangle\ . \end{aligned} \tag{5.26}$$

For the 14th summand in (5.21) we for example find that

$$\begin{aligned}\lim_{n_p,n_L\to\infty} \langle\ \partial_\nu \mathbf{A}_\mu(x) \partial_\alpha \mathbf{A}_\beta(x) \sum_{n=1}^{n_p} \sum_{j=1}^{n-1} y'^n_\mu \tilde{y}^n_\nu y'^j_\alpha \tilde{y}^j_\beta\ \rangle = \\ \partial_\nu \mathbf{A}_\mu(x) \partial_\alpha \mathbf{A}_\beta(x) \int_0^1 \mathrm{d}t \int_0^t \mathrm{d}t' \dots \langle\ \dot{y}_\mu(t) y_\nu(t) \dot{y}_\alpha(t') y_\beta(t')\ \rangle\ . \end{aligned} \tag{5.27}$$

Equation (5.23) requires the various terms containing worldline correlation functions in (5.21) to cancel each other in a very specific manner. How well these correlation functions are numerically calculated therefore governs how well (5.23) is realised by the computer and the correct result produced by worldline numerical calculations. In the case of the BPST instanton all the combinations of the field in (5.21) for big x fall off like x^{-4}, but the analytic a_1 falls off like x^{-8}. If the worldline correlation functions are not computed with sufficient accuracy, we are necessarily left with a term which shows the wrong large-x-behaviour that we see for a_1 obtained by the fitting procedure for the BPST instanton (see figure 5.7).

5.4 Worldline correlation functions

In this section we focus on the worldline numerical calculation of worldline correlation functions. As has been explained in the preceding section, being able to compute worldline correlation functions well enough is expected to make it possible to compute the Wilson loop expectation value and therefore the effective action.

5.4.1 Inverse mass expansion for an Abelian gauge theory

As is explained in section A.4.1, in the case of an Abelian gauge field a_1 is given by

$$\begin{aligned} a_1 = \partial_\nu\partial_\alpha\partial_\beta A_\mu(x) \int_0^1 \mathrm{d}t \,\langle\, \dot{y}_\mu(t) y_\nu(t) y_\alpha(t) y_\beta(t) \,\rangle \\ + \frac{1}{2}\,\partial_\nu A_\mu(x)\,\partial_\beta A_\alpha(x) \int_0^1 \mathrm{d}t \int_0^1 \mathrm{d}t' \,\langle\, \dot{y}_\mu(t) y_\nu(t) \dot{y}_\alpha(t') y_\beta(t') \,\rangle\,. \end{aligned} \tag{5.28}$$

We see that a_1 has two contributions. They are build out of two parts: One involving the gauge field and its derivatives and one involving a worldline correlation function. These correlation functions are about to be evaluated. But first we need to learn how.

5.4.2 How to calculate worldline correlation functions

To be able to calculate worldline correlation functions analytically, we need to know how to Wick contract as well as the solution of the worldline 2-point function

$$\begin{aligned} \langle\, y_\mu(t) y_\nu(t') \,\rangle =& \frac{1}{\mathcal{N}} \int \mathcal{D}y\, e^{-\int_0^1 \mathrm{d}t\, \frac{\dot{y}^2}{4}}\; y_\mu(t) y_\nu(t') \\ =& \frac{1}{\mathcal{N}} \int \mathcal{D}y\, e^{-\int_0^1 \mathrm{d}t\, \frac{1}{4} y(-\frac{d^2}{dt^2})y}\; y_\mu(t) y_\nu(t')\,, \end{aligned} \tag{5.29}$$

where $\mathcal{N}$ serves to normalise the integral and a partial integration was performed in the exponent. Expression (5.29) does not only look like the 2-point function in a free quantum field theory, with $-\int_0^1 \mathrm{d}t\, \frac{1}{4} y \frac{d^2}{dt^2} y$ serving as action, but can also be evaluated the same way. All we need is the inverse of the differential operator appearing in the exponent (acting on closed loops with common "centre of mass" zero, parametrised by a parameter $\in [0,1]$):

$$\langle t' | \frac{d^2}{dt^2}^{-1} | t'' \rangle = \frac{1}{2}\,\mathcal{G}(t',t'')\,, \tag{5.30}$$

with $\mathcal{G}(t',t'')$ being the worldline Green's function. It is given by

$$\mathcal{G}(t',t'') = |t'-t''| - (t'-t'')^2 - \frac{1}{6}\,. \tag{5.31}$$

Its derivatives with respect of the first variable are

$$\dot{\mathcal{G}}(t',t'') = \mathrm{sign}(t'-t'') - 2(t'-t'') \tag{5.32}$$

and

$$\ddot{\mathcal{G}}(t',t'') = 2\delta(t'-t'') - 2\ . \tag{5.33}$$

With the second derivative of $\mathcal{G}(t',t'')$ it is easy to show that the given Green's functions really satisfy (5.30). We simply have to plug (5.30) into the definition of an inverse operator. We see that the function on which both operators act is reproduced:

$$\begin{aligned}\frac{d^2}{dt^2}\int_0^1 \mathrm{d}t' \frac{1}{2}\mathcal{G}(t,t')y(t') &= \int_0^1 \mathrm{d}t' \frac{1}{2}\ddot{\mathcal{G}}(t,t')y(t') \\ &= \int_0^1 \mathrm{d}t'\delta(t-t')y(t') - \int_0^1 \mathrm{d}t' y(t') \\ &= y(t)\ ,\end{aligned} \tag{5.34}$$

where $y(t)$ is a function defined on a circle of circumference one, with a "centre of mass" of zero $\big(\int_0^1 \mathrm{d}t\ y(t) = 0\big)$. For the 2-point correlation function we therefore find that

$$\begin{aligned}\langle\ y_\mu(t)y_\nu(t')\ \rangle &= -\ \delta_{\mu\nu}\ \mathcal{G}(t,t') \\ &= -\ \delta_{\mu\nu}\ \big(|t-t'| - (t-t')^2 - \frac{1}{6}\big)\ ,\end{aligned} \tag{5.35}$$

and for the 2-point function involving derivatives that

$$\begin{aligned}\langle\ \dot{y}_\mu(t)y_\nu(t')\ \rangle &= -\ \langle\ y_\mu(t)\dot{y}_\nu(t')\ \rangle \\ &= -\ \delta_{\mu\nu}\ \dot{\mathcal{G}}(t,t') \\ &= \mathrm{sign}(t-t') - 2(t-t')\end{aligned} \tag{5.36}$$

and

$$\begin{aligned}\langle\ \dot{y}_\mu(t)\dot{y}_\nu(t')\ \rangle &= -\ \langle\ \ddot{y}_\mu(t)y_\nu(t')\ \rangle \\ &= \delta_{\mu\nu}\ \ddot{\mathcal{G}}(t,t') \\ &= 2\delta(t-t') - 2\ .\end{aligned} \tag{5.37}$$

5.4.3 Inverse mass expansion for an Abelian gauge theory (revisited)

The first summand in (5.28) contains an integration over a worldline correlation function. It looks like

$$\int_0^1 \mathrm{d}t\ \langle\ \dot{y}_\mu(t)y_\nu(t)y_\alpha(t)y_\beta(t)\ \rangle\ . \tag{5.38}$$

To evaluate it, we have to perform Wick contractions. The "fields", of which the expectation value is to be taken, are grouped in pairs and the resulting 2-point functions are multiplied. We do this in all possible ways and sum.

Equation (5.38) is particularly easy to evaluate. If cyclic permutations of ν, α and β are taken into account, all possible Wick contractions are given by

$$\begin{aligned}\langle\, \dot{y}_\mu(t) y_\nu(t)\,\rangle\langle\, y_\alpha(t) y_\beta(t)\,\rangle &= -\,\delta_{\mu\nu}\,\dot{\mathcal{G}}(t,t)\langle\, y_\alpha(t) y_\beta(t)\,\rangle \\ &= \operatorname{sign}(t-t) - 2(t-t)\rangle\langle\, y_\alpha(t) y_\beta(t)\,\rangle \\ &= 0\,, \end{aligned} \tag{5.39}$$

where we have used (5.36). We therefore find that

$$\int_0^1 \mathrm{d}t\,\langle\, \dot{y}_\mu(t) y_\nu(t) y_\alpha(t) y_\beta(t)\,\rangle \;=\; 0. \tag{5.40}$$

The evaluation of the other integral in (5.28)

$$\int_0^1 \mathrm{d}t \int_0^1 \mathrm{d}t'\,\langle\, \dot{y}_\mu(t) y_\nu(t) \dot{y}_\alpha(t') y_\beta(t')\,\rangle \tag{5.41}$$

is less boring. By the same argument as above, all but two Wick contractions are zero. This yields that

$$\begin{aligned}\int_0^1 \mathrm{d}t \int_0^1 \mathrm{d}t'\,\langle\, \dot{y}_\mu(t) y_\nu(t) \dot{y}_\alpha(t') y_\beta(t')\,\rangle = \int_0^1 \mathrm{d}t \int_0^1 \mathrm{d}t'\,\big[&\langle\, \dot{y}_\mu(t) \dot{y}_\alpha(t')\,\rangle\langle\, y_\nu(t) y_\beta(t')\,\rangle \\ &+ \langle\, \dot{y}_\mu(t) y_\beta(t')\,\rangle\langle\, y_\nu(t) \dot{y}_\alpha(t')\,\rangle\big]\,, \end{aligned} \tag{5.42}$$

and with (5.35) and (5.36) this is

$$\begin{aligned} &= -\int_0^1 \mathrm{d}t \int_0^1 \mathrm{d}t'\;\delta_{\mu\alpha}\,\ddot{\mathcal{G}}(t,t')\delta_{\nu\beta}\,\mathcal{G}(t,t') \\ &\quad -\int_0^1 \mathrm{d}t \int_0^1 \mathrm{d}t'\;\delta_{\mu\beta}\dot{\mathcal{G}}(t,t')\,\delta_{\nu\alpha}\dot{\mathcal{G}}(t,t')\,. \end{aligned} \tag{5.43}$$

Now we perform the integrations to get

$$\begin{aligned}\int_0^1 \mathrm{d}t \int_0^1 \mathrm{d}t'\,\ddot{\mathcal{G}}(t,t')\mathcal{G}(t,t') &= \int_0^1 \mathrm{d}t \int_0^1 \mathrm{d}t'\,\left[2\delta(t-t') - 2\right]\left[|t-t'| - (t-t')^2 - \frac{1}{6}\right] \\ &= \int_0^1 \mathrm{d}t \int_0^1 \mathrm{d}t'\,\left[2\delta(t-t')|t-t'| - 2\delta(t-t')(t-t')^2 - 2\delta(t-t')\frac{1}{6}\right. \\ &\qquad \left. - 2|t-t'| + 2(t-t')^2 + 2\frac{1}{6}\right] \\ &= 2\int_0^1 \mathrm{d}t\,\left[|t-t| - (t-t)^2 - \frac{1}{6} + \frac{1}{6}\right] \end{aligned}$$

$$
\begin{aligned}
&+ 2 \int_0^1 \mathrm{d}t \int_{-t}^{1-t} \mathrm{d}x \, [x^2 - |x|] \\
=&2 \int_0^1 \mathrm{d}t \left[\frac{1}{3}\big((1-t)^3 + t^3\big) + \int_{-t}^{0} \mathrm{d}x \, x - \int_0^{1-t} \mathrm{d}x \, x \right] \\
=&2 \int_0^1 \mathrm{d}t \left[\frac{1}{3}\big((1-t)^3 + t^3\big) - \frac{1}{2}(t^2 + (1-t)^2) \right] \\
=&2 \left[\frac{1}{12}(1+1) - \frac{1}{6}(1+1) \right] \\
=&-\frac{1}{3}
\end{aligned} \tag{5.44}
$$

and

$$
\begin{aligned}
\int_0^1 \mathrm{d}t \int_0^1 \mathrm{d}t' \, \dot{\mathcal{G}}(t,t')\dot{\mathcal{G}}(t,t') =& \int_0^1 \mathrm{d}t \int_0^1 \mathrm{d}t' \, \left[\mathrm{sign}(t-t') - 2(t-t')\right]^2 \\
=& \int_0^1 \mathrm{d}t \int_0^1 \mathrm{d}t' \, \left[1 - 4(t-t')\mathrm{sign}(t-t') + 4(t-t')^2\right] \\
=&1 + \int_0^1 \mathrm{d}t \int_{-t}^{1-t} \mathrm{d}x \, x^2 - 4 \int_0^1 \mathrm{d}t \int_{-t}^{1-t} \mathrm{d}x \, |x| \, .
\end{aligned} \tag{5.45}
$$

We have already solved these integrals in (5.44) and can therefore write that

$$
\begin{aligned}
\int_0^1 \mathrm{d}t \int_0^1 \mathrm{d}t' \, \dot{\mathcal{G}}(t,t')\dot{\mathcal{G}}(t,t') =&1 - \frac{4}{6} \\
=&\frac{1}{3} \, .
\end{aligned} \tag{5.46}
$$

Putting it all together, $\int_0^1 \mathrm{d}t \int_0^1 \mathrm{d}t' \, \langle \, \dot{y}_\mu(t) y_\nu(t) \dot{y}_\alpha(t') y_\beta(t') \, \rangle$ turns out to be

$$
\int_0^1 \mathrm{d}t \int_0^1 \mathrm{d}t' \, \langle \, \dot{y}_\mu(t) y_\nu(t) \dot{y}_\alpha(t') y_\beta(t') \, \rangle = \frac{1}{3} \, (\delta_{\mu\alpha}\delta_{\nu\beta} - \delta_{\mu\beta}\delta_{\nu\alpha}) \, . \tag{5.47}
$$

For the coefficient of order T^2 this means that

$$
\begin{aligned}
a_1 &= \frac{1}{2} \, \partial_\nu A_\mu(x) \, \partial_\beta A_\alpha(x) \, \frac{1}{3} \, (\delta_{\mu\alpha}\delta_{\nu\beta} - \delta_{\mu\beta}\delta_{\nu\alpha}) \\
&= \frac{1}{6}\big[\big(\partial_\nu A_\mu(x)\big)^2 - \partial_\nu A_\mu(x) \partial_\mu A_\nu(x)\big] \\
&= \frac{1}{12}\big[\partial_\mu A_\nu(x) - \partial_\nu A_\mu(x)\big]^2 \\
&= \frac{1}{12}\mathrm{tr}[(\mathbf{G}_{\mu\nu})^2] \, ,
\end{aligned} \tag{5.48}
$$

just as we would have expected.

5.4.4 Numerical results for a worldline correlation function

We are now going to investigate how well worldline numerics is able to reproduce the results of integrations over worldline correlation functions. This is done for the only one that in the Abelian case gives a nonzero contribution to a_1:

$$\int_0^1 \mathrm{d}t \int_0^1 \mathrm{d}t' \, \langle \, \dot{y}_\mu(t) y_\nu(t) \dot{y}_\alpha(t') y_\beta(t') \, \rangle = \frac{1}{3} \left(\delta_{\mu\alpha}\delta_{\nu\beta} - \delta_{\mu\beta}\delta_{\nu\alpha} \right) . \tag{5.49}$$

A sample of the results of a straightforward implementation is shown in table 5.1. The complete list of the numerical results can be found in section A.5 on table A.1. The combinations of μ, ν, α and β can be divided into three classes.

μ	ν	α	β	worldline result	μ	ν	α	β	worldline result
0	1	0	1	0.274591	0	1	0	2	-0.046134
0	1	0	3	0.00285352	0	1	1	0	-0.274591
0	1	1	2	-0.00971428	0	1	1	3	-0.0339902
0	1	2	0	0.046134	0	1	2	1	0.00971428
0	1	2	3	-0.00776091	0	1	3	0	-0.00285352
0	1	3	1	0.0339902	0	1	3	2	0.00776091
0	2	0	1	-0.046134	0	2	0	2	0.277747
0	2	0	3	-0.0207131	0	2	1	0	0.046134
0	2	1	2	0.0284149	0	2	1	3	-0.0131166
0	2	2	0	-0.277747	0	2	2	1	-0.0284149
0	2	2	3	-0.0555001	0	2	3	0	0.0207131
0	2	3	1	0.0131166	0	2	3	2	0.0555001
0	3	0	1	0.00285352	0	3	0	2	-0.0207131
0	3	0	3	0.319711	0	3	1	0	-0.00285352
0	3	1	2	-0.0687531	0	3	1	3	0.0299561
0	3	2	0	0.0207131	0	3	2	1	0.0687531
0	3	2	3	0.00385483	0	3	3	0	-0.319711
0	3	3	1	-0.0299561	0	3	3	2	-0.00385483

Table 5.1: Table with the numerical results for $\int_0^1 \mathrm{d}t \int_0^1 \mathrm{d}t' \, \langle \, \dot{y}_\mu(t) y_\nu(t) \dot{y}_\alpha(t') y_\beta(t') \, \rangle$; only components with $\mu = 0$ that are bigger than 10^{-15} are shown. 100 loops of 101 points were used for the computation

- Combinations for which $\delta_{\mu\alpha}\delta_{\nu\beta} - \delta_{\mu\beta}\delta_{\nu\alpha} \neq 0$:

  Worldline numerics gives an estimate of the expected value, which is $(\pm)\frac{1}{3}$.

- Combinations where the indices of two loops depending on the same integration variable are equal (not shown in table 5.1):

The expected value of zero is reproduced to a very high degree of precision. Only rounding errors contribute to the deviation from zero. Starting from the double sum, of which the computer calculates the mean value, we can quite easily see why this is the case:

$$\sum_{n=1}^{n} n_p \sum_{j=1}^{n_p} y'^n_\mu \tilde{y}^n_\mu y'^j_\alpha \tilde{y}^j_\beta = \sum_{n=1}^{n_p} y'^n_\mu \tilde{y}^n_\mu \underbrace{\sum_{j=1}^{n_p} y'^j_\alpha \tilde{y}^j_\beta}_{=C} ,$$

which is, with the definitions of y' and $\tilde{y}$ given in (5.22),

$$\begin{aligned} &= \frac{C}{2} \sum_{n=1}^{n_p} (y^n_\mu - y^{n-1}_\mu)(y^n_\mu + y^{n-1}_\mu) \\ &= \frac{C}{2} \sum_{n=1}^{n_p} (y^n_\mu)^2 - (y^{n-1}_\mu)^2 \\ &= \frac{C}{2} [\sum_{n=1}^{n_p} (y^n_\mu)^2 - \sum_{n=1}^{n_p} (y^{n-1}_\mu)^2] \end{aligned}$$

and finally since because of the periodicity of the loops both sums are equal

$$= 0 , \tag{5.50}$$

up to computer precision.

- Other combinations:

  The expected value zero is reproduced with Monte Carlo precision. The deviation from the analytical result is about as big as in the first case, where $\delta_{\mu\alpha}\delta_{\nu\beta} - \delta_{\mu\beta}\delta_{\nu\alpha} = 1$.

The numerical results show two possible problems: the first is that, like always with Monte Carlo calculations, the numerical results match the analytic results only up to an error. The second is that the numerical results do not exhibit the analytically expected Lorentz structure. Both contribute to the error of the computation of a_1. These errors can be reduced by enlarging the loop cloud. Improving how well the Lorentz structure is reproduced can, however, be done by a more efficient and elegant method: making the loop cloud Lorentz invariant.

5.4.5 The Lorentz invariant loop cloud

The Lorentz structure of the results is not reproduced by the numerical method because the loop cloud itself is not Lorentz invariant although the probability distribution according to which the cloud was generated is. We are working in a Euclidean

space and Lorentz invariance for us means nothing but invariance under rotations. One can force the loop cloud to be Lorentz invariant by rotating it in all possible ways. In three dimensions this can very conveniently be done by parametrising the group off all rotations SO(3) using the well known Euler angles and then integrating over the three angles. The Romberg integration routine `qromo` implemented with `midpnt` from [38] is used. We confine ourselves to three integration steps for each integration which results in $3^3 = 27$ evaluations of the correlation functions because `midpnt` triples the number of evaluations every step. With rotations about three angles the program is slowed down by a factor of $27^3 \approx 20,000$. A sample of the results can be seen on table 5.2. The table A.2, which contains the complete results, is shown in section A.5.

μ	ν	α	β	worldline result	μ	ν	α	β	worldline result
0	0	0	0	-1.8102e-20	0	0	0	1	-7.89111e-19
0	0	0	2	-2.49021e-19	0	0	1	0	-7.33227e-19
0	0	1	1	5.9163e-20	0	0	1	2	5.87649e-19
0	0	2	0	-7.10149e-19	0	0	2	1	-1.54681e-19
0	0	2	2	1.44158e-20	0	1	0	0	-1.06692e-20
0	1	0	1	0.317984	0	1	0	2	1.8443e-19
0	1	1	0	-0.317984	0	1	1	1	-5.10855e-20
0	1	1	2	9.41701e-18	0	1	2	0	-8.24743e-19
0	1	2	1	-8.79056e-18	0	1	2	2	-8.06524e-20
0	2	0	0	-1.57299e-20	0	2	0	1	-3.21263e-18
0	2	0	2	0.317984	0	2	1	0	1.09507e-17
0	2	1	1	9.52551e-21	0	2	1	2	7.30153e-18
0	2	2	0	-0.317984	0	2	2	1	-3.42136e-18
0	2	2	2	2.68142e-20					

Table 5.2: Table of the numerical results for $\int_0^1 \mathrm{d}t \int_0^1 \mathrm{d}t' \, \langle \, \dot{y}_\mu(t) y_\nu(t) \dot{y}_\alpha(t') y_\beta(t') \, \rangle$ in three dimensions; only components with $\mu = 0$ are shown. 27^3 Monte Carlo evaluations (corresponding to 27^3 rotated copies of one loop cloud) using 100 loops of 101 points were done.

Comparing the tables 5.2 and 5.1, we see that we have successfully restored the Lorentz structure of the analytical result. For example with $\mu = 0$, $\nu = 1$, $\alpha = 0$ and $\beta = 2$, the result without rotation was -0.046134. Using the modified method we get 1.8443×10^{-19}, which is a lot closer to zero. For this better result we paid a quite high price: the program is about $20,000$ times slower.

This brings up the question whether or not enlarging the loop cloud could have done the same thing, maybe even without such a big impact on the performance. On the tables 5.3 and 5.4 we see samples of the results obtained with loop clouds which have sizes that also slow down the program by factor of about $20,000$, without any rotations involved. The complete results can again be found in the appendix. For table 5.3 a loop cloud with $n_L = 2 \times 10^6$ loops and $n_p = 101$ points was used. For

μ	ν	α	β	worldline result	μ	ν	α	β	worldline result
0	0	0	0	-3.50847e-20	0	0	0	1	-5.50973e-19
0	0	0	2	4.71693e-19	0	0	1	0	8.19679e-19
0	0	1	1	5.8455e-20	0	0	1	2	3.70387e-19
0	0	2	0	-4.3467e-19	0	0	2	1	4.04886e-19
0	0	2	2	-5.17888e-20	0	1	0	0	1.82786e-20
0	1	0	1	0.331451	0	1	0	2	-0.000203934
0	1	1	0	-0.331451	0	1	1	1	-8.80596e-21
0	1	1	2	-8.31337e-05	0	1	2	0	0.000203934
0	1	2	1	8.31337e-05	0	1	2	2	-6.76788e-20
0	2	0	0	-5.69572e-20	0	2	0	1	-0.000203934
0	2	0	2	0.331186	0	2	1	0	0.000203934
0	2	1	1	1.99144e-20	0	2	1	2	-0.000298953
0	2	2	0	-0.331186	0	2	2	1	0.000298953
0	2	2	2	3.69985e-20					

Table 5.3: Table of the numerical results for $\int_0^1 \mathrm{d}t \int_0^1 \mathrm{d}t' \, \langle \, \dot{y}_\mu(t) y_\nu(t) \dot{y}_\alpha(t') y_\beta(t') \, \rangle$ in three dimensions; only components with $\mu = 0$ are shown. 2,000,000 loops of 101 points were used for the computation

μ	ν	α	β	worldline result	μ	ν	α	β	worldline result
0	0	0	0	-9.74435e-17	0	0	0	1	1.14381e-15
0	0	0	2	-9.3336e-15	0	0	1	0	-9.42832e-15
0	0	1	1	4.2262e-17	0	0	1	2	-1.26645e-15
0	0	2	0	2.81632e-15	0	0	2	1	-5.02664e-16
0	0	2	2	7.94665e-17	0	1	0	0	-1.34598e-17
0	1	0	1	0.297909	0	1	0	2	0.0333473
0	1	1	0	-0.297909	0	1	1	1	-1.70299e-17
0	1	1	2	-0.023779	0	1	2	0	-0.0333473
0	1	2	1	0.023779	0	1	2	2	-3.01939e-17
0	2	0	0	-8.18568e-17	0	2	0	1	0.0333473
0	2	0	2	0.318283	0	2	1	0	-0.0333473
0	2	1	1	-3.72052e-17	0	2	1	2	-0.0514883
0	2	2	0	-0.318283	0	2	2	1	0.0514883
0	2	2	2	5.93328e-17					

Table 5.4: Table of the numerical results for $\int_0^1 \mathrm{d}t \int_0^1 \mathrm{d}t' \, \langle \, \dot{y}_\mu(t) y_\nu(t) \dot{y}_\alpha(t') y_\beta(t') \, \rangle$ in three dimensions; only components with $\mu = 0$ are shown. 100 loops of 14,241 points were used for the computation

table 5.4 a loop cloud with $n_L = 100$ loops and $n_p = 14,241 \approx \sqrt{2} \times 10^4$ points was used. Because of the double sum that has to be evaluated, the time it takes to run the program is of order n_p^2. We see that in both cases the degree suppression of the nonzero results is not even close to the degree of suppression one finds rotating the loop cloud. Trying to obtain the correct Lorentz structure of worldline correlation functions using worldline numerics in three dimensions, to rotate the loop cloud is the method of choice. It should be noted that in three dimensions a rotation about one axis is enough to restore the Lorentz structure. We believe this to be a special feature of the worldline correlation function that is evaluated. There is no reason to assume that this also works for correlation functions with a much more complicated Lorentz structure.

In higher dimensional spaces, however, rotating the loop cloud might not be the method of choice because more and more rotations have to be performed. The dimension of the rotation group's algebra grows quickly as the dimension of the space, in which we want to rotate, grows. In four dimensions there are six generators. Six integrations are therefore necessary to make the loop cloud Lorentz invariant. Doing it with the same precision as for three dimensions (three integration steps), would need $27^6 \approx 3.9 \times 10^8$ Monte Carlo evaluations. With the computers that we have at our disposal this would render a sensible numerical treatment impossible. We have to be content with two integration steps and the resulting worse suppression of the undesirable nonzero components. Doing so, $9^6 \approx 5.4 \times 10^5$ Monte Carlo evaluations need to be performed. A sample of the results of this procedure is listed in tab 5.5 (the rest of the calculated results can be found in the appendix on tab A.5).

5.5 The a_1 of the BPST instanton and the rotated loop cloud

As we stated at the end of section 5.3, the bad results for a_1 are believed to have two possible sources

- Worldline correlation functions are computed poorly where they should not be zero, which disturbs the detailed balance of all the terms contributing to a_1.
- The Lorentz structure is computed poorly, which has the same effect.

The only cure we know for the first problem is to enlarge the loop cloud. As we have already seen in figure 5.5 and figure 5.6, this does not help much. In the previous section we saw that how well the Lorentz structure is reproduced can be improved by rotating the loop cloud. To test whether or not this helps us with the a_1 of the BPST instanton, we again fit the Wilson loop expectation value evaluated at fixed x and $T = 0.01n$, where $n = 1, \ldots, 10$, to the polynomial $P = 2 + a_1 T^2 + a_2 T^4 + a_3 T^6 + a_4 T^8$ and expect that

$$a_1 \approx \frac{1}{12}\mathrm{tr}[\mathbf{G}_{\mu\nu}\mathbf{G}_{\mu\nu}] = -\frac{8}{(x^2+1)^4} \,. \tag{5.51}$$

μ	ν	α	β	worldline result	μ	ν	α	β	worldline result
0	0	0	0	3.1331e-18	0	0	0	1	-3.02033e-17
0	0	0	2	-1.63548e-17	0	0	0	3	-4.86273e-19
0	0	1	0	-3.69468e-17	0	0	1	1	6.36205e-18
0	0	1	2	-1.93687e-17	0	0	1	3	1.30484e-18
0	0	2	0	3.55469e-17	0	0	2	1	8.6476e-18
0	0	2	2	5.01795e-18	0	0	2	3	-1.2988e-18
0	0	3	0	4.16456e-18	0	0	3	1	4.31963e-19
0	0	3	2	1.78885e-18	0	0	3	3	-9.52311e-21
0	1	0	0	-6.03821e-18	0	1	0	1	0.274591
0	1	0	2	0.0152587	0	1	0	3	-1.74607e-05
0	1	1	0	-0.274591	0	1	1	1	9.36357e-18
0	1	1	2	-0.0136663	0	1	1	3	-1.521e-05
0	1	2	0	-0.0152587	0	1	2	1	0.0136663
0	1	2	2	6.45227e-18	0	1	2	3	1.21264e-05

Table 5.5: Table of the numerical results for $\int_0^1 \mathrm{d}t \int_0^1 \mathrm{d}t' \, \langle \, \dot{y}_\mu(t) y_\nu(t) \dot{y}_\alpha(t') y_\beta(t') \, \rangle$ in four dimensions; only components with $\mu = 0$ are shown. 9^6 Monte Carlo evaluations with 100 loops of 101 points were used for the computation

Because of performance issues, we tried this only for one point with $x = 100$. In table 5.6 we can compare the results of a worldline numerical computation of a_1 with and without rotations for a loop cloud with 100 loops of 101 points. The rotation was done about all six angles and two integration steps were used. $10 \times 9^6 \approx 5.3 \times 10^6$ (we use ten points for the fit) evaluations of the Wilson loop expectation value had to be performed.

method	a_1
analytic computation	-7.9968×10^{-16}
without rotations	$-1.364102437 \times 10^{-07}$
with rotations	$-1.364226246 \times 10^{-07}$

Table 5.6: Table of the analytic value and the numerical results for a_1 obtained with and without rotations. A loop cloud of 100 loops of 101 points and, in the rotated case, 9^6 rotated copies of the same loop cloud were used for the computation.

It is plain to see that the result is not improved at all and we have no means to numerically extract the correct results for the a_1 of the BPST instanton within a reasonable time span.

6 The effective potential and the Polyakov loop

Worldline numerics can also be used to calculate finite temperature effects. In this chapter it is applied to the computation of the one-loop effective action of an SU(2) background gauge field at finite temperature. We will then be able to derive the effective potential of the background field, whose expectation value can be used to calculate an upper bound for the Polyakov loop expectation value. This is interesting because the Polyakov loop expectation value is interpreted as an order parameter for confinement (see [34,35]). The Polyakov loop expectation value being zero signals confinement; it being unequal to zero signals deconfinement. Rescaled components of the gauge field as defined in section 2.3 will be used in this chapter. The basics of the necessary method are now briefly explained.

6.1 QFT at finite temperature

A statistical treatment of quantum fields at finite temperature can be done using the imaginary-time formalism. The basic quantity necessary for a statistical treatment of a D-dimensional quantum system in thermal equilibrium is the partition function

$$Z = \operatorname{tr} e^{-\beta H} = \sum_n \langle \mathrm{n}|e^{-\beta H}|\mathrm{n}\rangle \ , \tag{6.1}$$

where the set of all $|\mathrm{n}\rangle$ is a basis of the Hilbert space under consideration. Having knowledge of it, *all* macroscopic physical quantities can be derived; the problem of the statistical description of the system can be considered solved. A path integral expression for a quantity looking very similar to the matrix elements in (6.1) is well known. It is the probability amplitude to find a system that is in the state $|\mathrm{n}\rangle$ at time zero to be found in the same state $|\mathrm{n}\rangle$ at time T, which is given by

$$\langle \mathrm{n}|e^{-iHT}|\mathrm{n}\rangle = \int \mathcal{D}\phi \ \langle \mathrm{n}|\phi(0)\rangle \ \langle \phi(T)|\mathrm{n}\rangle \ e^{i\int_0^T \mathrm{d}\tau \int \mathrm{d}^D x \, \mathcal{L}(\phi)} \ , \tag{6.2}$$

where $\mathcal{L}$ is the Lagrangian density of the system. Setting $T = -i\beta$ (hence the name imaginary-time formalism), we can use (6.2) to replace the matrix elements of the Hamiltonian in (6.1) and end up with

$$Z = \int \mathcal{D}\phi \, e^{-\int_0^\beta \mathrm{d}\tau \int \mathrm{d}^D x \, \mathcal{L}(\phi)} \ , \tag{6.3}$$

where the integration has to be taken over all ϕ that satisfy periodic boundary conditions in the case of bosons or anti-periodic boundary conditions in the case of fermions. A comparison with (2.8) shows that this is nothing else but the Euclidean generating functional (with the current $J = 0$) defined for a theory with one dimension compactified to a circle of circumference β. The space of this theory then looks like a cylinder. The whole machinery developed for the treatment of the generating functional can therefore be used for the study of finite temperature phenomena as well. The statistical quantity we will use in this thesis is the free energy density. Remembering the definition of the free energy

$$F = -\beta^{-1} \ln Z \ , \tag{6.4}$$

we see with the aid of section 2.1 that a quantity proportional to the free energy is given with the effective action (calculated with compactified time and as long as J=0). To get the free energy density, we can therefore compute the effective Lagrangian density (again with compactified time).

6.2 Worldline numerics at finite temperature

Worldline numerics can be used to investigate configurations of finite temperature, too. This brings about a new feature of the loops used in the worldline calculations: The loops x that the path integral is to be taken about can wind around the space-time cylinder. For this we have to accommodate the worldline numerical approach. We do this by separating every path into a part with winding number $n_0 = 0$ and a part with its original winding number n:

$$x_\mu(\tau) = \tilde{x}_\mu(\tau) - \delta_{\mu 0} \frac{\tau}{T} n\beta \ . \tag{6.5}$$

For the worldline path integration this means that

$$\begin{aligned} \int \mathcal{D}x \, e^{-\frac{1}{4}\int_0^T \mathrm{d}\tau \, \dot{x}^2} &= \int \mathcal{D}x \, e^{-\frac{1}{4}\int_0^T \mathrm{d}\tau \, (\dot{\tilde{x}}_\mu - \delta_{\mu 0}\frac{n\beta}{T})^2} \\ &= \int \mathcal{D}x \, e^{-\frac{1}{4}\int_0^T \mathrm{d}\tau \, (\dot{\tilde{x}}^2 - 2\dot{\tilde{x}}_\mu \delta_{\mu 0}\frac{n\beta}{T} + (\delta_{\mu 0}\frac{n\beta}{T})^2)} \ . \end{aligned} \tag{6.6}$$

Being an integration over a total derivative, the second term in the exponent gives zero. The other two terms yield

$$\begin{aligned} \int \mathcal{D}x \, e^{-\frac{1}{4}\int_0^T \mathrm{d}\tau \, \dot{x}^2} &= \int \mathcal{D}x \, e^{-\frac{1}{4}\int_0^T \mathrm{d}\tau \, \dot{\tilde{x}}^2} \, e^{\frac{(n\beta)^2}{4T}} \\ &= \sum_{n=-\infty}^{\infty} e^{-\frac{(n\beta)^2}{4T}} \int \mathcal{D}\tilde{x} \, e^{-\frac{1}{4}\int_0^T \mathrm{d}\tau \, \dot{\tilde{x}}^2} \ . \end{aligned} \tag{6.7}$$

The paths $\tilde{x}$, over which the path integral on the right hand side of (6.7) has to be taken, have the same properties as the ones used in the worldline calculations that

were done earlier in this thesis. The loops also have the same statistical weight as the ones used by us so far. We therefore can compute the integral in (6.7) using the Monte Carlo methods employed throughout the thesis. All we have to do is to take an additional sum into account.

6.3 The Polyakov loop and confinement

Consider a static quark in an SU(2) gauge field theory without any dynamic quarks (one also speaks of quenched QCD). Its worldline is a circle around the space-time cylinder. We can now define the Polyakov loop $L(x)$. It is given by the Wilson loop along the worldline of the static quark, i.e.

$$L(x) = \frac{1}{N_c}\mathrm{tr}\,\mathrm{P}\exp\left[-\int_0^\beta \mathrm{d}x_0 \mathbf{A}_0(x)\right] , \tag{6.8}$$

where N_c is the number of colours, which in our case is two. As shown in [48] the expectation value of $\langle L(x)\rangle$, which is given by

$$\langle L(x)\rangle = \frac{1}{Z}\int \mathcal{D}\mathbf{A}\, L(x)\, e^{-S(\beta,\mathbf{A}]} , \tag{6.9}$$

has a very simple relation to the free energy F_q of the system:

$$e^{-\beta F_q} = \langle L(x)\rangle. \tag{6.10}$$

An expression similar to (6.10) can also be given for $\langle L(x)L^\dagger(x+R)\rangle$. One finds (see again [48]) that

$$\langle L(x)L^\dagger(x+R)\rangle = e^{-\beta F_{q\bar{q}}^{|R|}} , \tag{6.11}$$

where $F_{q\bar{q}}^{|R|}$ denotes the free energy of a system with two static quarks that are separated by a distance of $|R|$. Assuming the cluster decomposition theorem to hold, we find that

$$\begin{aligned}\lim_{|R|\to\infty} e^{-\beta F_{q\bar{q}}^{|R|}} &= \lim_{|R|\to\infty}\langle L(x)L^\dagger(x+R)\rangle \\ &=\langle L(x)\rangle\,\langle L^\dagger(x+R)\rangle\ .\end{aligned} \tag{6.12}$$

This means that for $\langle L(x)\rangle = 0$ the free energy $F_{q\bar{q}}^{\infty}$ has to be infinite, which is interpreted as confining. For $\langle L(x)\rangle \neq 0$ the free energy $F_{q\bar{q}}^{\infty}$ is finite. This is interpreted as deconfining.

For the computation we are about to do, it is convenient to work in the Polyakov gauge, where

$$\partial_0 \mathbf{A}_0 = 0 \quad \text{and} \quad A_0^a(x) = a(x)\delta^{a3} . \tag{6.13}$$

In this gauge $L(x)$ evaluates to

$$\begin{aligned} L(x) =& \frac{1}{2}\mathrm{tr}\ \exp\left[-\int_0^\beta \mathrm{d}x_0\, \mathbf{A}_0(x)\right] \\ =& \frac{1}{2}\left[\exp\left[\frac{i}{2}\int_0^\beta \mathrm{d}x_0\, a(x)\right] + \exp\left[-\frac{i}{2}\int_0^\beta \mathrm{d}x_0\, a(x)\right]\right] \\ =& \cos\left(\frac{\beta\, a(x)}{2}\right)\ , \end{aligned} \tag{6.14}$$

where $\partial_0 \mathbf{A}_0 = \partial_0 a(x) = 0$ was used in the last step. Not only $\langle L\rangle$ can serve as a order parameter for confinement, but also $\langle a(x)\rangle$. By virtue of the Jensen inequality we find:

$$L[\langle a(x)\rangle] \geq \langle L[a(x)]\rangle\ . \tag{6.15}$$

Knowing the $\mathbf{A}_0$ expectation value, we can therefore easily find out whether or not the system has to be confined.

6.4 The one-loop effective action of a pure SU(2) gauge field

But what is the $\mathbf{A}_0$ expectation value? Sadly a general answer to this question has not yet been found. What we do is to restrict ourselves to a set of background gauge fields that are parametrised by one parameter and to calculate the effective potential $V_{\mathrm{eff}} = \frac{\Gamma}{\mathrm{Volume}}$, which is the effective Lagrangian density, which is proportional to the free energy density (there are no sources and J is therefore zero). Because the gauge field corresponding to the minimum of the effective potential has the minimal free energy, we treat it as the expectation value. In one-loop perturbation theory an analytical solution for the contribution to the effective action of a constant $a(x) = a$ that is caused by the temperature being nonzero was found by Weiss (see [36]):

$$V_{\mathrm{eff}}^{\mathrm{Weiss}}(a) = -\frac{2\pi^2}{\beta^4}\left(\frac{1}{45} - \frac{1}{24}\left\{1 - \left[\left(\frac{\beta a}{\pi}\right)_{\mathrm{mod}2} - 1\right]^2\right\}^2\right)\ . \tag{6.16}$$

A plot of the Weiss solution is shown in figure 6.1. The minima of the Weiss solution lie at $\beta a = 2\pi z$, where z is an integer. Plugging this into (6.14), we find $L = 1$ and interpret this as deconfining. Because of asymptotic freedom, that is the coupling constant g being small at high energies, we expect perturbation to be valid at high temperatures. The Weiss result therefore indicates a deconfined phase at high temperatures. In this thesis we will go beyond the Weiss solution and explore how things change if one chooses a spatially varying background gauge field. To do so, we add a perturbation to the constant field. The components of the background field we consider are given by

$$A_\mu^a = a(x)\delta^{3a}\delta_{0\mu}\ ,\text{with}\quad a(x) = a + \delta_a \cos(kx_1)\cos(kx_2)\ . \tag{6.17}$$

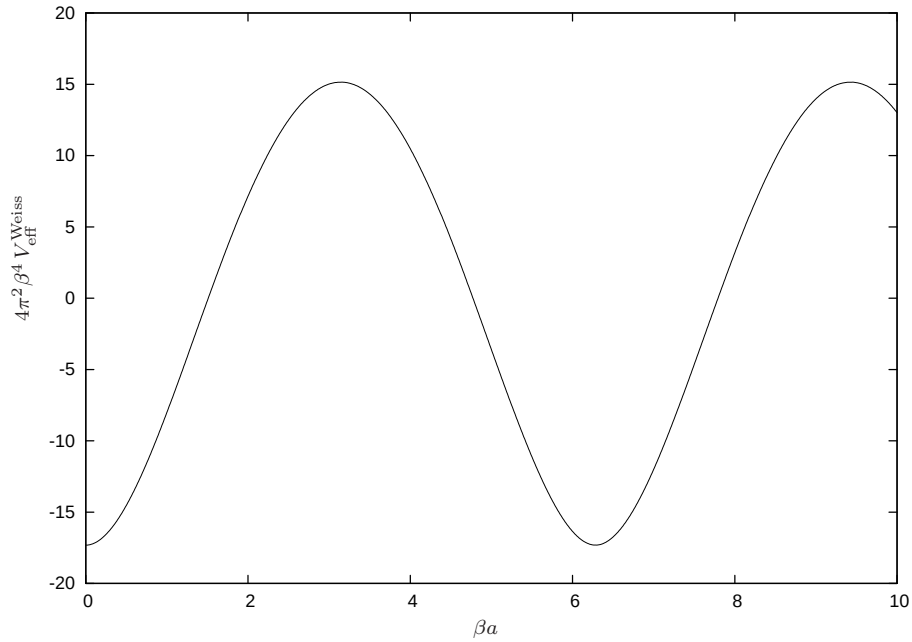

Figure 6.1: The Weiss solution of the effective potential for a constant background field $a(x) = a$.

The definition of the perturbation contains two parameters: δ_a is the amplitude and k is the frequency of the perturbation.

In order to calculate the effective action, we employ the background field method in Feynman gauge, which is explained in [49]. Although the overall gauge is then fixed, the resulting effective action is still gauge invariant under gauge transformations of the background field alone (which justifies the use of the Polyakov gauge). We analyse the effective action in one-loop approximation. The one-loop effective action is given by

$$\begin{aligned}\Gamma^{(1)} =& \frac{1}{2}\ln\det\left[-\mathbf{D}^2 - 2\mathbf{G}\right] - \ln\det\left[-\mathbf{D}^2\right] \\ =& \frac{1}{2}\mathrm{Tr}\ln\left[-\mathbf{D}^2 - 2\mathbf{G}\right] - \mathrm{Tr}\ln\left[-\mathbf{D}^2\right] \ , \end{aligned} \tag{6.18}$$

where the field strength tensor $\mathbf{G}$ has to be taken in the adjoint representation. This is where worldline numerics comes into play; as a tool to numerically compute the one-loop effective action.

6.5 The one-loop effective potential for $a(x)$

Starting from (6.18), we derive the expression for the one-loop effective potential of a gauge field with

$$A_0^a(x) = a(x)\delta^{a3}\delta_{\mu 0} \quad \text{and} \quad a(x) = a + \delta_a \cos(kx_1)\cos(kx_2) \ . \tag{6.19}$$

We write (6.18) in the proper time representation (see section A.1) and perform the trace as explained in section 2.4. We find that

$$\begin{aligned}\Gamma^{(1)} =& -\frac{1}{2}\mathrm{tr}\int_0^\infty \frac{\mathrm{d}T}{T^3}\int \mathrm{d}^D x \int_{x(0)=x}^{x(T)=x} \mathcal{D}x\, e^{-\int_0^T \mathrm{d}\tau \frac{\dot{x}^2}{4}}\, \mathrm{P} e^{-\int_0^T \mathrm{d}\tau [\dot{x}\mathbf{A}+2\mathbf{G}]} \\ &+ \mathrm{tr}\int_0^\infty \frac{\mathrm{d}T}{T^3}\int \mathrm{d}^D x \int_{x(0)=x}^{x(T)=x} \mathcal{D}x\, e^{-\int_0^T \mathrm{d}\tau \frac{\dot{x}^2}{4}}\, \mathrm{P} e^{-\int_0^T \mathrm{d}\tau \dot{x}\mathbf{A}} \,. \end{aligned} \tag{6.20}$$

Because $\mathbf{A}$ only points into one direction of the colour space, the problem is pseudo-abelian and the path ordering is not necessary. After dropping the path ordering, the one-loop effective action reads

$$\begin{aligned}\Gamma^{(1)} =& -\frac{1}{2}\int_0^\infty \frac{\mathrm{d}T}{T^3}\int \mathrm{d}^D x \int_{x(0)=x}^{x(T)=x} \mathcal{D}x\, e^{-\int_0^T \mathrm{d}\tau \frac{\dot{x}^2}{4}}\, \mathrm{tr}\, e^{-\int_0^T \mathrm{d}\tau [\dot{x}\mathbf{A}+2\mathbf{G}]} \\ &+ \int_0^\infty \frac{\mathrm{d}T}{T^3}\int \mathrm{d}^D x \int_{x(0)=x}^{x(T)=x} \mathcal{D}x\, e^{-\int_0^T \mathrm{d}\tau \frac{\dot{x}^2}{4}}\, \mathrm{tr}\, e^{-\int_0^T \mathrm{d}\tau \dot{x}\mathbf{A}} \\ =& \int_0^\infty \frac{\mathrm{d}T}{T^3}\int \mathrm{d}^D x \int_{x(0)=x}^{x(T)=x} \mathcal{D}x\, e^{-\int_0^T \mathrm{d}\tau \frac{\dot{x}^2}{4}} \left[\mathrm{tr}\, e^{-\int_0^T \mathrm{d}\tau \dot{x}\mathbf{A}} - \frac{1}{2}\mathrm{tr}\, e^{-\int_0^T \mathrm{d}\tau [\dot{x}\mathbf{A}+2\mathbf{G}]}\right] . \end{aligned} \tag{6.21}$$

6.5.1 Performing the traces

The next step is to perform the traces. We will turn to $\mathrm{tr}\, e^{-\int_0^T \mathrm{d}\tau \dot{x}\mathbf{A}}$ first. Using the definition of the gauge field (equation (6.19)), we get that

$$\begin{aligned}\mathrm{tr}\, e^{-\int_0^T \mathrm{d}\tau \dot{x}\mathbf{A}} =& \mathrm{tr}\, e^{i\int_0^T \mathrm{d}\tau\, \dot{x}_0\, a(x)\, \mathbf{T}^3} \\ =& \mathrm{tr}\, e^{\Theta\, \mathbf{T}^3} \,, \end{aligned} \tag{6.22}$$

where we defined $\Theta = i\int_0^T \mathrm{d}\tau\, \dot{x}_0\, a(x)$. If there exists an invertible matrix $\mathbf{U}$ that complies with

$$\mathbf{U}\,\mathbf{T}^3\,\mathbf{U}^{-1} = \mathrm{diag}(T_1, T_2, T_3) \,, \tag{6.23}$$

where $\mathbf{U}^{-1}$ is the inverse matrix of $\mathbf{U}$ and T_0, T_1, T_2 and T_3 are the eigenvalues of $\mathbf{T}^3$, we can easily perform the trace, because then

$$\begin{aligned}\mathrm{tr}\, e^{\Theta\, \mathbf{T}^3} =& \mathrm{tr}\, \mathbf{U}^{-1}\mathbf{U} e^{\Theta\, \mathbf{T}^3} \\ =& \mathrm{tr}\, \mathbf{U}\, e^{\Theta\, \mathbf{T}^3}\, \mathbf{U}^{-1} \\ =& \mathrm{tr}\, e^{\Theta\, \mathbf{U}\, \mathbf{T}^3\, \mathbf{U}^{-1}} \\ =& \mathrm{tr}\, e^{\Theta\, \mathrm{diag}(T_1,T_2,T_3)} \\ =& \sum_{i=0}^{3} e^{\Theta\, T_i} \,, \end{aligned} \tag{6.24}$$

where the second and forth step can be seen to be correct by expanding the exponential. According to (2.24), $\mathbf{T}^3$ is

$$\mathbf{T}^3 = i \begin{pmatrix} 0 & 1 & 0 \\ -1 & 0 & 0 \\ 0 & 0 & 0 \end{pmatrix} \tag{6.25}$$

and therefore Hermitian. A matrix that meets the requirements given above is therefore known to exist. The eigenvalues of $\mathbf{T}^3$ are: $T_1 = 1$, $T_2 = -1$ and $T_3 = 0$. Because of (6.24), we can write:

$$\begin{aligned} \operatorname{tr} e^{-\int_0^T \mathrm{d}\tau\, \dot{x}\mathbf{A}} =& \operatorname{tr} e^{i\int_0^T \mathrm{d}\tau\, \dot{x}_0\, a(x)\, \mathbf{T}^3} \\ =& 1 + e^{-i\int_0^T \mathrm{d}\tau\, \dot{x}_0\, a(x)} + e^{i\int_0^T \mathrm{d}\tau\, \dot{x}_0\, a(x)} \end{aligned} \tag{6.26}$$

The first trace in (6.21), $\operatorname{tr} e^{-\int_0^T \mathrm{d}\tau[\dot{x}\mathbf{A}+2\mathbf{G}]}$, is to be dealt with next. The trace here runs over colour *and* Lorentz labels. We will perform the Lorentz trace first. As a first step, we write the trace including the explicit Lorentz structure and give the trace the index L to remind us that we are only looking at the Lorentz trace:

$$\operatorname{tr}_{\mathrm{L}} e^{-\int_0^T \mathrm{d}\tau[\dot{x}\mathbf{A}+2\mathbf{G}]} = \operatorname{tr}_{\mathrm{L}} e^{-\int_0^T \mathrm{d}\tau[\dot{x}\mathbf{A}\,\delta_{\mu\nu}+2\mathbf{G}_{\mu\nu}]} \,. \tag{6.27}$$

Because of $\exp(k\mathbf{1} + \mathbf{A}) = \exp(k\mathbf{1})\exp(\mathbf{A}) = \exp(k)\exp(\mathbf{A})$, where k is a C-number, $\mathbf{1}$ the unit matrix and $\mathbf{A}$ an arbitrary matrix, the trace can also be written as

$$\operatorname{tr}_{\mathrm{L}} e^{-\int_0^T \mathrm{d}\tau[\dot{x}\mathbf{A}\,\delta_{\mu\nu}+2\mathbf{G}_{\mu\nu}]} = e^{-\int_0^T \mathrm{d}\tau\, \dot{x}\mathbf{A}}\, \operatorname{tr}_{\mathrm{L}} e^{-2\int_0^T \mathrm{d}\tau\, \mathbf{G}_{\mu\nu}} \,. \tag{6.28}$$

Now we compute the field strength tensor as defined in (2.30):

$$\mathbf{G}_{\mu\nu} = \partial_\mu \mathbf{A}_\nu - \partial_\nu \mathbf{A}_\mu + g[\mathbf{A}_\mu, \mathbf{A}_\nu] \,. \tag{6.29}$$

Because of the pseudo-abelian structure of the problem, the commutator vanishes. Plugging in the definition of the gauge field that we consider here (given in (6.19)), we get that

$$\mathbf{G}_{\mu\nu} = -\,i\big(\partial_\mu a(x)\delta_{\nu 0} - \partial_\nu a(x)\delta_{\mu 0}\big)\mathbf{T}^3 \,. \tag{6.30}$$

We see that the non-zero components of $\mathbf{G}_{\mu\nu}$, which we will call $F_{\mu\nu}$, are given by

$$\begin{aligned} F_{\mu\nu} =& G^3_{\mu\nu} \\ =& -E_\mu \delta_{\nu 0} + E_\nu \delta_{\mu 0} \,, \end{aligned} \tag{6.31}$$

where we introduced the electric field $E_\mu = -\partial_\mu a(x)$. The two electric field components that are not zero are given by

$$\begin{aligned} E_1 =& -\partial_1 a(x) = \delta_a\, k \sin(kx_1)\cos(kx_2) \\ E_2 =& -\partial_2 a(x) = \delta_a\, k \cos(kx_1)\sin(kx_2) \,. \end{aligned} \tag{6.32}$$

Given as a matrix $\mathbf{F}$ then looks like

$$\mathbf{F} = \begin{pmatrix} 0 & E_1 & E_2 & 0 \\ -E_1 & 0 & 0 & 0 \\ -E_2 & 0 & 0 & 0 \\ 0 & 0 & 0 & 0 \end{pmatrix} . \tag{6.33}$$

Putting it all back into the trace, we find that

$$\mathrm{tr_L}\, e^{-\int_0^T \mathrm{d}\tau [\dot{x}\mathbf{A}+2\mathbf{G}]} = e^{-\int_0^T \mathrm{d}\tau\, \dot{x}\mathbf{A}}\ \mathrm{tr_L}\, e^{2i\int_0^T \mathrm{d}\tau\, F_{\mu\nu}\mathbf{T}^3} . \tag{6.34}$$

As before in this section, since $iF_{\mu\nu}$ is Hermitian the problem of taking the trace reduces to the problem of finding the eigenvalues of $iF_{\mu\nu}$. They are: 0, 0, $\pm\sqrt{E_1^2+E_2^2}$. Finally we sum to get

$$\mathrm{tr_L}\, e^{-\int_0^T \mathrm{d}\tau [\dot{x}\mathbf{A}+2\mathbf{G}]} = e^{-\int_0^T \mathrm{d}\tau\, \dot{x}\mathbf{A}} \left(2 + e^{2\int_0^T \mathrm{d}\tau |\vec{E}|\,\mathbf{T}^3} + e^{-2\int_0^T \mathrm{d}\tau |\vec{E}|\,\mathbf{T}^3}\right) . \tag{6.35}$$

The only trace left is the colour trace over (6.35):

$$\begin{aligned} &\mathrm{tr}_c\, e^{-\int_0^T \mathrm{d}\tau\, \dot{x}\mathbf{A}} \left(2 + e^{2\int_0^T \mathrm{d}\tau |\vec{E}|\,\mathbf{T}^3} + e^{-2\int_0^T \mathrm{d}\tau |\vec{E}|\,\mathbf{T}^3}\right) \\ =&2\,\mathrm{tr}_c\, e^{i\int_0^T \mathrm{d}\tau\, \dot{x}_0\, a(x)\,\mathbf{T}^3} + \mathrm{tr}_c\, e^{\mathbf{T}^3 \int_0^T \mathrm{d}\tau\, \dot{x}_0 \left[i\, a(x)+2|\vec{E}|\right]} \\ &+ \mathrm{tr}_c\, e^{\mathbf{T}^3 \int_0^T \mathrm{d}\tau\, \dot{x}_0 \left[i\, a(x)-2|\vec{E}|\right]} . \end{aligned} \tag{6.36}$$

We can again use the fact that $\mathbf{T}^3$ is Hermitian and find that

$$\begin{aligned} \mathrm{tr}\, e^{-\int_0^T \mathrm{d}\tau [\dot{x}\mathbf{A}+2\mathbf{G}]} =&2\left(1 + e^{-i\int_0^T \mathrm{d}\tau\, \dot{x}_0\, a(x)} + e^{i\int_0^T \mathrm{d}\tau\, \dot{x}_0\, a(x)}\right) \\ &+ 1 + e^{\int_0^T \mathrm{d}\tau\, \dot{x}_0 \left[i\, a(x)+2|\vec{E}|\right]} + e^{-\int_0^T \mathrm{d}\tau\, \dot{x}_0 \left[i\, a(x)+2|\vec{E}|\right]} \\ &+ 1 + e^{\int_0^T \mathrm{d}\tau\, \dot{x}_0 \left[i\, a(x)-2|\vec{E}|\right]} + e^{-\int_0^T \mathrm{d}\tau\, \dot{x}_0 \left[i\, a(x)-2|\vec{E}|\right]} . \end{aligned} \tag{6.37}$$

6.5.2 Calculating $\Gamma^{(1)}$

Using our knowledge about the traces, we can write (6.21) as

$$\begin{aligned} \Gamma^{(1)} &= \int_0^\infty \frac{\mathrm{d}T}{T^3} \int \mathrm{d}^D x \int_{x(0)=x}^{x(T)=x} \mathcal{D}x\, e^{-\int_0^T \mathrm{d}\tau \frac{\dot{x}^2}{4}} \left[\mathrm{tr}\, e^{-\int_0^T \mathrm{d}\tau\, \dot{x}\mathbf{A}} - \frac{1}{2}\mathrm{tr}\, e^{-\int_0^T \mathrm{d}\tau [\dot{x}\mathbf{A}+2\mathbf{G}]}\right] \\ &= \int_0^\infty \frac{\mathrm{d}T}{T^3} \int \mathrm{d}^D x \int_{x(0)=x}^{x(T)=x} \mathcal{D}x\, e^{-\int_0^T \mathrm{d}\tau \frac{\dot{x}^2}{4}} \Big[-\frac{1}{2}\big(2 + e^{\int_0^T \mathrm{d}\tau\, \dot{x}_0 \left[i\, a(x)+2|\vec{E}|\right]} \\ &\qquad + e^{-\int_0^T \mathrm{d}\tau\, \dot{x}_0 \left[i\, a(x)+2|\vec{E}|\right]} + e^{\int_0^T \mathrm{d}\tau\, \dot{x}_0 \left[i\, a(x)-2|\vec{E}|\right]} \\ &\qquad + e^{-\int_0^T \mathrm{d}\tau\, \dot{x}_0 \left[i\, a(x)-2|\vec{E}|\right]}\big)\Big] \\ &= -\int_0^\infty \frac{\mathrm{d}T}{T^3} \int \mathrm{d}^D x \int_{x(0)=x}^{x(T)=x} \mathcal{D}x\, e^{-\int_0^T \mathrm{d}\tau \frac{\dot{x}^2}{4}} \Big[1 \\ &\qquad + \frac{1}{2}\big(e^{i\int_0^T \mathrm{d}\tau\, \dot{x}_0\, a(x)} + e^{-i\int_0^T \mathrm{d}\tau\, \dot{x}_0\, a(x)}\big)\big(e^{2\int_0^T \mathrm{d}\tau\, |\vec{E}|} + e^{2\int_0^T \mathrm{d}\tau\, |\vec{E}|}\big)\Big] . \end{aligned} \tag{6.38}$$

The 1 only amounts for a constant term which will be left out, and the first and second term in brackets are twice a hyperbolic and trigonometric cosine function respectively. This makes it possible to write the one-loop effective action in a very concise form:

$$\Gamma^{(1)} = -\int_0^\infty \frac{\mathrm{d}T}{T^3} \int \mathrm{d}^D x \int_{x(0)=x}^{x(T)=x} \mathcal{D}x\, e^{-\int_0^T \mathrm{d}\tau \frac{\dot{x}^2}{4}} \times 2\cos\left(\int_0^T \mathrm{d}\tau\, \dot{x}_0\, a(x)\right) \cosh\left(2\int_0^T \mathrm{d}\tau\, |\vec{E}|\right) . \tag{6.39}$$

6.5.3 Making the one-loop effective action suit numerical evaluation

To make the one-loop effective action numerically treatable, we normalise the path integral, which is to be evaluated using Monte Carlo techniques. We do this just as in section 2.5. Then

$$\Gamma^{(1)} = -\frac{2}{(4\pi)^2}\int_0^\infty \frac{\mathrm{d}T}{T^3} e^{-m^2 T} \int \mathrm{d}^D x\, \mathcal{N} \int_{x(0)=x}^{x(T)=x} \mathcal{D}x\, e^{-\int_0^T \mathrm{d}\tau \frac{\dot{x}^2}{4}} \times \cos\left(\int_0^T \mathrm{d}\tau\, \dot{x}_0\, a(x)\right) \cosh\left(2\int_0^T \mathrm{d}\tau\, |\vec{E}|\right) , \tag{6.40}$$

where

$$\mathcal{N} = \Big[\int_{x(0)=x}^{x(T)=x} \mathcal{D}x\, e^{-\int_0^T \mathrm{d}\tau \frac{\dot{x}^2}{4}}\Big]^{-1} . \tag{6.41}$$

We are investigating a quantum field theory at finite temperature. As is explained in section 6.2, (6.40) can therefore be written as

$$\begin{aligned}
\Gamma^{(1)} &= -\frac{2}{(4\pi)^2}\int_0^\infty \frac{\mathrm{d}T}{T^3} \int \mathrm{d}^D x\, \mathcal{N} \sum_{n=-\infty}^{\infty} e^{-\frac{(n\beta)^2}{4T}} \int \mathcal{D}\tilde{x}\, e^{-\frac{1}{4}\int_0^T \mathrm{d}\tau\, \dot{\tilde{x}}^2} \\
&\qquad \times \cos\Big(-\frac{n\beta}{T}\, a(x) + \int_0^T \mathrm{d}\tau\, \dot{\tilde{x}}_0\, a(x)\Big) \cosh\Big(2\int_0^T \mathrm{d}\tau\, |\vec{E}|\Big) \\
&= -\frac{2}{(4\pi)^2}\int_0^\infty \frac{\mathrm{d}T}{T^3} \int \mathrm{d}^D x\, \mathcal{N} \sum_{n=-\infty}^{\infty} e^{-\frac{(n\beta)^2}{4T}} \int \mathcal{D}\tilde{x}\, e^{-\frac{1}{4}\int_0^T \mathrm{d}\tau\, \dot{\tilde{x}}^2} \\
&\quad \times \cosh\Big(2\int_0^T \mathrm{d}\tau\, |\vec{E}|\Big)\Big[\cos\Big(\frac{n\beta}{T}\int_0^T \mathrm{d}\tau\, a(x)\Big)\cos\Big(\int_0^T \mathrm{d}\tau\, \dot{\tilde{x}}_0\, a(x)\Big) \\
&\qquad + \sin\Big(\frac{n\beta}{T}\int_0^T \mathrm{d}\tau\, a(x)\Big)\sin\Big(\int_0^T \mathrm{d}\tau\, \dot{\tilde{x}}_0\, a(x)\Big)\Big] .
\end{aligned} \tag{6.42}$$

We only want to investigate finite temperature effects and therefore exclude the zero temperature case by demanding that $n \neq 0$. Because

$$\sum_{n=-\infty, n\neq 0}^{\infty} f(n^2)\sin(\alpha n) = \sum_{n=1}^{\infty} f(n^2)\sin(\alpha n) + \sum_{n=1}^{\infty} f(n^2)\sin(-\alpha n) = 0 , \tag{6.43}$$

the term containing the sine function drops out. The same reasoning leads to a different result for the term with the cosine function since

$$\sum_{n=-\infty, n\neq 0}^{\infty} f(n^2)\cos(\alpha n) = \sum_{n=1}^{\infty} f(n^2)\cos(\alpha n) + \sum_{n=1}^{\infty} f(n^2)\cos(-\alpha n)$$
$$= 2\sum_{n=1}^{\infty} f(n^2)\cos(\alpha n)\ . \tag{6.44}$$

The finite temperature one-loop effective action $\Gamma_{\mathrm{e}}^{(1)}$ therefore is

$$\Gamma_{\mathrm{e}}^{(1)} = -\frac{4}{(4\pi)^2}\int_0^\infty \frac{\mathrm{d}T}{T^3}\int \mathrm{d}^D x\,\mathcal{N}\sum_{n=1}^{\infty} e^{-\frac{(n\beta)^2}{4T}}\int \mathcal{D}\tilde{x}\, e^{-\frac{1}{4}\int_0^T \mathrm{d}\tau\,\dot{\tilde{x}}^2}$$
$$\times\cos\Big(\frac{n\beta}{T}\int_0^T \mathrm{d}\tau\, a(x)\Big)\cos\Big(\int_0^T \mathrm{d}\tau\,\dot{\tilde{x}}_0\, a(x)\Big)$$
$$\times\cosh\Big(2\int_0^T \mathrm{d}\tau\,|\vec{E}|\Big)\ . \tag{6.45}$$

After the introduction of unit loops (see section 2.5) it looks like

$$\Gamma_{\mathrm{e}}^{(1)} = -\frac{4}{(4\pi)^2}\int_0^\infty \frac{\mathrm{d}T}{T^3}\int \mathrm{d}^D x\,\mathcal{N}\int \mathcal{D}y\sum_{n=1}^{\infty} e^{-\frac{(n\beta)^2}{4T}}\, e^{-\frac{1}{4}\int_0^1 \mathrm{d}t\,\dot{y}^2}$$
$$\times\cos\Big(n\beta\int_0^1 \mathrm{d}t\, a(x+\sqrt{T}y)\Big)\cos\Big(\sqrt{T}\int_0^1 \mathrm{d}t\,\dot{y}_0\, a(x+\sqrt{T}y)\Big)$$
$$\times\cosh\Big(2T\int_0^1 \mathrm{d}t\,|\vec{E}(x+\sqrt{T}y)|\Big)\ . \tag{6.46}$$

6.5.4 Deriving the one-loop effective potential

To get the one-loop effective potential $V_{\mathrm{eff}}^{(1)}$we have to divide the one-loop effective action $\Gamma_{\mathrm{e}}^{(1)}$ by the space-time volume:

$$V_{\mathrm{eff}}^{(1)} = -\frac{4}{(4\pi)^2}\Big[\int \mathrm{d}^D x\Big]^{-1}\int_0^\infty \frac{\mathrm{d}T}{T^3}\int \mathrm{d}^D x\,\mathcal{N}\int \mathcal{D}y\sum_{n=1}^{\infty} e^{-\frac{(n\beta)^2}{4T}}\, e^{-\frac{1}{4}\int_0^1 \mathrm{d}t\,\dot{y}^2}$$
$$\times\cos\Big(n\beta\int_0^1 \mathrm{d}t\, a(x+\sqrt{T}y)\Big)\cos\Big(\sqrt{T}\int_0^1 \mathrm{d}t\,\dot{y}_0\, a(x+\sqrt{T}y)\Big)$$
$$\times\cosh\Big(2T\int_0^1 \mathrm{d}t\,|\vec{E}(x+\sqrt{T}y)|\Big)\ . \tag{6.47}$$

The field $a(x)$ is given by $a(x) = a + \delta_a\cos(kx_1)\cos(kx_2)$. The two nonzero components of $\vec{E}$ are therefore given by

$$E_1 = k\delta_a\sin(kx_1)\cos(kx_2)$$
$$E_2 = k\delta_a\cos(kx_1)\sin(kx_2)\ . \tag{6.48}$$

If we plug this into the definition of the one-loop effective potential and perform the change of variables $T \to T/\beta^2$ and $x_\mu \to x_\mu/\beta$, we find that

$$\begin{aligned} V_{\text{eff}}^{(1)} = &- \frac{4}{(4\pi)^2\beta^4} \Big[\int \mathrm{d}^D x\Big]^{-1} \int \mathrm{d}^D x \int_0^\infty \frac{\mathrm{d}T}{T^3} \mathcal{N} \int \mathcal{D}y \sum_{n=1}^{\infty} e^{-\frac{n^2}{4T}}\, e^{-\frac{1}{4}\int_0^1 \mathrm{d}t\, \dot{y}^2} \\ &\times \cos\Big(n \int_0^1 \mathrm{d}t \Big[\hat{a} + \hat{\delta}_a \cos\big(\hat{k}(x_1 + \sqrt{T}y_1)\big) \cos\big(\hat{k}(x_2 + \sqrt{T}y_2)\big)\Big]\Big) \\ &\times \cos\Big(\sqrt{T} \int_0^1 \mathrm{d}t\, \dot{y}_0 \Big[\hat{a} + \hat{\delta}_a \cos\big(\hat{k}(x_1 + \sqrt{T}y_1)\big) \cos\big(\hat{k}(x_2 + \sqrt{T}y_2)\big)\Big]\Big) \\ &\times \cosh\Big(2T\,\hat{k}\hat{\delta}_a \int_0^1 \mathrm{d}t \Big[\sin^2\big(\hat{k}(x_1 + \sqrt{T}y_1)\big) \cos^2\big(k(x_2 + \sqrt{T}y_2)\big) + \\ &\qquad \times \cos^2\big(\hat{k}(x_1 + \sqrt{T}y_1)\big) \sin^2\big(\hat{k}(x_2 + \sqrt{T}y_2)\big)\Big]^{\frac{1}{2}}\Big)\,, \end{aligned} \tag{6.49}$$

where several new quantities were introduced: a, δ_a and k were rescaled to become $\hat{a} = \beta a$, $\hat{\delta}_a = \beta\delta_a$ and $\hat{k} = \beta k$. Because the x-integrand does not depend on x_0 and x_3, the integrations over the two variables cancel with the corresponding integrations that are in the denominator. Furthermore, the x-integrand is periodic in x_1 and x_2 with a period of $2\pi/\hat{k}$. Using this, we finally get the expression that is numerically evaluated:

$$\begin{aligned} V_{\text{eff}}^{(1)} = &- \frac{1}{4\pi^2\beta^4}\Big(\frac{\hat{k}}{2\pi}\Big)^2 \int_0^{\frac{2\pi}{\hat{k}}} \mathrm{d}x_1 \int_0^{\frac{2\pi}{\hat{k}}} \mathrm{d}x_2 \int_0^\infty \frac{\mathrm{d}T}{T^3} \mathcal{N} \int \mathcal{D}y \sum_{n=1}^{\infty} e^{-\frac{n^2}{4T}}\, e^{-\frac{1}{4}\int_0^1 \mathrm{d}t\, \dot{y}^2} \\ &\times \cos\Big(n \int_0^1 \mathrm{d}t \Big[\hat{a} + \hat{\delta}_a \cos\big(\hat{k}(x_1 + \sqrt{T}y_1)\big) \cos\big(\hat{k}(x_2 + \sqrt{T}y_2)\big)\Big]\Big) \\ &\times \cos\Big(\sqrt{T} \int_0^1 \mathrm{d}t\, \dot{y}_0 \Big[\hat{a} + \hat{\delta}_a \cos\big(\hat{k}(x_1 + \sqrt{T}y_1)\big) \cos\big(\hat{k}(x_2 + \sqrt{T}y_2)\big)\Big]\Big) \\ &\times \cosh\Big(2T\,\hat{k}\hat{\delta}_a \int_0^1 \mathrm{d}t \Big[\sin^2\big(\hat{k}(x_1 + \sqrt{T}y_1)\big) \cos^2\big(k(x_2 + \sqrt{T}y_2)\big) \\ &\qquad + \cos^2\big(\hat{k}(x_1 + \sqrt{T}y_1)\big) \sin^2\big(\hat{k}(x_2 + \sqrt{T}y_2)\big)\Big]^{\frac{1}{2}}\Big)\,. \end{aligned} \tag{6.50}$$

From (6.50) we can find another way to write the Weiss solution, which was given in equation (6.16), if we set $\hat{\delta}_a = 0$:

$$V_{\text{eff}}^{\text{Weiss}}(\hat{a}) = -\frac{1}{4\pi^2\beta^4} \int_0^\infty \frac{\mathrm{d}T}{T^3} \sum_{n=1}^{\infty} e^{-\frac{n^2}{4T}} \cos(n\hat{a})\,. \tag{6.51}$$

6.5.5 The pseudo Weiss approximation

The numerical results are compared to the Weiss solution and what we call the pseudo Weiss approximation. It can be obtained by simply inserting $a(x)$ into the Weiss solution and performing the x-integrations:

$$\begin{aligned} V_{\mathrm{eff}}^{\mathrm{psWei}}(\hat{\delta}_a,\hat{k}) &= -\frac{1}{4\pi^2\beta^4}\Big(\frac{\hat{k}}{2\pi}\Big)^2 \int_0^{\frac{2\pi}{\hat{k}}}\mathrm{d}x_1\int_0^{\frac{2\pi}{\hat{k}}}\mathrm{d}x_2\int_0^\infty\frac{\mathrm{d}T}{T^3}\sum_{n=1}^\infty e^{-\frac{n^2}{4T}} \\ &\quad\times\cos\Big(n\int_0^1\mathrm{d}t\,\Big[\hat{a}+\hat{\delta}_a\cos(\hat{k}x_1)\cos(\hat{k}x_2)\Big]\Big) \\ &= -\frac{1}{4\pi^2\beta^4}\Big(\frac{1}{2\pi}\Big)^2 \int_0^{2\pi}\mathrm{d}x_1\int_0^{2\pi}\mathrm{d}x_2\int_0^\infty\frac{\mathrm{d}T}{T^3}\sum_{n=1}^\infty e^{-\frac{n^2}{4T}} \\ &\quad\times\cos\Big(n\int_0^1\mathrm{d}t\,\Big[\hat{a}+\hat{\delta}_a\cos(x_1)\cos(x_2)\Big]\Big)\,. \end{aligned} \tag{6.52}$$

We see that the pseudo Weiss solution does not depend on $\hat{k}$, i.e.

$$V_{\mathrm{eff}}^{\mathrm{psWei}}(\hat{\delta}_a,\hat{k}) = V_{\mathrm{eff}}^{\mathrm{psWei}}(\hat{\delta}_a)\,. \tag{6.53}$$

In the pseudo Weiss approximation we take the field to be locally constant and then perform the x-integrations. The smaller we choose $\hat{k}$, the better this is fulfilled. With a small $\hat{k}$ the dominating contributions to the T-integral for $V_{\mathrm{eff}}^{(1)}$ are computed with a nearly constant background field as the frequency of its variation is small.

That for small $\hat{k}$ we expect the pseudo Weiss approximation to be the outcome of the calculation can also be seen by investigating the small-$\hat{k}$-behaviour of all the contributions to the path integral. At small $\hat{k}$ and at T values that dominate the proper time integrand $\hat{k}\sqrt{T}$ is also small. For the first cosine term in (6.52) this means that

$$\begin{aligned} &\mathcal{N}\int\mathcal{D}y\,e^{-\frac{1}{4}\int_0^1\mathrm{d}t\,\dot{y}^2}\cos\Big(n\int_0^1\mathrm{d}t\,\Big[\hat{a}+\hat{\delta}_a\cos\big(\hat{k}(x_1+\sqrt{T}y_1)\big)\cos\big(\hat{k}(x_2+\sqrt{T}y_2)\big)\Big]\Big) \\ &\approx\cos\Big(n\int_0^1\mathrm{d}t\,\Big[\hat{a}+\hat{\delta}_a\cos(\hat{k}x_1)\cos(\hat{k}x_2)\Big]\Big)\,. \end{aligned} \tag{6.54}$$

For the second term in (6.52) this means that

$$\begin{aligned} &\mathcal{N}\int\mathcal{D}y\,e^{-\frac{1}{4}\int_0^1\mathrm{d}t\,\dot{y}^2}\cos\Big(\sqrt{T}\int_0^1\mathrm{d}t\,\dot{y}_0\,\Big[\hat{a}+\hat{\delta}_a\cos\big(\hat{k}(x_1+\sqrt{T}y_1)\big)\cos\big(\hat{k}(x_2+\sqrt{T}y_2)\big)\Big]\Big) \\ &\approx 1 \end{aligned} \tag{6.55}$$

because with small $\hat{k}\sqrt{T}$ the integral in the cosine function is taken over a total

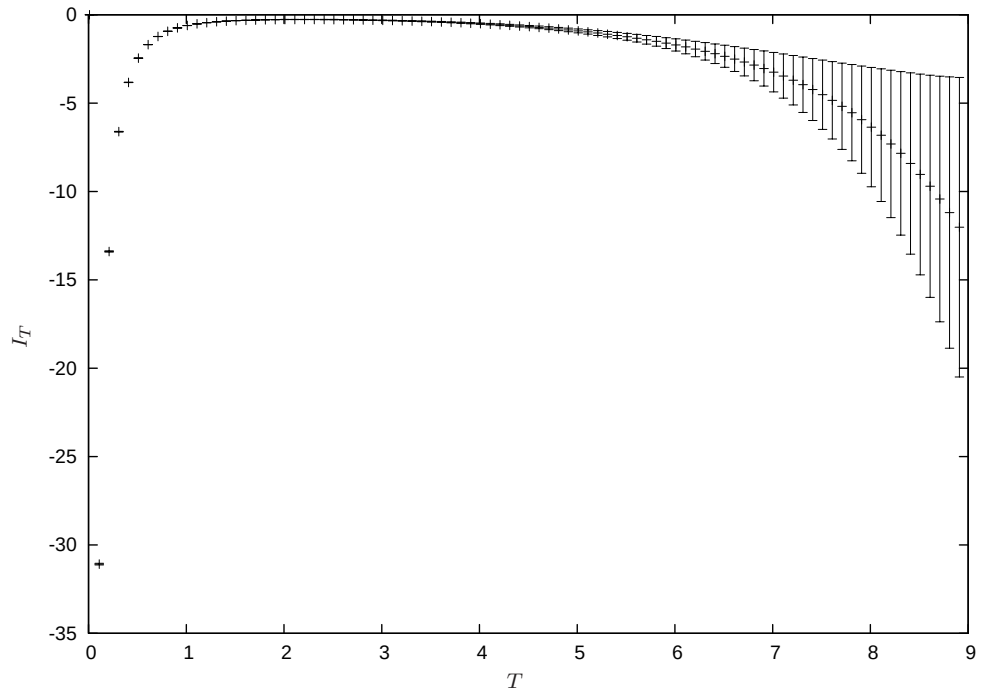

Figure 6.2: The proper time integrand I_T with $\hat{a} = \hat{k} = \hat{\delta}_a = 1$ and $x_1 = x_2 = 0$. 100 loops of 101 points were used for the computation.

derivative of a loop and therefore zero. For the third term we find that

$$\mathcal{N} \int \mathcal{D}y\, e^{-\frac{1}{4}\int_0^1 \mathrm{d}t\, \dot{y}^2} \cosh\left(2T\,\hat{k}\hat{\delta}_a \int_0^1 \mathrm{d}t \left[\sin^2\left(\hat{k}(x_1+\sqrt{T}y_1)\right)\cos^2\left(k(x_2+\sqrt{T}y_2)\right)\right.\right.$$
$$\left.\left. + \cos^2\left(\hat{k}(x_1+\sqrt{T}y_1)\right)\sin^2\left(\hat{k}(x_2+\sqrt{T}y_2)\right)\right]^{\frac{1}{2}}\right)$$
$$\approx 1 \tag{6.56}$$

because all the contributions to the argument that come from the integral are damped by a factor of $\hat{k}$. We again see that the pseudo Weiss approximation is the expected outcome for small $\hat{k}$.

6.6 The numerical treatment

In this section the numerical results are presented. The necessity of an integration cutoff is explained.

6.6.1 The integration cutoff

$V_{\text{eff}}^{(1)}$ is calculated using the techniques explained in chapter 3 and section 6.2. The evaluation of the proper time integrand I_T is somewhat troublesome. In figure 6.2 we have a typical plot of a proper time integrand, with the gauge field given by $\hat{a} = \hat{k} = \hat{\delta}_a = 1$, evaluated at $x_1 = x_2 = 0$. We see the typical behaviour of the T-integrands: The absolute value approaches a maximum and then the function goes to zero. At some point the numerical error will dominate. The integrand is given by

$$\begin{aligned} I_T =& \frac{\mathcal{N}}{T^3} \int \mathcal{D}y \sum_{n=1}^{\infty} e^{-\frac{n^2}{4T}} e^{-\frac{1}{4}\int_0^1 \mathrm{d}t\, \dot{y}^2} \\ & \times \cos\left(n \int_0^1 \mathrm{d}t \left[\hat{a} + \hat{\delta}_a \cos\left(\hat{k}(x_1 + \sqrt{T} y_1)\right) \cos\left(\hat{k}(x_2 + \sqrt{T} y_2)\right) \right] \right) \\ & \times \cos\left(\sqrt{T} \int_0^1 \mathrm{d}t\, \dot{y}_0 \left[\hat{a} + \hat{\delta}_a \cos\left(\hat{k}(x_1 + \sqrt{T} y_1)\right) \cos\left(\hat{k}(x_2 + \sqrt{T} y_2)\right) \right] \right) \\ & \times \cosh\left(2T\, \hat{k}\hat{\delta}_a \int_0^1 \mathrm{d}t \left[\sin^2\left(\hat{k}(x_1 + \sqrt{T} y_1)\right) \cos^2\left(k(x_2 + \sqrt{T} y_2)\right) \right.\right. \\ & \qquad \left.\left. + \cos^2\left(\hat{k}(x_1 + \sqrt{T} y_1)\right) \sin^2\left(\hat{k}(x_2 + \sqrt{T} y_2)\right) \right]^{\frac{1}{2}} \right) . \end{aligned} \tag{6.57}$$

Because of the hyperbolic cosine function in the integrand the smallest error in the Monte Carlo calculation will eventually become big. The difficult contribution looks like: $\cosh(2T\,\hat{k}\hat{\delta}_a \Phi_{\text{MC}})$, where Φ_{MC} is computed up to some (in general T dependent) error. We see that as T grows the effect of this error will be exponentially enhanced. We also see that to enlarge the range of validity of the computation of the T-integrand we have to choose $\hat{k}\hat{\delta}_a$ to be smaller. Not being able to compute the integrand we of course also cannot perform an integration. We will therefore have to abort the integration at some finite value of T. This requires us to find an abortion criterion to decide where to stop the integration.

We choose to cut off the integration where the absolute value of the integrand has its first minimum (that is not a zero crossing). Should this point have a value bigger than ten we cut off at $T = 10$. If the cutoff is done at a $T < 2$ the results are considered unusable and are not shown here. Cutting off the integration range causes an error which we cannot quantify. We therefore do not give any errors for the results as we have no means to estimate them, but believe them to be small as long as the main contribution to the integral is not cut off, which should be the case if the cutoff is done at a $T > 4$. The Romberg integration routine `qromo` implemented with `midpnt` from [38] was again used for the integration.

6.6.2 The effective potential

In figure 6.3 we see the effective potential for different values of the parameters $\hat{\delta}_a$ and $\hat{k}$. Figure 6.3 (a) shows that setting $\hat{\delta}_a = 0.1$ and $\hat{k} = 1.0$ does not have a notable effect either for the pseudo Weiss approximation or the worldline numerical

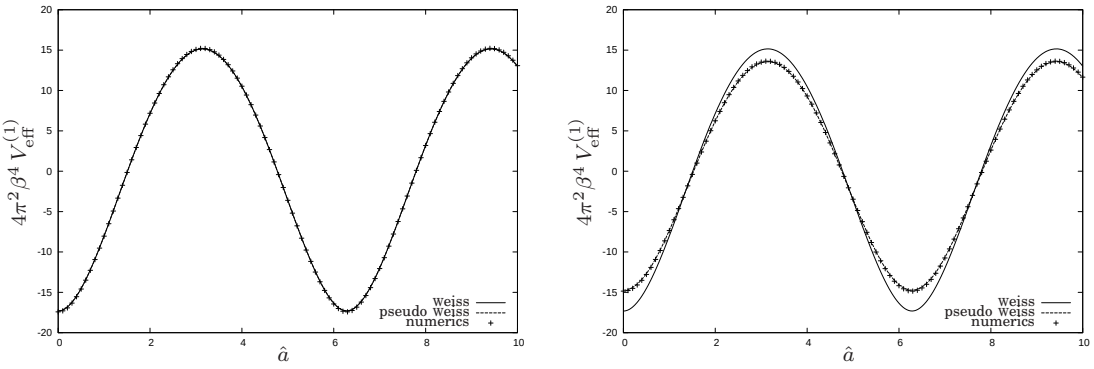

(a) $\hat{\delta}_a = 0.1$, $\hat{k} = 1.0$ (b) $\hat{\delta}_a = 1.0$, $\hat{k} = 0.1$

Figure 6.3: The one-loop effective potential with two different values of $\hat{\delta}_a$ and $\hat{k}$. 100 loops of 101 points were used for the computation.

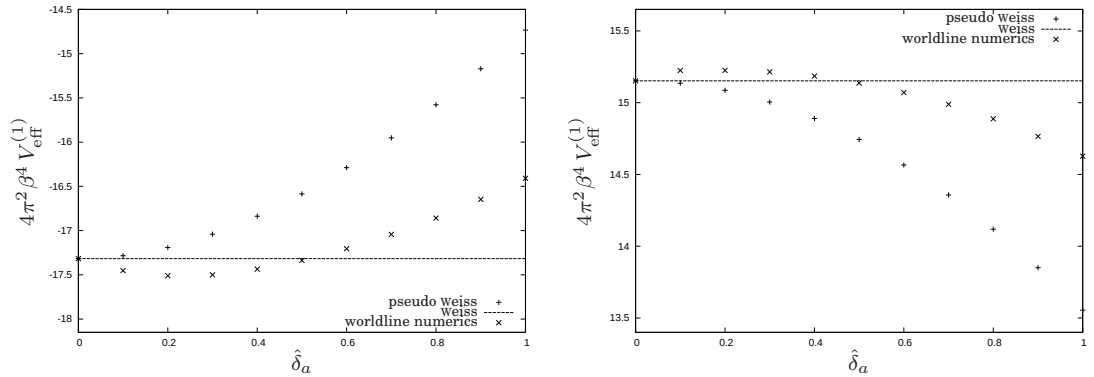

(a) $\hat{a} = 0$ (b) $\hat{a} = \pi$

Figure 6.4: The one-loop effective potential as a function of $\hat{\delta}_a$ at $\hat{k} = 1$. 100 loops of 101 points were used for the computation.

results. This is different when one sets $\hat{\delta}_a = 1.0$ and $\hat{k} = 0.1$. The corresponding plot is given in figure 6.3 (b). The pseudo Weiss approximation and the worldline numerical results deviate from the Weiss solution, but they agree with each other. As expected, the pseudo Weiss approximation is useful in the case of small $\hat{k}$. The minima of the numerical results lie above the minima in the constant field case (Weiss solution) and the maxima of the numerical results underneath the maxima in the constant field case.

Altogether, we can state that the overall structure of the Weiss solution is preserved and the maxima and minima stay at the same values of $\hat{a}$, which are zero and π respectively.

To get a better idea of the effect of varying the two parameters, we now turn to

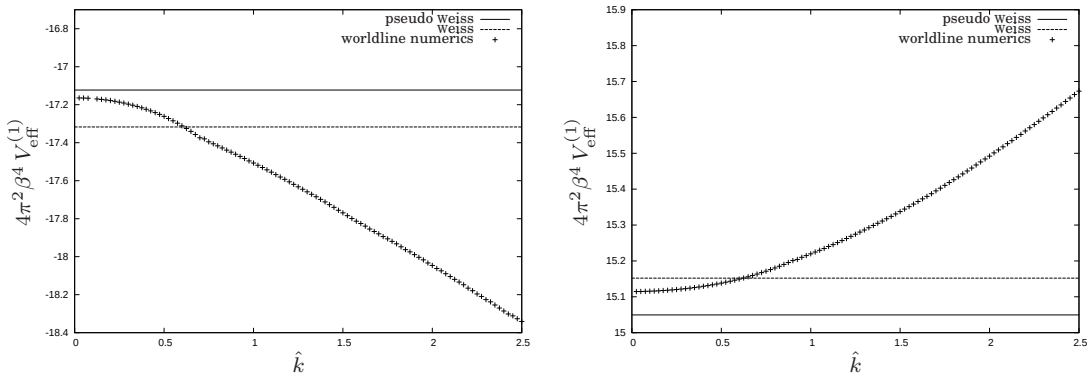

(a) $\hat{a} = 0$ (b) $\hat{a} = \pi$

Figure 6.5: The one-loop effective potential as a function of $\hat{k}$ at $\hat{\delta}_a = 0.25$. 100 loops of 101 points were used for the computation.

figures in which the effective potential, with one of the parameters fixed, is shown. These plot are done at the minimum and the maximum, i.e. $\hat{a} = 0$ and $\hat{a} = \pi$. The Weiss solution and the pseudo Weiss approximation are also shown. The parameter range on the abscissa includes values that allow for a cutoff bigger than three.

At $\hat{\delta}_a$ or $\hat{k}$ equal to zero the numerical treatment we use breaks down. The problem we have is in fact that there is no numerical difficulty and a cutoff of the integration is not necessary. The algorithm that searches for the cutoff value of T therefore gives a useless result. For $\hat{k} = 0$ there is the additional problem that the integration together with the fraction in front of the integral cannot be handled numerically as they have to be treated as a limiting process. We again get useless results. For this reason at $\hat{\delta}_a = 0$ and $\hat{k} = 0$ there are no worldline numerical results given.

In figure 6.4 we see the one-loop effective potential as a function of $\hat{\delta}_a$ with $\hat{k} = 1$. We can see something quite remarkable and unexpected. In figure 6.4 (a) the data shows a minimum that lies beneath the minimum of the Weiss solution at about $\hat{\delta}_a = 0.25$. This indicates that the varying field might be favoured over a constant field. As can be seen on figure 6.4 (b) at $\hat{\delta}_a = 0.25$, where the minimum was in figure 6.4 (a), there is a maximum that exceeds the maximum of the Weiss solution.

To find out how this minimum (maximum) depends on the value of $\hat{k}$, we now turn to plots in which $\hat{\delta}_a = 0.25$ and $\hat{k}$ is varied. Figure 6.5 is the first of a whole series of similar plots. The kink that can be seen in the figures 6.5 (a)-6.9 (a) is caused by the numerical integration. When the point, where the kink is, is passed, to get the required relative error of 10^{-5} one integration step less is needed and performed.

Since the pseudo Weiss approximation does not depend on $\hat{k}$, both, the Weiss solution and the pseudo Weiss approximation, are given as horizontal lines. In the case of $\hat{a} = 0$, the one-loop effective potential starts above the Weiss minimum

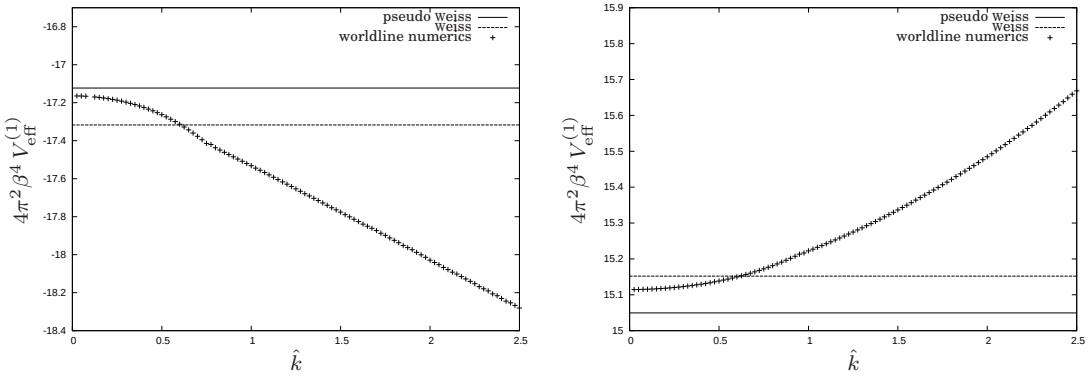

(a) $\hat{a} = 0$ (b) $\hat{a} = \pi$

Figure 6.6: The one-loop effective potential as a function of $\hat{k}$ at $\hat{\delta}_a = 0.25$. A different loop cloud than in figure 6.5 was used for the computation. The loop cloud consisted of 100 loops of 101 points.

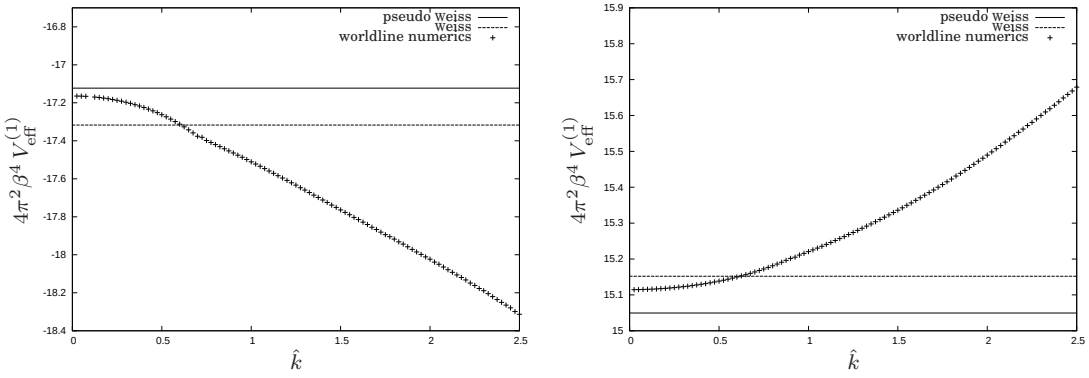

(a) $\hat{a} = 0$ (b) $\hat{a} = \pi$

Figure 6.7: The one-loop effective potential as a function of $\hat{k}$ at $\hat{\delta}_a = 0.25$. A bigger loop cloud than in figure 6.5 was used for the computation. The loop cloud consisted of 100 loops of 1001 points.

with a negative slope and then intersects the Weiss solution. It keeps decreasing until finally the numerics becomes unreliable. In the case of $\hat{a} = \pi$, the one-loop effective potential starts beneath the Weiss maximum with a positive slope and then intersects the Weiss solution. It keeps increasing until finally the numerics becomes unreliable.

In order to clarify whether or not this behaviour is caused by a numerical artefact we take a look at the same plot, but this time different loop clouds were used to get the data.

A different loop cloud than for the data shown in figure 6.5, that was of the same size as the loop cloud used for the data in figure 6.5, was employed to generate the

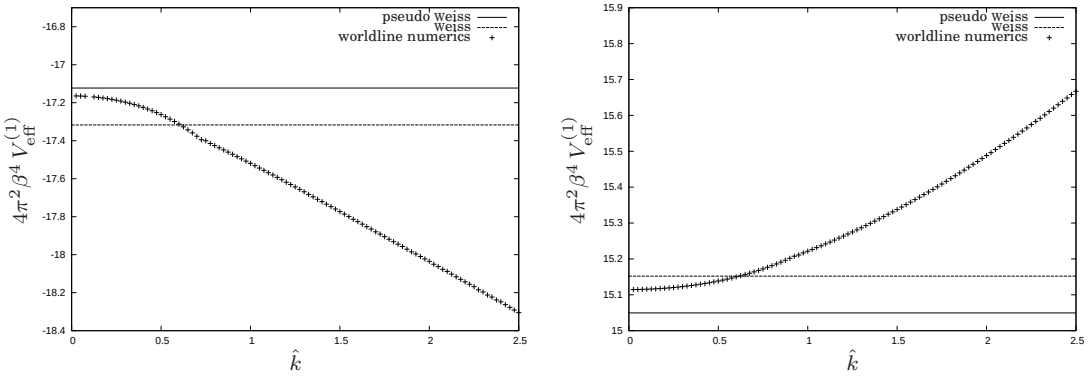

(a) $\hat{a} = 0$ (b) $\hat{a} = \pi$

Figure 6.8: The one-loop effective potential as a function of $\hat{k}$ at $\hat{\delta}_a = 0.25$. A bigger loop cloud than in figure 6.5 was used for the computation. The loop cloud consisted of 1000 loops of 101 points.

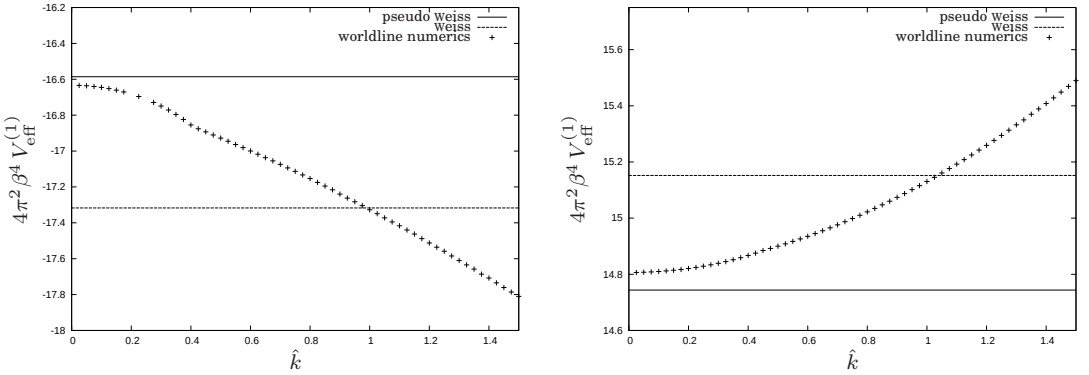

(a) $\hat{a} = 0$ (b) $\hat{a} = \pi$

Figure 6.9: The one-loop effective potential as a function of $\hat{k}$ at $\hat{\delta}_a = 0.5$. 100 loops of 101 points were used for the computation.

data shown in figure 6.6. The data that is shown in the figures 6.7 and 6.8 was generated with clouds of 100 loops of 1001 points and clouds of 1000 loops of 101 points respectively. We see that the result worldline numerics delivers remains the same. Although this is hardly a proof of the results not just being some numerical junk that is collected by the algorithm at some point during the calculation, this makes us trust our findings insofar as we would assume numerical problems to depend notably on the loop cloud that is used. Furthermore, we would expect such problems to become bigger as we choose either $\hat{\delta}_a$ or $\hat{k}$ bigger since the numerical stability depends on them. Assuming this, figure 6.4 tells us that the minimum (maximum) at $\hat{\delta}_a = 0.25$ cannot be the result of numerical problems because choosing $\hat{\delta}_a$ bigger makes the minimum (maximum) disappear.

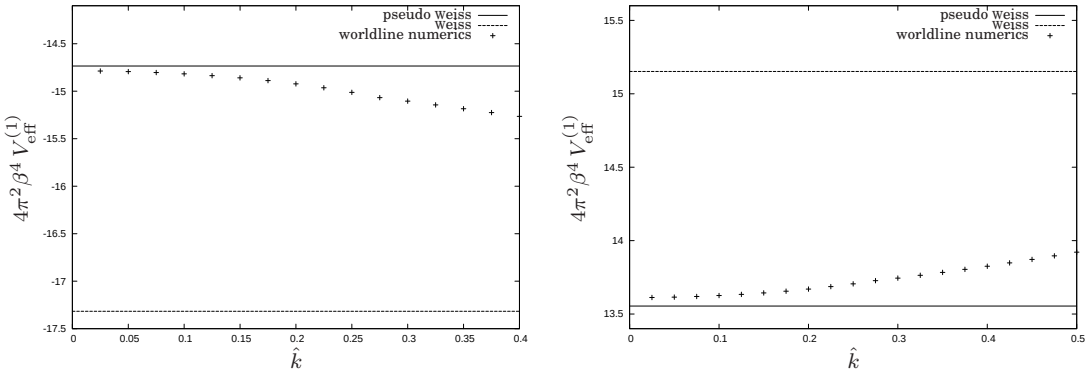

(a) $\hat{a} = 0$ (b) $\hat{a} = \pi$

Figure 6.10: The one-loop effective potential as a function of $\hat{k}$ at $\hat{\delta}_a = 1$. 100 loops of 101 points were used for the computation.

We, however, do not fully understand the numerical data at small $\hat{k}$. The plots in the figures 6.5-6.7 show an unexpected behaviour. Instead of approaching the pseudo Weiss solution, the numerical data goes to a different value. Since the result is the same for different loop clouds, it cannot simply be dismissed as an effect of the uncertainty which Monte Carlo methods necessarily entail. Further research is required in order to understand this puzzling behaviour.

In figure 6.9 and figure 6.10 the one-loop effective potential is plotted as in figure 6.4 but this time with $\hat{\delta}_a = 0.5$ and $\hat{\delta}_a = 1$ respectively. We see that the qualitative picture does not change. In the minimum the pseudo Weiss approximation moves upwards with the numerical data following it as $\hat{\delta}_a$ is chosen bigger. In the maximum it is just the other way around. The pseudo Weiss approximation moves downwards with the numerical data following it as $\hat{\delta}_a$ is chosen bigger. The point where the Weiss solution is intersected moves to the right. In figure 6.10 the intersection point does not lie in the accessible parameter range.

The data obtained clearly indicates a varying field to be favoured over the constant field.

7 Conclusions and Outlook

In chapter 4 the application of the worldline numerical method to the pseudoabelian background field and the PNA field was presented. We saw that the pseudoabelian field is well treatable in two gauges, which shows that there are fields for which worldline numerics is able to compute the Wilson loop expectation value and to conserve the gauge invariance of the Wilson loop expectation value (see figure 4.2). For the first time the one-loop effective Lagrangian density of the PNA field was calculated (see figure 4.7).

Although it is possible to calculate an analytic expression for the one-loop effective Lagrangian density of the PNA field [40], this has not yet been done.

In chapter 5 we investigated how useful worldline numerics is to calculate the one-loop effective action of an instanton background field. The Wilson loop expectation value in an instanton background field has been computed in two gauges: the regular gauge (BPST instanton) and the singular gauge (singular instanton). The results in both gauges did *not* match (see figure 5.2). Because the Wilson loop expectation value is gauge invariant, this indicates a failure of the straightforward method used. We compared the analytically known a_1, which is the coefficient of order T^2 in the inverse mass expansion, with the estimates computed using a fitting procedure. While the Wilson loop expectation value of the singular instanton gave good results in the parameter range we expected it to be well treatable (small x), the BPST instanton did so only very close to the origin and showed very bad agreement with the true value anywhere else although the gauge field itself was well behaved throughout the whole 4-dimensional space we worked in (see figures 5.3 and 5.4). In the limit of big x, instead of falling off like x^{-8}, it fell off like x^{-4} as x grew. As pointed out in section 5.3, this wrong behaviour could be retraced to a flawed computation of integrations over worldline correlation functions which spoiled a non-trivial cancellation of terms of order x^{-4}, which was responsible for the analytical decay like x^{-8}. Because this cancellation was not reproduced precisely enough we were left with a term of order x^{-4}, which dominated the behaviour of the numerically obtained a_1 in the BPST case. In section 5.4, how well the numerical method conserves the Lorentz structure of such integrations over worldline correlation functions was improved by rotating the loop cloud. This, however, did not improve the results for the a_1 of the BPST instanton. Enlarging the loop cloud improved the results but did so at such terrible speed (see figure 5.5 and figure 5.6) that loop clouds seemed to be needed that exceed today's possibilities by far. We saw no way for us to get reliable results for the Wilson loop expectation value in the whole range of integration necessary to compute the one-loop effective action of the

BPST instanton within a reasonable time span. For the time being, we therefore considered the use of worldline numerics to calculate the one-loop effective action in a BPST instanton background field to be suboptimal. Although we did not succeed to compute the one-loop effective action, we have discovered a new feature of worldline numerics that only appears when one tries to treat non-abelian fields: should the computation involve non-trivial cancellations of terms that contribute to the inverse mass expansion, the worldline numerical method might not be able to compute the correct Wilson loop expectation value. Using worldline numerics to compute the one-loop effective action, one should choose the field in a way that no such cancellations take place, but the large-x-behaviour of every contribution to the coefficient of order T^2 in the inverse mass expansion as given in (5.21) coincides with the large-x-behaviour of $\mathrm{tr}[\mathbf{G}_{\mu\nu}\mathbf{G}_{\mu\nu}]$.

Using worldline numerics, the one-loop effective action of the instanton has so far not been calculated. We believe this to be possible using the singular instanton. As has been stated, the standard discretisation will run into the same difficulties as the ones known from the path integral formulation of the hydrogen problem in quantum mechanics. But since these problems have been solved (see [44]), one should be able to perform the calculation utilising the solution for the hydrogen problem employing hybrid Monte Carlo methods.

We stated that in three dimensions rotating the cloud about only one axis results in numerical computations for $\int_0^1 \mathrm{d}t \int_0^1 \mathrm{d}t' \, \langle \, \dot{y}_\mu(t) y_\nu(t) \dot{y}_\alpha(t') y_\beta(t') \, \rangle$ that show the analytically expected Lorentz structure. We have not gained any insight into why or how this is the case.

In chapter 6 we computed the effect the perturbation by $\delta_a \cos(kx_1)\cos(kx_2)$ has on the one-loop effective potential of the zero-component of an SU(2) gauge field in thermal equilibrium. We found the overall structure of the constant field solution to be unchanged by the fact that the field varys (see figure 6.3). While the results are not fully understood in the whole parameter range, the numerical data clearly indicated that a varying field is favoured over the constant field (see the figures 6.4-6.10).

This calls for further research in order to clarify and verify the results obtained. The most urgent step is to enlarge the loop clouds in order to stabilise the numerical treatment.

A Appendix

A.1 Proper time representation

In this section we show that for Hermitian and positive definite matrices $\mathbf{A}$ and $\mathbf{B}$

$$\operatorname{tr}\left(\ln(\mathbf{A}) - \ln(\mathbf{B})\right) = -\int_0^\infty \frac{\mathrm{d}T}{T} \operatorname{tr}\left(e^{-\mathbf{A}T} - e^{-\mathbf{B}T}\right) . \tag{A.1}$$

Let a_i and b_i be the eigenvalues of $\mathbf{A}$ and $\mathbf{B}$. We find that

$$\begin{aligned}
\int_0^\infty \frac{\mathrm{d}T}{T} \operatorname{tr}\left(e^{-\mathbf{A}T} - e^{-\mathbf{B}T}\right) &= \lim_{\alpha\to 0} \int_\alpha^\infty \frac{\mathrm{d}T}{T} \operatorname{tr}\left(e^{-\mathbf{A}T} - e^{-\mathbf{B}T}\right) \\
&= \lim_{\alpha\to 0} \Big[\int_\alpha^\infty \frac{\mathrm{d}T}{T} \operatorname{tr} e^{-\mathbf{A}T} - \int_\alpha^\infty \frac{\mathrm{d}T}{T} \operatorname{tr} e^{-\mathbf{B}T} \Big] \\
&= \lim_{\alpha\to 0} \Big[\sum_i \int_\alpha^\infty \frac{\mathrm{d}T}{T} e^{-a_i T} - \int_\alpha^\infty \frac{\mathrm{d}T}{T} e^{-b_i T} \Big] \\
&= \sum_i \lim_{\alpha\to 0} \Big[\int_{a_i\alpha}^\infty \frac{\mathrm{d}x}{x} e^{-x} - \int_{b_i\alpha}^\infty \frac{\mathrm{d}x}{x} e^{-x} \Big] .
\end{aligned} \tag{A.2}$$

With the exponential integral

$$\begin{aligned}
\operatorname{Ei}(x) &= \int_{-\infty}^x \frac{\mathrm{d}t}{t} e^t \\
&= -\int_x^\infty \frac{\mathrm{d}t}{t} e^{-t} \\
&= \mathrm{C_E} + \ln|x| + \sum_{k=1}^\infty \frac{x^k}{k\,k!} ,
\end{aligned} \tag{A.3}$$

where $\mathrm{C_E} = 0.577215665...$ is the Euler constant, we can write:

$$\begin{aligned}
\int_0^\infty \frac{\mathrm{d}T}{T} \operatorname{tr}\left(e^{-\mathbf{A}T} - e^{-\mathbf{B}T}\right) &= \sum_i \lim_{\alpha\to 0} \Big[-\operatorname{Ei}(-a_i\alpha) + \operatorname{Ei}(-b_i\alpha) \Big] \\
&= \sum_i \lim_{\alpha\to 0} \Big[\mathrm{C_E} + \ln(b_i\alpha) + \sum_{k=1}^\infty \frac{(b_i\alpha)^k}{k\,k!} - \mathrm{C_E} - \ln(a_i\alpha) - \sum_{k=1}^\infty \frac{(a_i\alpha)^k}{k\,k!} \Big] \\
&= \sum_i \ln(b_i) - \ln(a_i) \\
&= -\operatorname{tr}\left(\ln(\mathbf{A}) - \ln(\mathbf{B})\right) .
\end{aligned} \tag{A.4}$$

This concludes the proof.

A.2 The matrix element in the trace

In this section a path integral expression for the matrix elements $\langle x|e^{-(-\mathbf{D}^2+m^2)T}|x\rangle$, which we encountered calculating the trace of the fluctuation operator in (2.47), is derived. Since

$$\langle x|e^{-(-\mathbf{D}^2+m^2)T}|x\rangle = e^{-m^2T}\langle x|e^{\mathbf{D}^2T}|x\rangle \;, \tag{A.5}$$

the only difficult part is calculating $\langle x|e^{\mathbf{D}^2T}|x\rangle$. This can be done in the same way as the introduction of Feynman path integrals in a quantum mechanics course. First we define $\tau = \frac{T}{N}$, with τ very small (and N very big), write the exponential as a product of N exponentials, with T replaced by τ, and use $N-1$ sets of the space basis $|x\rangle$ to separate the product's N factors. We can then write:

$$\begin{aligned}\langle x|e^{\mathbf{D}^2T}|x\rangle &= \lim_{N\to\infty}\langle x|\prod_{i=1}^{N} e^{\mathbf{D}^2\tau}|x\rangle \\ &= \lim_{N\to\infty}\Big[\int \mathrm{d}^d x_1 \,\ldots\, \int \mathrm{d}^d x_{N-1}\,\langle x|e^{\mathbf{D}^2\tau}|x_1\rangle \,\ldots\, \langle x_{N-1}|e^{\mathbf{D}^2\tau}|x\rangle\Big] \;,\end{aligned} \tag{A.6}$$

where we use d instead of D to denote the number of space-time dimensions. Since τ is very small, we can expand the exponentials and keep only the term of order one. For every factor in (A.6), this yields that

$$\begin{aligned}\langle x_i|e^{\mathbf{D}^2\tau}|x_{i+1}\rangle &= \langle x_i|x_{i+1}\rangle + \langle x_i|(\partial_\mu + \mathbf{A}_\mu)(\partial_\mu + \mathbf{A}_\mu)\tau|x_{i+1}\rangle \\ &= \delta(x_i - x_{i+1}) + \langle x_i|(\partial^2 + \partial_\mu\mathbf{A}_\mu + \mathbf{A}_\mu\partial_\mu + \mathbf{A}^2)\tau|x_{i+1}\rangle \\ &= \delta(x_i - x_{i+1}) + \langle x_i|\partial^2|x_{i+1}\rangle\tau \\ &\quad + \langle x_i|(\partial_\mu\mathbf{A}_\mu)|x_{i+1}\rangle\tau + 2\langle x_i|\mathbf{A}_\mu\,\partial_\mu|x_{i+1}\rangle\tau \\ &\quad + \langle x_i|\mathbf{A}^2|x_{i+1}\rangle\tau \\ &= \delta(x_i - x_{i+1}) + \langle x_i|(\partial^2 + \partial_\mu\mathbf{A}_\mu + \mathbf{A}_\mu\partial_\mu + \mathbf{A}^2)\tau|x_{i+1}\rangle \\ &= \delta(x_i - x_{i+1}) + \langle x_i|\partial^2|x_{i+1}\rangle\tau \\ &\quad + 2\langle x_i|\mathbf{A}_\mu\,\partial_\mu|x_{i+1}\rangle\tau \;+ \mathbf{A}^2\big(\frac{x_i + x_{i+1}}{2}\big)\langle x_i|x_{i+1}\rangle\tau \\ &\quad + \partial_\mu\mathbf{A}_\mu\big(\frac{x_i + x_{i+1}}{2}\big)\langle x_i|x_{i+1}\rangle\tau \;.\end{aligned} \tag{A.7}$$

As Schulman shows in [50], it is correct to choose $\langle x_i|\mathbf{A}_\mu|x_{i+1}\rangle = \mathbf{A}_\mu(\frac{x_i+x_{i+1}}{2}) := \mathbf{A}_\mu(\zeta_i)$. Assuming $\mathbf{A}_\mu$ to vanish sufficiently quickly, we can use Gauß' law to get rid of the last term in (A.7). Expanding in terms of momentum eigenstates, we find that

$$\begin{aligned}\langle x_i|e^{\mathbf{D}^2\tau}|x_{i+1}\rangle &= \frac{1}{(2\pi)^d}\int \mathrm{d}^d p_i\, e^{ip_i(x_i - x_{i+1})}\Big[1 + \tau(-p_i^2 + i2\mathbf{A}(\zeta_i)p_i + \mathbf{A}(\zeta_i)^2)\Big] \\ &= \frac{1}{(2\pi)^d}\int \mathrm{d}^d p_i\, e^{ip_i(x_i - x_{i+1})}e^{\tau(-p_i^2 + i2\mathbf{A}(\zeta_i)p_i + \mathbf{A}(\zeta_i)^2)} \\ &= \frac{1}{(2\pi)^d}\int \mathrm{d}^d p_i\, e^{-\tau(p_i^2 - ip_i(\frac{x_i - x_{i+1}}{\tau} + 2\mathbf{A}(\zeta_i)) - \mathbf{A}(\zeta_i)^2)} \;.\end{aligned} \tag{A.8}$$

Completing the square in the exponent, we derive:

$$\begin{aligned}\langle x_i|e^{\mathbf{D}^2\tau}|x_{i+1}\rangle =& \frac{1}{(2\pi)^d}\int \mathrm{d}^d p_i\, e^{-\tau\left[(p_i+\frac{1}{2i}(2\mathbf{A}(\zeta_i)+\frac{x_i-x_{i+1}}{\tau}))^2+\mathbf{A}(\zeta_i)\frac{x_i-x_{i+1}}{\tau}+\frac{1}{4}(\frac{x_i-x_{i+1}}{\tau})^2\right]}\\ =&\mathcal{N}_i\, e^{-\tau(\mathbf{A}(\zeta_i)\frac{x_i-x_{i+1}}{\tau}+\frac{1}{4}(\frac{x_i-x_{i+1}}{\tau})^2)}\ , \end{aligned} \tag{A.9}$$

where

$$\mathcal{N}_i = \frac{1}{(2\pi)^d}\int \mathrm{d}^d p_i e^{-\tau(p_i+\frac{1}{2i}(2\mathbf{A}(\zeta_i)+\frac{x_i-x_{i+1}}{\tau}))^2}\ . \tag{A.10}$$

If we now plug (A.9) into (A.6), we arrive at our final destination:

$$\begin{aligned}\langle x|e^{\mathbf{D}^2 T}|x\rangle \ =\ \lim_{N\to\infty}\big[\mathcal{N}\int \mathrm{d}^d x_1\ \ldots\ \int \mathrm{d}^d x_{N-1} e^{-\tau(\mathbf{A}(\zeta_0)\frac{x-x_1}{\tau}+\frac{1}{4}(\frac{x-x_1}{\tau})^2)}\ \ldots\\ \times\, e^{-\tau(\mathbf{A}(\zeta_{N-1})\frac{x_{N-1}-x}{\tau}+\frac{1}{4}(\frac{x_{N-1}-x}{\tau})^2)}\big]\\ =:\ \int_{x(0)=x}^{x(T)=x}\mathcal{D}x\ \mathrm{P}\, e^{-\int_0^T \mathrm{d}\tau[\frac{\dot{x}^2}{4}+\dot{x}_\mu \mathbf{A}_\mu]}\ ,\end{aligned} \tag{A.11}$$

where

$$\mathcal{N} = \prod_{i=0}^{N-1}\mathcal{N}_i\ . \tag{A.12}$$

The P denotes path ordering. It is required because the gauge field evaluated for different arguments in general does not commute with itself. It is defined by

$$\begin{aligned}\mathrm{P}e^{\mathbf{A}(t_1)+\mathbf{A}(t_2)+\cdots+\mathbf{A}(t_n)} &:= e^{\mathbf{A}(t_1)}e^{\mathbf{A}(t_2)}\ldots e^{\mathbf{A}(t_n)}\ ,\\ &\text{with } t_1>\cdots>t_n\ .\end{aligned} \tag{A.13}$$

Writing (A.11) without the path ordering, as one does it with an Abelian gauge field, is therefore false. The path ordered integral in (A.11) is an example of a product integral. More information on product integration can be found in [47].

A.3 The v-loop algorithm

Apart from omissions, this section follows the treatment given in [15]. The v-loop algorithm is a very effective tool to generate a set of n_p numbers $\hat{y}=y_i$ distributed as

$$P[\hat{y}] = P[\{y_i\}] = \frac{1}{\mathcal{N}}\delta(y_1+\ldots y_{n_p})\exp\Big[-\frac{n_p}{4}\sum_{k=1}^{n_p}(y_k-y_{k-1})^2\Big] \tag{A.14}$$

so that the expectation value of some quantity $Q(\hat{y})$ can be calculated by

$$\begin{aligned}\langle Q\rangle =& \frac{1}{\mathcal{N}}\int \mathrm{d}\hat{y} P[\hat{y}]Q(\hat{y})\\ =& \lim_{k\to\infty}\Big[\frac{1}{k}\sum_{i=1}^{k}Q(\hat{y}_k)\Big]\ .\end{aligned} \tag{A.15}$$

The idea of its derivation, which can be found in [15], is to perform a linear variable transformation $\hat{y} \to \hat{v}$ so that $P[\hat{v}]$ becomes a product of Gaussian distributions, which are easy to generate. As a recipe the v-loop algorithm can be summarised in just a few steps:

(1) generate $n_p - 1$ numbers w_i, $i = 1, \ldots, n_p - 1$ such that they are distributed according to $\exp(-w_i^2)$

(2) compute $\bar{v}_i$, $i = 1, \ldots, n_p - 1$, by normalising the w_i:

$$\begin{aligned} \bar{v}_1 &= \sqrt{\frac{2}{n_p}}\, w_1, \\ \bar{v}_i &= \frac{2}{\sqrt{n_p}} \sqrt{\frac{n_p + 1 - i}{n_p + 2 - i}}\, w_i, \quad i = 2, \ldots, n_p - 1 \end{aligned} \tag{A.16}$$

(3) compute v_i, $i = 2, \ldots, n_p - 1$, using

$$v_i = \bar{v}_i - \frac{1}{n_p + 2 - i}\, v_{i-1,1}, \quad \text{where } v_{i-1,1} = \sum_{j=2}^{i-1} v_j \tag{A.17}$$

(4) construct the unit loops according to

$$\begin{aligned} y_1 &= \frac{1}{n_p} \left(\bar{v}_1 - \sum_{i=2}^{n_p - 1} \left(n_p - i + \frac{1}{2} \right) v_i \right), \\ y_i &= y_{i-1} + v_i, \quad i = 2, \ldots, n_p - 1, \\ y_{n_p} &= -\sum_{i=1}^{n_p - 1} y_i \, . \end{aligned} \tag{A.18}$$

A.4 The inverse mass expansion in terms of the gauge field

As is well known and has been used throughout this thesis, the Wilson loop expectation value possesses an expansion of the form:

$$\begin{aligned} \langle \, \mathrm{tr} \mathrm{P}\, e^{-\oint \mathrm{d}x_\mu \mathbf{A}_\mu} \, \rangle &= a_0 + a_1\, T^2 + O(T^4) \\ &= \mathrm{tr}\mathbf{1} - \frac{1}{12} \mathrm{tr}[(\mathbf{G}_{\mu\nu})^2] T^2 + O(T^4) \, . \end{aligned} \tag{A.19}$$

In this section of the appendix we will derive a_1, i.e. the coefficient of order T^2 of the inverse mass expansion. The derivation is done purely in terms of the gauge field and not as it is usually done in Fock-Schwinger gauge (see e.g. [8]), which makes it possible to express the gauge fields in terms of the field strength tensor. This will be done for an Abelian as well as for a non-abelian gauge theory. In an Abelian gauge theory the path ordering in the definition of the Wilson loop has no effect and can thus be dropped. This makes the derivation we are about to undertake much more convenient. We will therefore turn to the Abelian case first.

A.4.1 Abelian case

Starting with the definition of the Wilson loop, we first drop the path ordering and write the exponential using all the notation we are used to. The path, along which the integration needs to be done, is denoted by y. We again use T for the proper time and x is the "centre of mass" of the loop, for which we calculate the Wilson loop. In an Abelian gauge theory the only generator of the gauge group is 1. For the sake of notational simplicity we will scale the coupling constant into the fields and take the field to be a purely imaginary number: $\mathrm{Re}(A) = 0$. The Wilson loop then looks like

$$W = e^{-\sqrt{T}\int_0^1 \mathrm{d}t\, \dot{y}_\mu(t)\, A_\mu(x+\sqrt{T}y(t))} ,$$

which is after expanding the exponential

$$= \sum_{k=0}^{\infty} \frac{(-1)^k}{k!}\, T^{\frac{k}{2}} \Big[\int_0^1 \mathrm{d}t\, \dot{y}_\mu(t)\, A_\mu(x+\sqrt{T}y(t)) \Big]^k . \tag{A.20}$$

Now we expand the gauge field itself:

$$\int_0^1 \mathrm{d}t\, \dot{y}_\mu(t)\, A_\mu(x+\sqrt{T}y(t)) = \int_0^1 \mathrm{d}t\, \dot{y}_\mu(t) \sum_{r=0}^{\infty} \frac{T^{\frac{r}{2}}}{r!} \partial_\nu^{(r)} A_\mu(x)\, y_\nu^r(t) , \tag{A.21}$$

where $\partial_\nu^{(r)} A_\mu(x)\, y_\nu^r(t)^r$ in (A.21) is short for

$$\partial_\nu^{(r)} A_\mu(x)\, \tilde{y}_\nu^r = \underbrace{\partial_\alpha \partial_\beta \ldots \partial_\omega}_{r\text{times}} A_\mu(x) \underbrace{y_\alpha(t) y_\beta(t) \ldots y_\omega(t)}_{r\text{times}} . \tag{A.22}$$

For the Wilson loop we then have:

$$W = \sum_{k=0}^{\infty} \frac{(-1)^k}{k!}\, T^{\frac{k}{2}} \Big[\int_0^1 \mathrm{d}t\, \dot{y}_\mu(t) \sum_{r=0}^{\infty} \frac{T^{\frac{r}{2}}}{r!} \partial_\nu^{(r)} A_\mu(x)\, y_\nu^r(t) \Big]^k . \tag{A.23}$$

Because the paths that we consider are loops, the first term (corresponding to $r = 0$) of the sum in (A.21) vanishes:

$$\begin{aligned} \int_0^1 \mathrm{d}t\, \dot{y}_\mu(t)\, T^0 A_\mu(x) &= A_\mu(x) \int_0^1 \mathrm{d}t\, \dot{y}_\mu(t) \\ &= 0 . \end{aligned} \tag{A.24}$$

To get the coefficient of order T^2 of the inverse mass expansion a_1, we simply have to count powers, add all contributions in (A.23) that are of order T^2 and calculate its expectation value. There are only two terms in (A.23) that contribute to the coefficient of order T^2. They correspond to $k = 1$ and $k = 2$:

$$-T^2 \int_0^1 \mathrm{d}t\, \dot{y}_\mu(t)\, \partial_\nu \partial_\alpha \partial_\beta A_\mu(x)\, y_\nu(t) y_\alpha(t) y_\beta(t)$$

and

$$T^2\,\frac{1}{2}\int_0^1 \mathrm{d}t\,\dot{y}_\mu(t)\,\partial_\nu A_\mu(x)\,y_\nu(t)\;\int_0^1 \mathrm{d}t'\,\dot{y}_\alpha(t')\,\partial_\beta A_\alpha(x)\,y_\beta(t')\;. \tag{A.25}$$

The coefficient a_1 is now just the expectation value of the sum of the two contributions:

$$\begin{aligned} a_1 =& \Big\langle\; -\partial_\nu\partial_\alpha\partial_\beta A_\mu(x)\;\int_0^1 \mathrm{d}t\,\dot{y}_\mu(t)y_\nu(t)y_\alpha(t)y_\beta(t) \\ &+\;\frac{1}{2}\,\partial_\nu A_\mu(x)\,\partial_\beta A_\alpha(x)\;\int_0^1 \mathrm{d}t\int_0^1 \mathrm{d}t'\;\dot{y}_\mu(t)y_\nu(t)\dot{y}_\alpha(t')y_\beta(t')\Big\rangle \\ =&\frac{1}{2}\,\partial_\nu A_\mu(x)\,\partial_\beta A_\alpha(x)\;\int_0^1 \mathrm{d}t\int_0^1 \mathrm{d}t'\;\langle\;\dot{y}_\mu(t)y_\nu(t)\dot{y}_\alpha(t')y_\beta(t')\;\rangle \\ &-\partial_\nu\partial_\alpha\partial_\beta A_\mu(x)\;\int_0^1 \mathrm{d}t\,\langle\;\dot{y}_\mu(t)y_\nu(t)y_\alpha(t)y_\beta(t)\;\rangle\;. \end{aligned} \tag{A.26}$$

A.4.2 Non-abelian case

We start with the exponential that appears in the definition of the Wilson loop, writing it using all the notation we are used to. The path, along which the integration needs to be done, is denoted by y. We again use T for the proper time and x is the "centre of mass" of the loop, for which we calculate the Wilson loop. We find that

$$\begin{aligned} \mathrm{P}\,e^{-\oint \mathrm{d}x_\mu \mathbf{A}_\mu} =& \mathrm{P}\,e^{-\sqrt{T}\,\int_0^1 \mathrm{d}t\,\dot{y}_\mu(t)\,\mathbf{A}_\mu(x+\sqrt{T}y(t))} \\ &= \lim_{N\to\infty}\prod_{n=1}^{N} e^{-\sqrt{T}\,(y_\mu^n - y_\mu^{n-1})\,\mathbf{A}_\mu(x+\sqrt{T}\frac{y^n+y^{n-1}}{2})} \\ &= \lim_{N\to\infty}\prod_{n=1}^{N} e^{-\sqrt{T}\,y'^n_\mu\,\mathbf{A}_\mu(x+\sqrt{T}\tilde{y}^n)}\;, \end{aligned} \tag{A.27}$$

where y_μ^n denotes the μ component of the loop $y_\mu(t)$ evaluated at $t = n/N$ and we introduced two new quantities:

$$y'^n_\mu = (y_\mu^n - y_\mu^{n-1}) \quad \text{and} \quad \tilde{y}_\mu^n = \frac{y_\mu^n + y_\mu^{n-1}}{2}\;. \tag{A.28}$$

We now expand first the exponential and then the gauge field about $T = 0$. We find:

$$\begin{aligned} \mathrm{P}\,e^{-\oint \mathrm{d}x_\mu \mathbf{A}_\mu} &= \lim_{N\to\infty}\prod_{n=1}^{N}\sum_{k=0}^{\infty}\frac{1}{k!}\,T^{\frac{k}{2}}\Big[-y'^n_\mu\mathbf{A}_\mu(x+\sqrt{T}\frac{y^n+y^{n-1}}{2})\Big]^k \\ &= \lim_{N\to\infty}\prod_{n=1}^{N}\sum_{k=0}^{\infty}\frac{T^{\frac{k}{2}}}{k!}\Big[-y'^n_\mu\sum_{r=0}^{\infty}\frac{T^{\frac{r}{2}}}{r!}\,\partial_\nu^{(r)}\mathbf{A}_\mu(x)\,(\tilde{y}_\nu^n)^r\Big]^k\;, \end{aligned} \tag{A.29}$$

where $\partial_\nu^{(r)}\mathbf{A}_\mu(x)\,(\tilde{y}_\nu^n)^r$ in (A.29) is short for

$$\partial_\nu^{(r)}\mathbf{A}_\mu(x)\,(\tilde{y}_\nu^n)^r = \underbrace{\partial_\alpha\partial_\beta\ldots\partial_\omega}_{r\text{times}}\mathbf{A}_\mu(x)\,\underbrace{\tilde{y}_\alpha^n\tilde{y}_\beta^n\ldots\tilde{y}_\omega^n}_{r\text{times}}\,. \tag{A.30}$$

This yields that

$$\begin{aligned}
\mathrm{P}\,e^{-\oint \mathrm{d}x_\mu\mathbf{A}_\mu} = \lim_{N\to\infty}\prod_{n=1}^{N}\Big[\mathbf{1} - \quad & T^{\frac{1}{2}}\,y'^n_\mu\sum_{r=0}^{\infty}\frac{T^{\frac{r}{2}}}{r!}\,\partial_\nu^{(r)}\mathbf{A}_\mu(x)\,(\tilde{y}_\nu^n)^r \\
& + \frac{1}{2}T\;\; y'^n_\mu\sum_{r=0}^{\infty}\frac{T^{\frac{r}{2}}}{r!}\,\partial_\nu^{(r)}\mathbf{A}_\mu(x)\,(\tilde{y}_\nu^n)^r \\
& \qquad \times y'^n_\alpha\sum_{s=0}^{\infty}\frac{T^{\frac{s}{2}}}{s!}\,\partial_\beta^{(s)}\mathbf{A}_\alpha(x)\,(\tilde{y}_\beta^n)^s \\
& - \frac{1}{6}T^{\frac{3}{2}}\,y'^n_\mu\sum_{r=0}^{\infty}\frac{T^{\frac{r}{2}}}{r!}\,\partial_\nu^{(r)}\mathbf{A}_\mu(x)\,(\tilde{y}_\nu^n)^r \\
& \qquad \times y'^n_\alpha\sum_{s=0}^{\infty}\frac{T^{\frac{s}{2}}}{s!}\,\partial_\beta^{(s)}\mathbf{A}_\alpha(x)\,(\tilde{y}_\beta^n)^s \\
& \qquad \times y'^n_\kappa\sum_{l=0}^{\infty}\frac{T^{\frac{l}{2}}}{l!}\,\partial_\lambda^{(l)}\mathbf{A}_\kappa(x)\,(\tilde{y}_\lambda^n)^l \\
& + \frac{1}{24}T^2 y'^n_\mu\sum_{r=0}^{\infty}\frac{T^{\frac{r}{2}}}{r!}\,\partial_\nu^{(r)}\mathbf{A}_\mu(x)\,(\tilde{y}_\nu^n)^r \\
& \qquad \times y'^n_\alpha\sum_{s=0}^{\infty}\frac{T^{\frac{s}{2}}}{s!}\,\partial_\beta^{(s)}\mathbf{A}_\alpha(x)\,(\tilde{y}_\beta^n)^s \\
& \qquad \times y'^n_\kappa\sum_{l=0}^{\infty}\frac{T^{\frac{l}{2}}}{l!}\,\partial_\lambda^{(l)}\mathbf{A}_\kappa(x)\,(\tilde{y}_\lambda^n)^l \\
& \qquad \times y'^n_\eta\sum_{k=0}^{\infty}\frac{T^{\frac{k}{2}}}{k!}\,\partial_\zeta^{(k)}\mathbf{A}_\eta(x)\,(\tilde{y}_\zeta^n) \\
& - \ldots\Big]\,.
\end{aligned} \tag{A.31}$$

The Taylor series of $\mathbf{A}_\mu$ is now performed and the result is ordered in powers of T:

$$\begin{aligned}
\mathrm{P}\,e^{-\oint \mathrm{d}x_\mu\mathbf{A}_\mu} = \lim_{N\to\infty}\prod_{n=1}^{N}\Big[\mathbf{1} - \quad & T^{\frac{1}{2}}\;\; \mathbf{A}_\mu(x)y'^n_\mu \\
& - \quad T\;\; \partial_\nu\mathbf{A}_\mu(x)\,y'^n_\mu\tilde{y}_\nu^n \\
& + \frac{1}{2}T\;\; \mathbf{A}_\mu(x)\mathbf{A}_\nu(x)\,y'^n_\mu y'^n_\nu
\end{aligned}$$

$$
\begin{aligned}
&- \frac{1}{2}\, T^{\frac{3}{2}}\ \partial_\nu \partial_\alpha \mathbf{A}_\mu(x)\, y'^n_\mu \tilde{y}^n_\nu \tilde{y}^n_\alpha \\
&+ \quad T^{\frac{3}{2}}\ \partial_\nu \mathbf{A}_\mu(x) \mathbf{A}_\beta(x)\, y'^n_\mu y'^n_\beta \tilde{y}^n_\nu \\
&- \frac{1}{6}\, T^{\frac{3}{2}}\ \mathbf{A}_\mu(x) \mathbf{A}_\alpha(x) \mathbf{A}_\beta(x)\, y'^n_\beta y'^n_\alpha y'^n_\mu \\
&- \frac{1}{6}\, T^2\ \partial_\nu \partial_\alpha \partial_\beta \mathbf{A}_\mu(x)\, y'^n_\mu \tilde{y}^n_\nu \tilde{y}^n_\alpha \tilde{y}^n_\beta \\
&+ \frac{1}{4} T^2\ \partial_\nu \partial_\alpha \mathbf{A}_\mu(x) \mathbf{A}_\beta(x)\, y'^n_\beta y'^n_\mu \tilde{y}^n_\nu \tilde{y}^n_\alpha \\
&+ \frac{1}{4} T^2\ \mathbf{A}_\beta(x)\, \partial_\nu \partial_\alpha \mathbf{A}_\mu(x)\, y'^n_\beta y'^n_\mu \tilde{y}^n_\nu \tilde{y}^n_\alpha \\
&+ \frac{1}{2}\, T^2\ \partial_\nu \mathbf{A}_\mu(x) \partial_\beta \mathbf{A}_\alpha(x)\, y'^n_\alpha y'^n_\mu \tilde{y}^n_\beta \tilde{y}^n_\nu \\
&- \frac{1}{6}\, T^2\ \partial_\nu \mathbf{A}_\mu(x) \mathbf{A}_\alpha(x) \mathbf{A}_\beta(x)\, y'^n_\mu y'^n_\alpha y'^n_\beta \tilde{y}^n_\nu \\
&- \frac{1}{6}\, T^2\ \mathbf{A}_\alpha(x) \partial_\nu \mathbf{A}_\mu(x) \mathbf{A}_\beta(x)\, y'^n_\alpha y'^n_\mu y'^n_\beta \tilde{y}^n_\nu \\
&- \frac{1}{6}\, T^2\ \mathbf{A}_\alpha(x) \mathbf{A}_\beta(x) \partial_\nu \mathbf{A}_\mu(x)\, y'^n_\alpha y'^n_\beta y'^n_\mu \tilde{y}^n_\nu \\
&+ \frac{1}{24}\, T^2 \mathbf{A}_\mu(x) \mathbf{A}_\alpha(x) \mathbf{A}_\beta(x) \mathbf{A}_\nu)\, y'^n_\mu y'^n_\alpha y'^n_\beta y'^n_\nu \\
&+ \dots \Big] \,. \qquad \text{(A.32)}
\end{aligned}
$$

Note that the derivatives only act on the field next to them and that the order of the derivatives of the fields and the fields themselves is important because they in general do not commute. We now perform the product in (A.27).

The path ordering requires us to perform the product in (A.27) in the correct order, i.e. multiplying the factor with $n = N$ from the left onto the factor with $n = N - 1 \dots$. Since we are only interested in the coefficient of order T^2, we will only perform those multiplications which yield a contribution of that order. The easiest contributions to find are those corresponding to summands in (A.32) that are of order T^2. Let K_2^n be a representative of those summands evaluated at time n. We can perform the product and write:

$$
\begin{aligned}
\mathrm{P}\, e^{-\oint \mathrm{d}x_\mu \mathbf{A}_\mu} = \lim_{N\to\infty} [(\mathbf{1} + \dots + K_2^N + \dots)(\mathbf{1} + \dots + K_2^{N-1} + \dots) \cdots \\
(\mathbf{1} + \dots + K_2^1 + \dots)] \,. \qquad \text{(A.33)}
\end{aligned}
$$

We only get something of order T^2 if a K_2^n is multiplied with all the $\mathbf{1}$s belonging to the other ns. This means that we get n summands of order T^2:

$$
\begin{aligned}
\mathrm{P}\, e^{-\oint \mathrm{d}x_\mu \mathbf{A}_\mu} &= \lim_{N\to\infty} [K_2^N + K_2^{N-1} + \dots + K_2^1 + \dots)] \\
&= \lim_{N\to\infty} [\sum_{n=1}^{N} K_2^n + \dots] \,. \qquad \text{(A.34)}
\end{aligned}
$$

If we for example take K_2^n to be the first summand of order T^2 in (A.32), we find the contribution to the coefficient of order T^2 in the inverse mass expansion a_1 to be

$$\begin{aligned}\frac{1}{T^2}\lim_{N\to\infty}\Big[\sum_{n=1}^{N}K_2^n\Big] &= \lim_{N\to\infty}\Big[\sum_{n=1}^{N}\frac{1}{6}\,\partial_\nu\partial_\alpha\partial_\beta\mathbf{A}_\mu(x)\,y'^n_\mu\tilde{y}^n_\nu\tilde{y}^n_\alpha\tilde{y}^n_\beta\Big]\\ &= \lim_{N\to\infty}\Big[\frac{1}{6}\,\partial_\nu\partial_\alpha\partial_\beta\mathbf{A}_\mu(x)\sum_{n=1}^{N}y'^n_\mu\tilde{y}^n_\nu\tilde{y}^n_\alpha\tilde{y}^n_\beta\Big]\,. \end{aligned}\tag{A.35}$$

Now let $K_{1/2}^n$ and $K_{3/2}^{n'}$ be representatives of summands in (A.32) that need to be multiplied with each other so that the result is of order T^2. In the same fashion as above we can find the corresponding contribution to a_1:

$$\begin{aligned}\mathrm{P}\,e^{-\oint \mathrm{d}x_\mu\mathbf{A}_\mu} = \lim_{N\to\infty}[&(\mathbf{1}+\cdots+K^N_{\frac{1}{2}}+\cdots+K^N_{\frac{3}{2}}\cdots)\\ &(\mathbf{1}+\cdots+K^{N-1}_{\frac{1}{2}}+\cdots+K^{N-1}_{\frac{3}{2}}+\cdots)\cdots\\ &(\mathbf{1}+\cdots+K^{1}_{\frac{1}{2}}+\cdots+K^{1}_{\frac{3}{2}}+\cdots)]\,.\end{aligned}\tag{A.36}$$

We have various possibilities to combine the Ks. We could, for example, multiply $K^N_{1/2}$ with $\cdots+K^{N-1}_{3/2}$ and the remaining $N-2$ **1**s, or we could multiply $K^N_{1/2}$ with $\cdots+K^{N-2}_{3/2}$ and the other **1**s. This would give the sum $\sum_{n=1}^{N-1}K^N_{1/2}K^n_{3/2}$. Doing the same, starting with $K^{N-1}_{1/2}$, we would get $\sum_{n=1}^{N-2}K^{N-1}_{1/2}K^n_{3/2}$. Note that the exponent and the upper limit of the summation have been reduced by one. This procedure can be used to get another $N-3$ of such sums all contributing additively. Because of the very simple relation between them, we can easily combine them to one double sum. We therefore find that

$$\mathrm{P}\,e^{-\oint \mathrm{d}x_\mu\mathbf{A}_\mu} = \lim_{N\to\infty}[\sum_{n=1}^{N}\sum_{j=1}^{n-1}K^n_{\frac{1}{2}}K^j_{\frac{3}{2}}+\cdots]\,.\tag{A.37}$$

Following the same reasoning, with the roles of $K^n_{1/2}$ and $K^n_{3/2}$ interchanged, we find another contribution:

$$\mathrm{P}\,e^{-\oint \mathrm{d}x_\mu\mathbf{A}_\mu} = \lim_{N\to\infty}[\sum_{n=1}^{N}\sum_{j=1}^{n-1}K^n_{\frac{3}{2}}K^j_{\frac{1}{2}}+\cdots]\,.\tag{A.38}$$

$K^n_{1/2}$ and $K^n_{3/2}$ therefore give a contribution to a_1 equal to

$$\frac{1}{T^2}\lim_{N\to\infty}\Big[\sum_{n=1}^{N}\sum_{j=1}^{n-1}K^n_{\frac{1}{2}}K^j_{\frac{3}{2}}+\sum_{n=1}^{N}\sum_{j=1}^{n-1}K^n_{\frac{3}{2}}K^j_{\frac{1}{2}}\Big]\,.\tag{A.39}$$

Should $K^n_{1/2}$ and $K^n_{3/2}$ be equal, we only get one of the sums in (A.39).

For three Ks involved, say K_1^n, $K_{1/2}^{n'}$ and $K_{1/2}^{n''}$, we get three sums, as can be seen by repeating the argument above. The summand contributing to the coefficient of order T^2 is

$$\frac{1}{T^2}\lim_{N\to\infty}\Big[\sum_{n=1}^{N}\sum_{j=1}^{n-1}\sum_{r=1}^{j-1}K_{\frac{1}{2}}^{n}K_1^jK_1^r+\sum_{n=1}^{N}\sum_{j=1}^{n-1}\sum_{r=1}^{j-1}K_1^nK_{\frac{1}{2}}^jK_1^r+\sum_{n=1}^{N}\sum_{j=1}^{n-1}\sum_{r=1}^{j-1}K_1^nK_1^jK_{\frac{1}{2}}^r\Big]\,. \tag{A.40}$$

There is one summand, let us call it $K_{1/2}^n$ in (A.32) which is of order $T^{\frac{1}{2}}$. Multiplying it four times onto itself (at different times) we get the contribution

$$\frac{1}{T^2}\lim_{N\to\infty}\Big[\sum_{n=1}^{N}\sum_{j=1}^{n-1}\sum_{r=1}^{j-1}\sum_{l=1}^{r-1}K_{\frac{1}{2}}^{n}K_{\frac{1}{2}}^{j}K_{\frac{1}{2}}^{r}K_{\frac{1}{2}}^{l}\Big]\,. \tag{A.41}$$

Putting everything together, we find for a_1, which is the trace over the expectation value of the sum of the contributions we have found in this section, that

$$\begin{aligned}
a_1=\operatorname{tr}\Big\langle\lim_{N\to\infty}\Big[\quad & -\frac{1}{6}\,\partial_\nu\partial_\alpha\partial_\beta\mathbf{A}_\mu(x)\sum_{n=1}^{N}y_\mu'^n\tilde{y}_\nu^n\tilde{y}_\alpha^n\tilde{y}_\beta^n\\
&+\frac{1}{4}\,\partial_\nu\partial_\alpha\mathbf{A}_\mu(x)\mathbf{A}_\beta(x)\sum_{n=1}^{N}y_\beta'^n y_\mu'^n\tilde{y}_\nu^n\tilde{y}_\alpha^n\\
&+\frac{1}{4}\,\mathbf{A}_\beta(x)\partial_\nu\partial_\alpha\mathbf{A}_\mu(x)\sum_{n=1}^{N}y_\beta'^n y_\mu'^n\tilde{y}_\nu^n\tilde{y}_\alpha^n\\
&+\frac{1}{2}\,\partial_\nu\mathbf{A}_\mu(x)\partial_\beta\mathbf{A}_\alpha(x)\sum_{n=1}^{N}y_\alpha'^n y_\mu'^n\tilde{y}_\beta^n\tilde{y}_\nu^n\\
&-\frac{1}{6}\,\partial_\nu\mathbf{A}_\mu(x)\mathbf{A}_\alpha(x)\mathbf{A}_\beta(x)\sum_{n=1}^{N}y_\mu'^n y_\alpha'^n y_\beta'^n\tilde{y}_\nu^n\\
&-\frac{1}{6}\,\mathbf{A}_\alpha(x)\partial_\nu\mathbf{A}_\mu(x)\mathbf{A}_\beta(x)\sum_{n=1}^{N}y_\alpha'^n y_\mu'^n y_\beta'^n\tilde{y}_\nu^n\\
&-\frac{1}{6}\quad\mathbf{A}_\alpha(x)\mathbf{A}_\beta(x)\partial_\nu\mathbf{A}_\mu(x)\sum_{n=1}^{N}y_\alpha'^n y_\beta'^n y_\mu'^n\tilde{y}_\nu^n\\
&+\frac{1}{24}\,\mathbf{A}_\mu(x)\mathbf{A}_\alpha(x)\mathbf{A}_\nu(x)\mathbf{A}_\beta(x)\sum_{n=1}^{N}y_\mu'^n y_\alpha'^n y_\nu'^n y_\beta'^n\\
&+\frac{1}{2}\,\partial_\nu\partial_\alpha\mathbf{A}_\mu(x)\mathbf{A}_\beta(x)\sum_{n=1}^{N}\sum_{j=1}^{n-1}y_\beta'^j y_\mu'^n\tilde{y}_\nu^n\tilde{y}_\alpha^n\\
&+\frac{1}{2}\,\mathbf{A}_\beta(x)\partial_\nu\partial_\alpha\mathbf{A}_\mu(x)\sum_{n=1}^{N}\sum_{j=1}^{n-1}y_\beta'^n y_\mu'^j\tilde{y}_\nu^j\tilde{y}_\alpha^j
\end{aligned}$$

$$
\begin{aligned}
&- \partial_\nu \mathbf{A}_\mu(x)\mathbf{A}_\beta(x)\mathbf{A}_\nu(x) \sum_{n=1}^{N}\sum_{j=1}^{n-1} y_\nu'^{j} y_\mu'^{n} y_\beta'^{n} \tilde{y}_\nu^{n} \\
&- \mathbf{A}_\nu(x)\partial_\nu \mathbf{A}_\mu(x)\mathbf{A}_\beta(x) \sum_{n=1}^{N}\sum_{j=1}^{n-1} y_\nu'^{n} y_\mu'^{j} y_\beta'^{j} \tilde{y}_\nu^{j} \\
&+\frac{1}{6}\,\mathbf{A}_\mu(x)\mathbf{A}_\alpha(x)\mathbf{A}_\beta(x)\mathbf{A}_\nu(x) \sum_{n=1}^{N}\sum_{j=1}^{n-1} y_\nu'^{j} y_\beta'^{n} y_\alpha'^{n} y_\mu'^{n} \\
&+\frac{1}{6}\,\mathbf{A}_\nu(x)\mathbf{A}_\mu(x)\mathbf{A}_\alpha(x)\mathbf{A}_\beta(x) \sum_{n=1}^{N}\sum_{j=1}^{n-1} y_\nu'^{n} y_\beta'^{j} y_\alpha'^{j} y_\mu'^{j} \\
&+\partial_\nu \mathbf{A}_\mu(x)\partial_\alpha \mathbf{A}_\beta(x) \sum_{n=1}^{N}\sum_{j=1}^{n-1} y_\mu'^{n} \tilde{y}_\nu^{n} y_\alpha'^{j} \tilde{y}_\beta^{j} \\
&-\frac{1}{2}\partial_\nu \mathbf{A}_\mu(x)\mathbf{A}_\beta(x)\mathbf{A}_\alpha(x) \sum_{n=1}^{N}\sum_{j=1}^{n-1} y_\mu'^{n} \tilde{y}_\nu^{n} y_\alpha'^{j} y_\beta'^{j} \\
&-\frac{1}{2}\mathbf{A}_\beta(x)\mathbf{A}_\alpha(x)\partial_\nu \mathbf{A}_\mu(x) \sum_{n=1}^{N}\sum_{j=1}^{n-1} y_\mu'^{j} \tilde{y}_\nu^{j} y_\alpha'^{n} y_\beta'^{n} \\
&-\mathbf{A}_\mu(x)\mathbf{A}_\alpha(x)\partial_\beta \mathbf{A}_\nu(x) \sum_{n=1}^{N}\sum_{j=1}^{n-1}\sum_{r=1}^{j-1} y_\mu'^{n} y_\alpha'^{j} y_\nu'^{r} \tilde{y}_\beta^{r} \\
&-\mathbf{A}_\mu(x)\partial_\beta \mathbf{A}_\nu(x)\mathbf{A}_\alpha(x) \sum_{n=1}^{N}\sum_{j=1}^{n-1}\sum_{r=1}^{j-1} y_\mu'^{n} y_\alpha'^{r} y_\nu'^{j} \tilde{y}_\beta^{j} \\
&-\partial_\beta \mathbf{A}_\nu(x)\mathbf{A}_\mu(x)\mathbf{A}_\alpha(x) \sum_{n=1}^{N}\sum_{j=1}^{n-1}\sum_{r=1}^{j-1} y_\mu'^{j} y_\alpha'^{r} y_\nu'^{n} \tilde{y}_\beta^{n} \\
&+\frac{1}{2}\mathbf{A}_\mu(x)\mathbf{A}_\alpha(x)\mathbf{A}_\beta(x)\mathbf{A}_\nu(x) \sum_{n=1}^{N}\sum_{j=1}^{n-1}\sum_{r=1}^{j-1} y_\mu'^{n} y_\alpha'^{j} y_\beta'^{r} y_\nu'^{r} \\
&+\frac{1}{2}\mathbf{A}_\mu(x)\mathbf{A}_\alpha(x)\mathbf{A}_\beta(x)\mathbf{A}_\nu(x) \sum_{n=1}^{N}\sum_{j=1}^{n-1}\sum_{r=1}^{j-1} y_\mu'^{n} y_\alpha'^{j} y_\beta'^{j} y_\nu'^{r} \\
&+\frac{1}{2}\mathbf{A}_\mu(x)\mathbf{A}_\alpha(x)\mathbf{A}_\beta(x)\mathbf{A}_\nu(x) \sum_{n=1}^{N}\sum_{j=1}^{n-1}\sum_{r=1}^{j-1} y_\mu'^{n} y_\alpha'^{n} y_\beta'^{j} y_\nu'^{r} \\
&+\mathbf{A}_\mu(x)\mathbf{A}_\alpha(x)\mathbf{A}_\beta(x)\mathbf{A}_\nu(x) \sum_{n=1}^{N}\sum_{j=1}^{n-1}\sum_{r=1}^{j-1}\sum_{l=1}^{r-1} y_\mu'^{n} y_\alpha'^{j} y_\beta'^{r} y_\nu'^{l}\Big]\Big\rangle\,. \qquad \text{(A.42)}
\end{aligned}
$$

Because of the cyclic invariance of the trace, some terms that include only a single sum can be simplified. The final expression for a_1 then reads:

$$
\begin{aligned}
a_1 = \operatorname{tr}\Big\langle \lim_{N\to\infty} \Big[\quad & -\frac{1}{6}\,\partial_\nu\partial_\alpha\partial_\beta \mathbf{A}_\mu(x) \sum_{n=1}^{N} y'^n_\mu \tilde{y}^n_\nu \tilde{y}^n_\alpha \tilde{y}^n_\beta \\
& +\frac{1}{2}\,\partial_\nu\partial_\alpha \mathbf{A}_\mu(x)\mathbf{A}_\beta(x) \sum_{n=1}^{N} y'^n_\beta y'^n_\mu \tilde{y}^n_\nu \tilde{y}^n_\alpha \\
& +\frac{1}{2}\,\partial_\nu \mathbf{A}_\mu(x)\partial_\beta \mathbf{A}_\alpha(x) \sum_{n=1}^{N} y'^n_\alpha y'^n_\mu \tilde{y}^n_\beta \tilde{y}^n_\nu \\
& -\frac{1}{2}\,\partial_\nu \mathbf{A}_\mu(x)\mathbf{A}_\alpha(x)\mathbf{A}_\beta(x) \sum_{n=1}^{N} y'^n_\mu y'^n_\alpha y'^n_\beta \tilde{y}^n_\nu \\
& +\frac{1}{24}\,\mathbf{A}_\mu(x)\mathbf{A}_\alpha(x)\mathbf{A}_\nu(x)\mathbf{A}_\beta(x) \sum_{n=1}^{N} y'^n_\mu y'^n_\alpha y'^n_\nu y'^n_\beta \\
& +\frac{1}{2}\,\partial_\nu\partial_\alpha \mathbf{A}_\mu(x)\mathbf{A}_\beta(x) \sum_{n=1}^{N}\sum_{j=1}^{n-1} y'^j_\beta y'^n_\mu \tilde{y}^n_\nu \tilde{y}^n_\alpha \\
& +\frac{1}{2}\,\mathbf{A}_\beta(x)\partial_\nu\partial_\alpha \mathbf{A}_\mu(x) \sum_{n=1}^{N}\sum_{j=1}^{n-1} y'^n_\beta y'^j_\mu \tilde{y}^j_\nu \tilde{y}^j_\alpha \\
& -\partial_\nu \mathbf{A}_\mu(x)\mathbf{A}_\beta(x)\mathbf{A}_\nu(x) \sum_{n=1}^{N}\sum_{j=1}^{n-1} y'^j_\nu y'^n_\mu y'^n_\beta \tilde{y}^n_\nu \\
& -\mathbf{A}_\nu(x)\partial_\nu \mathbf{A}_\mu(x)\mathbf{A}_\beta(x) \sum_{n=1}^{N}\sum_{j=1}^{n-1} y'^n_\nu y'^j_\mu y'^j_\beta \tilde{y}^j_\nu \\
& +\frac{1}{6}\,\mathbf{A}_\mu(x)\mathbf{A}_\alpha(x)\mathbf{A}_\beta(x)\mathbf{A}_\nu(x) \sum_{n=1}^{N}\sum_{j=1}^{n-1} y'^j_\nu y'^n_\beta y'^n_\alpha y'^n_\mu \\
& +\frac{1}{6}\,\mathbf{A}_\nu(x)\mathbf{A}_\mu(x)\mathbf{A}_\alpha(x)\mathbf{A}_\beta(x) \sum_{n=1}^{N}\sum_{j=1}^{n-1} y'^n_\nu y'^j_\beta y'^j_\alpha y'^j_\mu \\
& +\partial_\nu \mathbf{A}_\mu(x)\partial_\alpha \mathbf{A}_\beta(x) \sum_{n=1}^{N}\sum_{j=1}^{n-1} y'^n_\mu \tilde{y}^n_\nu y'^j_\alpha \tilde{y}^j_\beta \\
& -\frac{1}{2}\partial_\nu \mathbf{A}_\mu(x)\mathbf{A}_\beta(x)\mathbf{A}_\alpha(x) \sum_{n=1}^{N}\sum_{j=1}^{n-1} y'^n_\mu \tilde{y}^n_\nu y'^j_\alpha y'^j_\beta \\
& -\frac{1}{2}\mathbf{A}_\beta(x)\mathbf{A}_\alpha(x)\partial_\nu \mathbf{A}_\mu(x) \sum_{n=1}^{N}\sum_{j=1}^{n-1} y'^j_\mu \tilde{y}^j_\nu y'^n_\alpha y'^n_\beta \\
& -\mathbf{A}_\mu(x)\mathbf{A}_\alpha(x)\partial_\beta \mathbf{A}_\nu(x) \sum_{n=1}^{N}\sum_{j=1}^{n-1}\sum_{r=1}^{j-1} y'^n_\mu y'^j_\alpha y'^r_\nu \tilde{y}^r_\beta
\end{aligned}
$$

$$
\begin{aligned}
&-\mathbf{A}_\mu(x)\partial_\beta\mathbf{A}_\nu(x)\mathbf{A}_\alpha(x)\sum_{n=1}^{N}\sum_{j=1}^{n-1}\sum_{r=1}^{j-1}y_\mu'^n y_\alpha'^r y_\nu'^j \tilde{y}_\beta^j \\
&-\partial_\beta\mathbf{A}_\nu(x)\mathbf{A}_\mu(x)\mathbf{A}_\alpha(x)\sum_{n=1}^{N}\sum_{j=1}^{n-1}\sum_{r=1}^{j-1}y_\mu'^j y_\alpha'^r y_\nu'^n \tilde{y}_\beta^n \\
&+\frac{1}{2}\mathbf{A}_\mu(x)\mathbf{A}_\alpha(x)\mathbf{A}_\beta(x)\mathbf{A}_\nu(x)\sum_{n=1}^{N}\sum_{j=1}^{n-1}\sum_{r=1}^{j-1}y_\mu'^n y_\alpha'^j y_\beta'^r y_\nu'^r \\
&+\frac{1}{2}\mathbf{A}_\mu(x)\mathbf{A}_\alpha(x)\mathbf{A}_\beta(x)\mathbf{A}_\nu(x)\sum_{n=1}^{N}\sum_{j=1}^{n-1}\sum_{r=1}^{j-1}y_\mu'^n y_\alpha'^j y_\beta'^j y_\nu'^r \\
&+\frac{1}{2}\mathbf{A}_\mu(x)\mathbf{A}_\alpha(x)\mathbf{A}_\beta(x)\mathbf{A}_\nu(x)\sum_{n=1}^{N}\sum_{j=1}^{n-1}\sum_{r=1}^{j-1}y_\mu'^n y_\alpha'^n y_\beta'^j y_\nu'^r \\
&+\mathbf{A}_\mu(x)\mathbf{A}_\alpha(x)\mathbf{A}_\beta(x)\mathbf{A}_\nu(x)\sum_{n=1}^{N}\sum_{j=1}^{n-1}\sum_{r=1}^{j-1}\sum_{l=1}^{r-1}y_\mu'^n y_\alpha'^j y_\beta'^r y_\nu'^l\Big]\Big\rangle\,. \qquad \text{(A.43)}
\end{aligned}
$$

A.5 Tables of the computation of a worldline correlation function

In this section tables of numerical results for the worldline correlation function $\int_0^1 \mathrm{d}t \int_0^1 \mathrm{d}t' \,\langle\, \dot{y}_\mu(t) y_\nu(t) \dot{y}_\alpha(t') y_\beta(t') \,\rangle$ are shown.

Table A.1: Table with the numerical results for $\int_0^1 \mathrm{d}t \int_0^1 \mathrm{d}t' \,\langle\, \dot{y}_\mu(t) y_\nu(t) \dot{y}_\alpha(t') y_\beta(t') \,\rangle$ obtained by a straightforward implementation. 100 loops of 101 points were used for the computation.

μ	ν	α	β	worldline result	μ	ν	α	β	worldline result
0	0	0	0	5.91974e-19	0	0	0	1	3.68972e-17
0	0	0	2	-7.51835e-17	0	0	0	3	-6.90089e-17
0	0	1	0	3.47636e-18	0	0	1	1	1.0655e-18
0	0	1	2	-5.31315e-17	0	0	1	3	5.1131e-18
0	0	2	0	2.30596e-18	0	0	2	1	-8.93242e-17
0	0	2	2	5.83755e-18	0	0	2	3	5.71999e-17
0	0	3	0	-1.00381e-17	0	0	3	1	2.24462e-17
0	0	3	2	-8.86113e-17	0	0	3	3	-8.42967e-18
0	1	0	0	-8.05766e-18	0	1	0	1	0.274591
0	1	0	2	-0.046134	0	1	0	3	0.00285352
0	1	1	0	-0.274591	0	1	1	1	-4.07443e-18
0	1	1	2	-0.00971428	0	1	1	3	-0.0339902
0	1	2	0	0.046134	0	1	2	1	0.00971428

continued on next page

Table A.1: Table with the numerical results for $\int_0^1 \mathrm{d}t \int_0^1 \mathrm{d}t' \, \langle \, \dot{y}_\mu(t) y_\nu(t) \dot{y}_\alpha(t') y_\beta(t') \, \rangle$ obtained by a straightforward implementation. 100 loops of 101 points were used for the computation.

continued from previous page									
μ	ν	α	β	worldline result	μ	ν	α	β	worldline result
0	1	2	2	5.1669e-18	0	1	2	3	-0.00776091
0	1	3	0	-0.00285352	0	1	3	1	0.0339902
0	1	3	2	0.00776091	0	1	3	3	-5.13261e-18
0	2	0	0	7.7351e-18	0	2	0	1	-0.046134
0	2	0	2	0.277747	0	2	0	3	-0.0207131
0	2	1	0	0.046134	0	2	1	1	-2.5373e-18
0	2	1	2	0.0284149	0	2	1	3	-0.0131166
0	2	2	0	-0.277747	0	2	2	1	-0.0284149
0	2	2	2	-4.73019e-18	0	2	2	3	-0.0555001
0	2	3	0	0.0207131	0	2	3	1	0.0131166
0	2	3	2	0.0555001	0	2	3	3	-3.53558e-18
0	3	0	0	-1.19682e-17	0	3	0	1	0.00285352
0	3	0	2	-0.0207131	0	3	0	3	0.319711
0	3	1	0	-0.00285352	0	3	1	1	1.02999e-18
0	3	1	2	-0.0687531	0	3	1	3	0.0299561
0	3	2	0	0.0207131	0	3	2	1	0.0687531
0	3	2	2	-4.44292e-18	0	3	2	3	0.00385483
0	3	3	0	-0.319711	0	3	3	1	-0.0299561
0	3	3	2	-0.00385483	0	3	3	3	7.96672e-18
1	0	0	0	1.00248e-18	1	0	0	1	-0.274591
1	0	0	2	0.046134	1	0	0	3	-0.00285352
1	0	1	0	0.274591	1	0	1	1	4.14599e-18
1	0	1	2	0.00971428	1	0	1	3	0.0339902
1	0	2	0	-0.046134	1	0	2	1	-0.00971428
1	0	2	2	2.02698e-18	1	0	2	3	0.00776091
1	0	3	0	0.00285352	1	0	3	1	-0.0339902
1	0	3	2	-0.00776091	1	0	3	3	-8.5305e-18
1	1	0	0	9.6204e-18	1	1	0	1	6.85758e-18
1	1	0	2	-2.42241e-17	1	1	0	3	2.25579e-17
1	1	1	0	4.84497e-17	1	1	1	1	-6.43582e-18
1	1	1	2	1.72844e-17	1	1	1	3	1.04786e-16
1	1	2	0	-6.34706e-17	1	1	2	1	-1.30679e-17
1	1	2	2	-1.37977e-17	1	1	2	3	-1.27502e-18
1	1	3	0	-5.34208e-17	1	1	3	1	-5.91541e-17
1	1	3	2	3.65105e-17	1	1	3	3	-9.36751e-19
1	2	0	0	-8.35967e-18	1	2	0	1	-0.00971428
continued on next page									

Table A.1: Table with the numerical results for $\int_0^1 \mathrm{d}t \int_0^1 \mathrm{d}t' \, \langle \, \dot{y}_\mu(t) y_\nu(t) \dot{y}_\alpha(t') y_\beta(t') \, \rangle$ obtained by a straightforward implementation. 100 loops of 101 points were used for the computation.

continued from previous page

μ	ν	α	β	worldline result	μ	ν	α	β	worldline result
1	2	0	2	0.0284149	1	2	0	3	-0.0687531
1	2	1	0	0.00971428	1	2	1	1	7.9201e-18
1	2	1	2	0.300189	1	2	1	3	-0.0293346
1	2	2	0	-0.0284149	1	2	2	1	-0.300189
1	2	2	2	-9.45502e-18	1	2	2	3	0.0534002
1	2	3	0	0.0687531	1	2	3	1	0.0293346
1	2	3	2	-0.0534002	1	2	3	3	-1.50921e-18
1	3	0	0	2.71159e-18	1	3	0	1	-0.0339902
1	3	0	2	-0.0131166	1	3	0	3	0.0299561
1	3	1	0	0.0339902	1	3	1	1	-4.51028e-19
1	3	1	2	-0.0293346	1	3	1	3	0.258561
1	3	2	0	0.0131166	1	3	2	1	0.0293346
1	3	2	2	-2.07462e-18	1	3	2	3	0.0203626
1	3	3	0	-0.0299561	1	3	3	1	-0.258561
1	3	3	2	-0.0203626	1	3	3	3	-2.55004e-18
2	0	0	0	1.05733e-18	2	0	0	1	0.046134
2	0	0	2	-0.277747	2	0	0	3	0.0207131
2	0	1	0	-0.046134	2	0	1	1	-5.79045e-18
2	0	1	2	-0.0284149	2	0	1	3	0.0131166
2	0	2	0	0.277747	2	0	2	1	0.0284149
2	0	2	2	-6.7661e-18	2	0	2	3	0.0555001
2	0	3	0	-0.0207131	2	0	3	1	-0.0131166
2	0	3	2	-0.0555001	2	0	3	3	6.1355e-18
2	1	0	0	7.33117e-18	2	1	0	1	0.00971428
2	1	0	2	-0.0284149	2	1	0	3	0.0687531
2	1	1	0	-0.00971428	2	1	1	1	-2.62485e-18
2	1	1	2	-0.300189	2	1	1	3	0.0293346
2	1	2	0	0.0284149	2	1	2	1	0.300189
2	1	2	2	-3.39406e-18	2	1	2	3	-0.0534002
2	1	3	0	-0.0687531	2	1	3	1	-0.0293346
2	1	3	2	0.0534002	2	1	3	3	-2.97722e-18
2	2	0	0	-4.37838e-18	2	2	0	1	6.97053e-17
2	2	0	2	-4.52544e-18	2	2	0	3	5.19116e-18
2	2	1	0	-6.85866e-17	2	2	1	1	7.47761e-18
2	2	1	2	9.93526e-18	2	2	1	3	3.57407e-18
2	2	2	0	1.91921e-17	2	2	2	1	1.07556e-17

continued on next page

Table A.1: Table with the numerical results for $\int_0^1 \mathrm{d}t \int_0^1 \mathrm{d}t' \, \langle \, \dot{y}_\mu(t) y_\nu(t) \dot{y}_\alpha(t') y_\beta(t') \, \rangle$ obtained by a straightforward implementation. 100 loops of 101 points were used for the computation.

continued from previous page									
μ	ν	α	β	worldline result	μ	ν	α	β	worldline result
2	2	2	2	9.63917e-18	2	2	2	3	3.40933e-17
2	2	3	0	-5.00566e-17	2	2	3	1	2.06936e-17
2	2	3	2	7.39084e-17	2	2	3	3	1.03888e-17
2	3	0	0	6.79822e-18	2	3	0	1	-0.00776091
2	3	0	2	-0.0555001	2	3	0	3	0.00385483
2	3	1	0	0.00776091	2	3	1	1	5.09575e-20
2	3	1	2	0.0534002	2	3	1	3	0.0203626
2	3	2	0	0.0555001	2	3	2	1	-0.0534002
2	3	2	2	-1.97596e-18	2	3	2	3	0.346751
2	3	3	0	-0.00385483	2	3	3	1	-0.0203626
2	3	3	2	-0.346751	2	3	3	3	3.29164e-18
3	0	0	0	7.36471e-18	3	0	0	1	-0.00285352
3	0	0	2	0.0207131	3	0	0	3	-0.319711
3	0	1	0	0.00285352	3	0	1	1	8.23994e-18
3	0	1	2	0.0687531	3	0	1	3	-0.0299561
3	0	2	0	-0.0207131	3	0	2	1	-0.0687531
3	0	2	2	-9.26315e-20	3	0	2	3	-0.00385483
3	0	3	0	0.319711	3	0	3	1	0.0299561
3	0	3	2	0.00385483	3	0	3	3	-7.8583e-18
3	1	0	0	7.72386e-18	3	1	0	1	0.0339902
3	1	0	2	0.0131166	3	1	0	3	-0.0299561
3	1	1	0	-0.0339902	3	1	1	1	-1.56949e-17
3	1	1	2	0.0293346	3	1	1	3	-0.258561
3	1	2	0	-0.0131166	3	1	2	1	-0.0293346
3	1	2	2	-4.09368e-18	3	1	2	3	-0.0203626
3	1	3	0	0.0299561	3	1	3	1	0.258561
3	1	3	2	0.0203626	3	1	3	3	-8.84709e-19
3	2	0	0	-9.765e-18	3	2	0	1	0.00776091
3	2	0	2	0.0555001	3	2	0	3	-0.00385483
3	2	1	0	-0.00776091	3	2	1	1	-1.90603e-18
3	2	1	2	-0.0534002	3	2	1	3	-0.0203626
3	2	2	0	-0.0555001	3	2	2	1	0.0534002
3	2	2	2	-9.93346e-18	3	2	2	3	-0.346751
3	2	3	0	0.00385483	3	2	3	1	0.0203626
3	2	3	2	0.346751	3	2	3	3	-7.15573e-20
3	3	0	0	1.25084e-17	3	3	0	1	-2.29157e-17
continued on next page									

Table A.1: Table with the numerical results for $\int_0^1 \mathrm{d}t \int_0^1 \mathrm{d}t' \, \langle \, \dot{y}_\mu(t) y_\nu(t) \dot{y}_\alpha(t') y_\beta(t') \, \rangle$ obtained by a straightforward implementation. 100 loops of 101 points were used for the computation.

continued from previous page									
μ	ν	α	β	worldline result	μ	ν	α	β	worldline result
3	3	0	2	-1.54819e-17	3	3	0	3	1.3553e-16
3	3	1	0	2.63982e-17	3	3	1	1	9.97466e-19
3	3	1	2	-2.81741e-17	3	3	1	3	-4.34201e-17
3	3	2	0	6.00225e-17	3	3	2	1	6.70384e-17
3	3	2	2	-3.03685e-18	3	3	2	3	-1.17094e-19
3	3	3	0	6.55595e-17	3	3	3	1	1.79978e-17
3	3	3	2	1.55865e-17	3	3	3	3	1.38778e-18

Table A.2: Table of the numerical results for $\int_0^1 \mathrm{d}t \int_0^1 \mathrm{d}t' \, \langle \, \dot{y}_\mu(t) y_\nu(t) \dot{y}_\alpha(t') y_\beta(t') \, \rangle$ in three dimensions. 3^4 evaluations (corresponding to 3^4 rotated copies of the loop cloud) using 100 loops of 101 points were used for the computation.

μ	ν	α	β	worldline result	μ	ν	α	β	worldline result
0	0	0	0	-1.8102e-20	0	0	0	1	-7.89111e-19
0	0	0	2	-2.49021e-19	0	0	1	0	-7.33227e-19
0	0	1	1	5.9163e-20	0	0	1	2	5.87649e-19
0	0	2	0	-7.10149e-19	0	0	2	1	-1.54681e-19
0	0	2	2	1.44158e-20	0	1	0	0	-1.06692e-20
0	1	0	1	0.317984	0	1	0	2	1.8443e-19
0	1	1	0	-0.317984	0	1	1	1	-5.10855e-20
0	1	1	2	9.41701e-18	0	1	2	0	-8.24743e-19
0	1	2	1	-8.79056e-18	0	1	2	2	-8.06524e-20
0	2	0	0	-1.57299e-20	0	2	0	1	-3.21263e-18
0	2	0	2	0.317984	0	2	1	0	1.09507e-17
0	2	1	1	9.52551e-21	0	2	1	2	7.30153e-18
0	2	2	0	-0.317984	0	2	2	1	-3.42136e-18
0	2	2	2	2.68142e-20	1	0	0	0	6.72871e-21
1	0	0	1	-0.317984	1	0	0	2	1.06769e-17
1	0	1	0	0.317984	1	0	1	1	4.64745e-20
1	0	1	2	2.12872e-17	1	0	2	0	2.09525e-18
1	0	2	1	-2.13718e-18	1	0	2	2	2.56088e-20
1	1	0	0	9.65557e-21	1	1	0	1	-1.97221e-20
1	1	0	2	1.31336e-19	1	1	1	0	-4.96705e-19
1	1	1	1	6.51009e-20	1	1	1	2	4.40717e-19
1	1	2	0	-1.25658e-19	1	1	2	1	1.22015e-18
continued on next page									

Table A.2: Table of the numerical results for $\int_0^1 \mathrm{d}t \int_0^1 \mathrm{d}t' \, \langle \, \dot{y}_\mu(t) y_\nu(t) \dot{y}_\alpha(t') y_\beta(t') \, \rangle$ in three dimensions. 3^4 evaluations (corresponding to 3^4 rotated copies of the loop cloud) using 100 loops of 101 points were used for the computation.

continued from previous page

μ	ν	α	β	worldline result	μ	ν	α	β	worldline result
1	1	2	2	-2.75072e-21	1	2	0	0	1.39187e-20
1	2	0	1	1.10618e-17	1	2	0	2	3.39515e-18
1	2	1	0	1.73922e-17	1	2	1	1	-7.1318e-20
1	2	1	2	0.317984	1	2	2	0	-6.51974e-18
1	2	2	1	-0.317984	1	2	2	2	2.07666e-21
2	0	0	0	-5.49081e-20	2	0	0	1	-4.10234e-19
2	0	0	2	-0.317984	2	0	1	0	4.31337e-18
2	0	1	1	-6.39641e-20	2	0	1	2	-1.2246e-17
2	0	2	0	0.317984	2	0	2	1	-2.34662e-18
2	0	2	2	2.43293e-20	2	1	0	0	1.6796e-20
2	1	0	1	-8.13594e-18	2	1	0	2	-7.78334e-18
2	1	1	0	-3.87647e-18	2	1	1	1	1.44414e-20
2	1	1	2	-0.317984	2	1	2	0	-3.19195e-18
2	1	2	1	0.317984	2	1	2	2	-2.64457e-21
2	2	0	0	4.02212e-20	2	2	0	1	4.22303e-19
2	2	0	2	6.44196e-19	2	2	1	0	-9.31781e-20
2	2	1	1	-4.11199e-20	2	2	1	2	2.90902e-19
2	2	2	0	-7.98923e-19	2	2	2	1	-5.79444e-19
2	2	2	2	3.10095e-19					

Table A.3: Table of the numerical results for $\int_0^1 \mathrm{d}t \int_0^1 \mathrm{d}t' \, \langle \, \dot{y}_\mu(t) y_\nu(t) \dot{y}_\alpha(t') y_\beta(t') \, \rangle$ in three dimensions. 2,000,000 loops of 101 points were used for the computation.

μ	ν	α	β	worldline result	μ	ν	α	β	worldline result
0	0	0	0	-3.50847e-20	0	0	0	1	-5.50973e-19
0	0	0	2	4.71693e-19	0	0	1	0	8.19679e-19
0	0	1	1	5.8455e-20	0	0	1	2	3.70387e-19
0	0	2	0	-4.3467e-19	0	0	2	1	4.04886e-19
0	0	2	2	-5.17888e-20	0	1	0	0	1.82786e-20
0	1	0	1	0.331451	0	1	0	2	-0.000203934
0	1	1	0	-0.331451	0	1	1	1	-8.80596e-21
0	1	1	2	-8.31337e-05	0	1	2	0	0.000203934
0	1	2	1	8.31337e-05	0	1	2	2	-6.76788e-20
0	2	0	0	-5.69572e-20	0	2	0	1	-0.000203934

continued on next page

Table A.3: Table of the numerical results for $\int_0^1 \mathrm{d}t \int_0^1 \mathrm{d}t' \ \langle \ \dot{y}_\mu(t) y_\nu(t) \dot{y}_\alpha(t') y_\beta(t') \ \rangle$ in three dimensions. 2,000,000 loops of 101 points were used for the computation.

continued from previous page

μ	ν	α	β	worldline result	μ	ν	α	β	worldline result
0	2	0	2	0.331186	0	2	1	0	0.000203934
0	2	1	1	1.99144e-20	0	2	1	2	-0.000298953
0	2	2	0	-0.331186	0	2	2	1	0.000298953
0	2	2	2	3.69985e-20	1	0	0	0	1.3936e-20
1	0	0	1	-0.331451	1	0	0	2	0.000203934
1	0	1	0	0.331451	1	0	1	1	6.96224e-20
1	0	1	2	8.31337e-05	1	0	2	0	-0.000203934
1	0	2	1	-8.31337e-05	1	0	2	2	6.6418e-20
1	1	0	0	5.15469e-20	1	1	0	1	-2.071e-19
1	1	0	2	5.9772e-20	1	1	1	0	4.56647e-21
1	1	1	1	-6.16994e-20	1	1	1	2	5.80297e-19
1	1	2	0	-1.08255e-18	1	1	2	1	-1.06973e-18
1	1	2	2	2.75009e-20	1	2	0	0	-7.0594e-20
1	2	0	1	-8.31337e-05	1	2	0	2	-0.000298953
1	2	1	0	8.31337e-05	1	2	1	1	-8.85429e-20
1	2	1	2	0.330872	1	2	2	0	0.000298953
1	2	2	1	-0.330872	1	2	2	2	1.04298e-19
2	0	0	0	1.18161e-19	2	0	0	1	0.000203934
2	0	0	2	-0.331186	2	0	1	0	-0.000203934
2	0	1	1	8.5625e-20	2	0	1	2	0.000298953
2	0	2	0	0.331186	2	0	2	1	-0.000298953
2	0	2	2	-1.89715e-20	2	1	0	0	-4.35189e-20
2	1	0	1	8.31337e-05	2	1	0	2	0.000298953
2	1	1	0	-8.31337e-05	2	1	1	1	9.47017e-20
2	1	1	2	-0.330872	2	1	2	0	-0.000298953
2	1	2	1	0.330872	2	1	2	2	1.51013e-21
2	2	0	0	-7.25514e-20	2	2	0	1	-6.50983e-20
2	2	0	2	-3.98984e-19	2	2	1	0	-2.9079e-19
2	2	1	1	-6.75725e-21	2	2	1	2	1.38454e-19
2	2	2	0	-3.32316e-19	2	2	2	1	-1.15626e-18
2	2	2	2	8.11829e-20					

Table A.4: Table of the numerical results for $\int_0^1 \mathrm{d}t \int_0^1 \mathrm{d}t' \, \langle \, \dot{y}_\mu(t) y_\nu(t) \dot{y}_\alpha(t') y_\beta(t') \, \rangle$ in three dimensions. 100 loops of 14,241 points were used for the computation.

μ	ν	α	β	worldline result	μ	ν	α	β	worldline result
0	0	0	0	-9.74435e-17	0	0	0	1	1.14381e-15
0	0	0	2	-9.3336e-15	0	0	1	0	-9.42832e-15
0	0	1	1	4.2262e-17	0	0	1	2	-1.26645e-15
0	0	2	0	2.81632e-15	0	0	2	1	-5.02664e-16
0	0	2	2	7.94665e-17	0	1	0	0	-1.34598e-17
0	1	0	1	0.297909	0	1	0	2	0.0333473
0	1	1	0	-0.297909	0	1	1	1	-1.70299e-17
0	1	1	2	-0.023779	0	1	2	0	-0.0333473
0	1	2	1	0.023779	0	1	2	2	-3.01939e-17
0	2	0	0	-8.18568e-17	0	2	0	1	0.0333473
0	2	0	2	0.318283	0	2	1	0	-0.0333473
0	2	1	1	-3.72052e-17	0	2	1	2	-0.0514883
0	2	2	0	-0.318283	0	2	2	1	0.0514883
0	2	2	2	5.93328e-17	1	0	0	0	3.06013e-17
1	0	0	1	-0.297909	1	0	0	2	-0.0333473
1	0	1	0	0.297909	1	0	1	1	1.38635e-17
1	0	1	2	0.023779	1	0	2	0	0.0333473
1	0	2	1	-0.023779	1	0	2	2	5.23405e-18
1	1	0	0	-4.01419e-17	1	1	0	1	-2.81529e-15
1	1	0	2	4.43025e-15	1	1	1	0	-1.7684e-15
1	1	1	1	1.01031e-17	1	1	1	2	8.54911e-16
1	1	2	0	2.59074e-15	1	1	2	1	-4.04357e-15
1	1	2	2	-4.90665e-17	1	2	0	0	-4.92515e-17
1	2	0	1	-0.023779	1	2	0	2	-0.0514883
1	2	1	0	0.023779	1	2	1	1	5.56632e-17
1	2	1	2	0.320992	1	2	2	0	0.0514883
1	2	2	1	-0.320992	1	2	2	2	6.62522e-18
2	0	0	0	-2.47921e-17	2	0	0	1	-0.0333473
2	0	0	2	-0.318283	2	0	1	0	0.0333473
2	0	1	1	-2.25956e-17	2	0	1	2	0.0514883
2	0	2	0	0.318283	2	0	2	1	-0.0514883
2	0	2	2	1.02233e-17	2	1	0	0	8.23672e-17
2	1	0	1	0.023779	2	1	0	2	0.0514883
2	1	1	0	-0.023779	2	1	1	1	-3.72179e-17
2	1	1	2	-0.320992	2	1	2	0	-0.0514883
2	1	2	1	0.320992	2	1	2	2	4.40814e-17
2	2	0	0	2.49313e-17	2	2	0	1	-4.62021e-15

continued on next page

Table A.4: Table of the numerical results for $\int_0^1 \mathrm{d}t \int_0^1 \mathrm{d}t' \, \langle \, \dot{y}_\mu(t) y_\nu(t) \dot{y}_\alpha(t') y_\beta(t') \, \rangle$ in three dimensions. 100 loops of 14,241 points were used for the computation.

continued from previous page

μ	ν	α	β	worldline result	μ	ν	α	β	worldline result
2	2	0	2	6.77951e-15	2	2	1	0	-8.9194e-15
2	2	1	1	4.20786e-17	2	2	1	2	4.18565e-15
2	2	2	0	-5.51472e-15	2	2	2	1	-1.57275e-15
2	2	2	2	-4.902e-17					

Table A.5: Table of the numerical results for $\int_0^1 \mathrm{d}t \int_0^1 \mathrm{d}t' \, \langle \, \dot{y}_\mu(t) y_\nu(t) \dot{y}_\alpha(t') y_\beta(t') \, \rangle$ in four dimensions; only components with $\mu = 0$ are shown. 9^6 Monte Carlo evaluations with 100 loops of 101 points were used for the computation.

μ	ν	α	β	worldline result	μ	ν	α	β	worldline result
0	0	0	0	3.1331e-18	0	0	0	1	-3.02033e-17
0	0	0	2	-1.63548e-17	0	0	0	3	-4.86273e-19
0	0	1	0	-3.69468e-17	0	0	1	1	6.36205e-18
0	0	1	2	-1.93687e-17	0	0	1	3	1.30484e-18
0	0	2	0	3.55469e-17	0	0	2	1	8.6476e-18
0	0	2	2	5.01795e-18	0	0	2	3	-1.2988e-18
0	0	3	0	4.16456e-18	0	0	3	1	4.31963e-19
0	0	3	2	1.78885e-18	0	0	3	3	-9.52311e-21
0	1	0	0	-6.03821e-18	0	1	0	1	0.274591
0	1	0	2	0.0152587	0	1	0	3	-1.74607e-05
0	1	1	0	-0.274591	0	1	1	1	9.36357e-18
0	1	1	2	-0.0136663	0	1	1	3	-1.521e-05
0	1	2	0	-0.0152587	0	1	2	1	0.0136663
0	1	2	2	6.45227e-18	0	1	2	3	1.21264e-05
0	1	3	0	1.74607e-05	0	1	3	1	1.521e-05
0	1	3	2	-1.21264e-05	0	1	3	3	6.66322e-20
0	2	0	0	2.56515e-18	0	2	0	1	0.0152587
0	2	0	2	0.31605	0	2	0	3	0.000101377
0	2	1	0	-0.0152587	0	2	1	1	4.54158e-18
0	2	1	2	0.0130284	0	2	1	3	-3.23125e-05
0	2	2	0	-0.31605	0	2	2	1	-0.0130284
0	2	2	2	9.22331e-18	0	2	2	3	6.94696e-06
0	2	3	0	-0.000101377	0	2	3	1	3.23125e-05
0	2	3	2	-6.94696e-06	0	2	3	3	-1.94998e-19
0	3	0	0	-1.64831e-19	0	3	0	1	-1.74607e-05

continued on next page

Table A.5: Table of the numerical results for $\int_0^1 \mathrm{d}t \int_0^1 \mathrm{d}t' \ \langle \ \dot{y}_\mu(t) y_\nu(t) \dot{y}_\alpha(t') y_\beta(t') \ \rangle$ in four dimensions; only components with $\mu = 0$ are shown. 9^6 Monte Carlo evaluations with 100 loops of 101 points were used for the computation.

continued from previous page

μ	ν	α	β	worldline result	μ	ν	α	β	worldline result
0	3	0	2	0.000101377	0	3	0	3	0.251449
0	3	1	0	1.74607e-05	0	3	1	1	-7.49145e-19
0	3	1	2	5.46195e-05	0	3	1	3	-0.012305
0	3	2	0	-0.000101377	0	3	2	1	-5.46195e-05
0	3	2	2	9.45696e-20	0	3	2	3	-0.00150833
0	3	3	0	-0.251449	0	3	3	1	0.012305
0	3	3	2	0.00150833	0	3	3	3	4.61477e-19

Bibliography

[1] W. Heisenberg, H. Euler, Folgerungen aus der Diracschen Theorie des Positrons (Consequences of Dirac's theory of positrons), Z. Phys. 98 (1936) 714–732.

[2] V. Weisskopf, Über die Elektrodynamik des Vakuums auf Grund der Quantentheorie des Elekrons (The electrodynamics of the vacuum based on the quantum theory of the electron), Kong. Dans. Vid. Selsk. Math-fys. Medd. XIV No. 6.

[3] G. V. Dunne, Functional Determinants in Quantum Field Theory.

[4] G. V. Dunne, Heisenberg-Euler effective Lagrangians: Basics and extensions.

[5] E. Brezin, C. Itzykson, Pair production in vacuum by an alternating field, Phys. Rev. D 2 (7) (1970) 1191–1199.

[6] V. S. Popov, Pair production in a variable external field (quasiclassical approximation), Sov.Phys.JETP 34 (1972) 709.

[7] V. S. Popov, M. S. Marinov, e+ e- pair production in an alternating electric field, Yad. Fiz. 16 (1972) 809–822.

[8] C. Schubert, Perturbative quantum field theory in the string-inspired formalism, Phys. Rept. 355 (2001) 73–234.

[9] D. Fliegner, P. Haberl, M. G. Schmidt, C. Schubert, Application of the worldline path integral method to the calculation of inverse mass expansions, Nucl. Instrum. Meth. A389 (1997) 374–377.

[10] D. Fliegner, P. Haberl, M. G. Schmidt, C. Schubert, The higher derivative expansion of the effective action by the string inspired method. II, Annals Phys. 264 (1998) 51–74.

[11] D. V. Vassilevich, Heat kernel expansion: User's manual, Phys. Rept. 388 (2003) 279–360.

[12] H. Gies, K. Langfeld, Quantum diffusion of magnetic fields in a numerical worldline approach, Nucl. Phys. B613 (2001) 353–365.

[13] H. Gies, K. Langfeld, Loops and loop clouds: A numerical approach to the worldline formalism in QED, Int. J. Mod. Phys. A17 (2002) 966–978.

[14] H. Gies, K. Klingmüller, Pair production in inhomogeneous fields, Phys. Rev. D72 (2005) 065001.

[15] H. Gies, K. Langfeld, L. Moyaerts, Casimir effect on the worldline, JHEP 06 (2003) 018.

[16] L. Moyaerts, K. Langfeld, H. Gies, Worldline approach to the Casimir effect.

[17] H. Gies, K. Klingmüller, Casimir effect for curved geometries: PFA validity limits, Phys. Rev. Lett. 96 (2006) 220401.

[18] H. Gies, K. Klingmüller, Worldline algorithms for Casimir configurations, Phys. Rev. D74 (2006) 045002.

[19] H. Gies, K. Klingmüller, Casimir edge effects, Phys. Rev. Lett. 97 (2006) 220405.

[20] H. Gies, K. Klingmüller, Geothermal Casimir Phenomena, J. Phys. A41 (2008) 164042.

[21] K. Langfeld, G. Dunne, H. Gies, K. Klingmüller, Worldline Approach to Chiral Fermions, PoS LATTICE2007 (2006) 202.

[22] R. P. Feynman, Mathematical Formulation of the Quantum Theory of Electromagnetic Interaction, Phys. Rev. 80 (3) (1950) 440–457.

[23] Z. Bern, D. A. Kosower, Color decomposition of one loop amplitudes in gauge theories, Nucl. Phys. B362 (1991) 389–448.

[24] Z. Bern, D. A. Kosower, The Computation of loop amplitudes in gauge theories, Nucl. Phys. B379 (1992) 451–561.

[25] M. J. Strassler, Field theory without Feynman diagrams: One loop effective actions, Nucl. Phys. B385 (1992) 145–184.

[26] M. G. Schmidt, C. Schubert, On the calculation of effective actions by string methods, Phys. Lett. B318 (1993) 438–446.

[27] M. Reuter, M. G. Schmidt, C. Schubert, Constant external fields in gauge theory and the spin 0, 1/2, 1 path integrals, Annals Phys. 259 (1997) 313–365.

[28] M. G. Schmidt, I.-O. Stamatescu, Determinant calculations using random walk worldline loops, Nucl. Phys. Proc. Suppl. 119 (2003) 1030–1032.

[29] T. Schäfer, E. V. Shuryak, Instantons in QCD, Rev. Mod. Phys. 70 (1998) 323–426.

[30] S. Coleman, Aspects of Symmetry: Selected Erice Lectures, Cambridge University Press, 1988.

[31] M. A. Shifman, ITEP lectures on particle physics and field theory, World Scientific (Singapore), 1999.

[32] M. A. Shifman, Instantons in Gauge Theories, World Scientific (Singapore), 1994.

[33] G. V. Dunne, J. Hur, C. Lee, H. Min, Precise quark mass dependence of instanton determinant, Phys. Rev. Lett. 94 (2005) 072001.

[34] A. M. Polyakov, Thermal Properties of Gauge Fields and Quark Liberation, Phys. Lett. B72 (1978) 477–480.

[35] L. Susskind, Lattice models of quark confinement at high temperature, Phys. Rev. D 20 (10) (1979) 2610–2618.

[36] N. Weiss, Effective potential for the order parameter of gauge theories at finite temperature, Phys. Rev. D 24 (2) (1981) 475–480.

[37] G. E. Box, M. E. Müller, A Note on the Generation of Random Normal Deviates, Ann. Math. Stat. 29 (1958) 610.

[38] W. H. Press, S. A. Teukolsky, W. T. Vetterling, B. P. Flannery, Numerical Recipes in C: The Art of Scientific Computing, Cambridge University Press, New York, NY, USA, 1992.

[39] S. Huang, A. R. Levi, A non-Abelian variation on the Savvidy vacuum of the Yang- Mills gauge theory, Phys. Rev. D49 (1994) 6849–6856.

[40] H. Gies, private communication.

[41] A. A. Belavin, A. M. Polyakov, A. S. Schwartz, Y. S. Tyupkin, Pseudoparticle solutions of the Yang-Mills equations, Phys. Lett. B59 (1975) 85.

[42] R. Jackiw, C.Rebbi, Conformal properties of a Yang-Mills pseudoparticle, Phys. Rev. D14 (12) (1976) 517.

[43] M. Böhm, A. Denner, H. Joos, Gauge Theories of the Strong and Electroweak Interaction, Vieweg+Teubner, 2001.

[44] H. Kleinert, Path Integrals in Quantum Mechanics, Statistics, Polymer Physics, and Financial Markets, World Scientific (Singapore), 2004.

[45] G. V. Dunne, J. Hur, C. Lee, H. Min, Instanton determinant with arbitrary quark mass: WKB phase-shift method and derivative expansion, Phys. Lett. B600 (2004) 302–313.

[46] G. V. Dunne, C. Schubert, Two-loop self-dual Euler-Heisenberg Lagrangians. I: Real part and helicity amplitudes, JHEP 08 (2002) 053.

[47] R. L. Karp, F. Mansouri, J. S. Rno, Product integral representations of Wilson lines and Wilson loops, and non-Abelian Stokes theorem, Turk. J. Phys. 24 (2000) 365–384.

[48] B. Svetitsky, Symmetry Aspencts of Finite Temperature Confinement Transitions, Phys. Rept. 132 (1986) 1–53.

[49] W. Dittrich, M. Reuter, Selected Topics in Gauge Theories, Springer-Verlag, Berlin, Heidelberg, New York, Tokio, 1986.

[50] L. S. Schulman, Techniques and Applications of Path Integration, Wiley, New York, 1981.

Danksagung

Am Gelingen dieser Diplomarbeit hatten viele Menschen, ob sie sich dessen bewusst sein mögen oder nicht, ihren Anteil. Auch wenn es mir nicht möglich ist sie alle namentlich zu nennen, möchte ich ihnen hiermit danken. Denjenigen, die neben mir am meisten dazu beigetragen haben, dass es mir möglich war eine, wie ich finde, recht ordentliche Arbeit abzuliefern, möchte ich nun aber auch gesondert meinen Dank aussprechen.

Allen voran und ganz besonders möchte ich Herrn Prof. Dr. Holger Gies danken. Er hat mich nicht nur an diesem lehrreichen und interessanten Thema arbeiten lassen, sondern stand mir auch während der gesamten Dauer meiner Forschungen je nach Bedarf mit fachlicher Kompetenz, Zuspruch oder Enthusiasmus zur Seite.

Der Belegschaft des Westzimmers möchte ich für eine Arbeits- und Pausenatmosphäre danken, von der ich überzeugt bin, dass sie ihres gleichen sucht. Es wird mir wohl nicht wieder vergönnt sein, mit 3 Physikern den Arbeitsraum zu teilen, mit denen zusammenzuwohnen mir nicht wie eine Bestrafung vorkäme.

Dank möchte ich auch den Korrekturlesern Michael Scherer, Richard Schmidt, Jessica Thornton und Thomas Ebi aussprechen, die es in unermüdlicher Fleißarbeit bewerkstelligt haben mein gesamtes Werk nach Fehlern zu durchsuchen. Auch Nico Wintergerst möchte ich in diesem Zusammenhang danken, der die Arbeit zwar nicht korrekturgelesen hat, sie aber dennoch in weiten Teilen kennt.

Michael Scherer und Daniel Spielmann bin ich dafür dankbar, dass sie mir halfen die Grausamkeiten, zu denen ich, wenn ich deutsche Sätze schreibe, insbesondere, was die Zeichensetzung angeht, durchaus in der Lage bin, aufzuspühren und weniger grausam zu machen.

Zu guter Letzt danke ich meinen Eltern. Ohne sie wäre ich nicht am Leben. Ohne ihre Unterstützung wäre es zu dieser Diplomarbeit mit Sicherheit nicht gekommen.